NASA
Reference
Publication
1284

August 1992

Nimbus-7 Scanning Multichannel Microwave Radiometer (SMMR) PARM Tape User's Guide

D. Han,
P. Gloersen,
S. T. Kim,
C. C. Fu,
R. P. Cebula,
and D. MacMillan

NASA

NASA Reference Publication 1284

1992

Nimbus-7 Scanning Multichannel Microwave Radiometer (SMMR) PARM Tape User's Guide

D. Han and P. Gloersen
Goddard Space Flight Center
Greenbelt, Maryland

S. T. Kim and C. C. Fu
Computer Sciences Corporation (CSC)
Rockville, Maryland

R. P. Cebula
Hughes STX Corporation
Lanham, Maryland

D. MacMillan
Interferometrics, Inc.
Vienna, Virginia

NASA
National Aeronautics and Space Administration
Office of Management
Scientific and Technical Information Program

TABLE OF CONTENTS

TABLE OF CONTENTS (Continued)

TABLE OF CONTENTS (Continued)

1. INTRODUCTION

1.1 Purpose

This document describes in detail the format and contents of PARM tapes derived from Nimbus–7 Scanning Multichannel Microwave Radiometer (SMMR) data for the period November 1978 through October 1985. The description includes the algorithms used to retrieve geophysical parameters and quality assessment of the derived parameters.

1.2 Overview

There are three types of SMMR PARM tapes: PARM-LO, PARM-SS, and PARM-30. A PARM-LO tape contains land/ocean parameters. The list of parameters on a PARM-LO tape is given in Table A.1 in Appendix A along with their units and resolutions. A PARM-SS tape contains ocean, ice, snow, and ice-sheet parameters as listed in Table A.3 in Appendix A. A PARM-30 tape contains sea-ice concentration with 30-km resolution. Detailed descriptions of PARM tape formats are given in Appendix A.

1.3 Data Processing Flow

In Figure 1.1, the overall SMMR data processing flowchart is shown. Figure 1.2 shows the logical flow of parameter computations. The SMMR PARM tape generation program reads SMMR CELL-ALL tapes. For each cell* position, the program determines the geography flag. If the cell is entirely over land, it computes land parameters. If the latitude of the cell position is over land and more than 58° north or south of the snow indicator† latitude (the snow indicator varies day to day), then the program computes snow parameters. If the cell lies entirely over the ocean and the latitude is north of 45° N or south of 45° S, then ice parameters are computed. If the cell is flagged as ocean and contains no ice, then the program computes ocean parameters. Sea-surface temperatures (SST's) are computed only north of 55° S during the descending part of the orbit. If a cell contains both land and ocean, it is flagged as NO-OP, and the program does not compute any parameters. Greenland and Antarctica are flagged as ice sheets, and ice-sheet parameters are computed. The algorithms for deriving parameters for the Year-1 through Year-7 production are given in detail in Section 2.5.

---

*Cells are defined in four different sizes: 156 by 158 km, 97.5 by 98.5 km, 60 by 61 km, and 30 by 30 km. See *User's Guide for the Nimbus–7 SMMR CELL-ALL Tape* for details (Fu et al., 1988).

†Snow indicator latitude is defined as the following: SLAT = 23.5*SIN((Day – 90)*2π/365) If |Latitude-SLAT| >58, compute snow parameters.

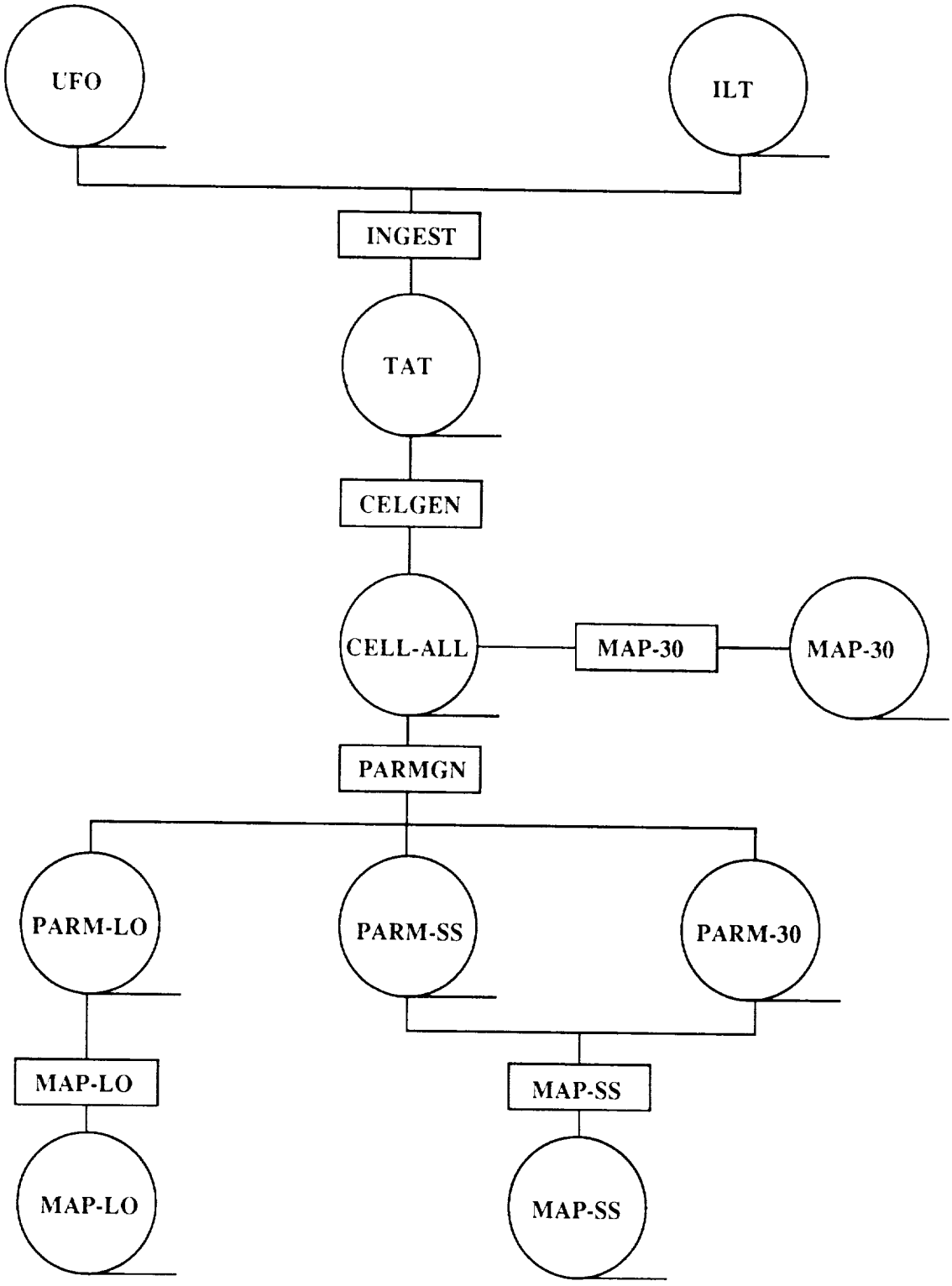

Figure 1.1. Flow of Nimbus–7 SMMR processing system.

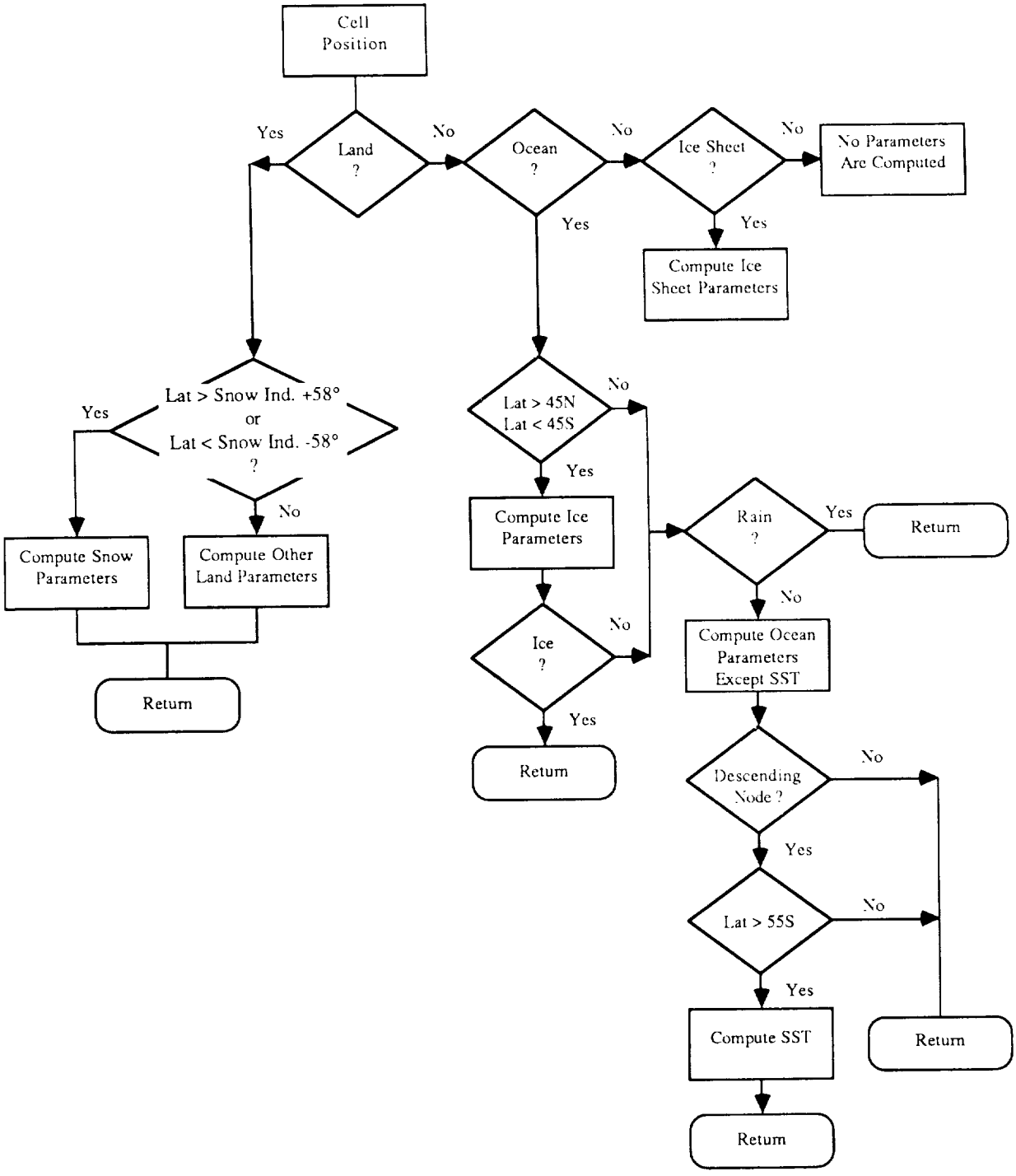

Figure 1.2. Flowchart of geophysical parameter calculations.

2. SEA-SURFACE TEMPERATURE

2.1 Introduction

During the 7-year data time span of the Nimbus–7 SMMR, five different versions of the geophysical algorithms have been used to derive sea-surface temperatures (SST's). Each subsequent version, except for Version V, has sought an improved compensation for one of two problems: (1) previously unmodeled physics of the ocean microwave emission; (2) previously unmodeled instrument losses and thermal cycling. Version V was introduced to account for the shutdown of the 21-GHz radiometer starting March 1985. Table 2.1 shows pertinent characteristics of the SST algorithm versions and which version was used for each year.

SST is calculated from the calibrated brightness temperatures with spatial resolution of 156 km measured in some of the 10 SMMR channels, housekeeping engineering data, and incidence angles. SST is retrieved only for those ocean areas that are at least 600 km away from land mass and north of 55° S latitude. In addition, if a severe rainstorm is in the field of view, no SST is calculated.

Sections 2.2 through 2.8 describe in detail the SST retrieval algorithm versions used for Years 1, 2, 4, 5, 3, 6, and 7 PARM production, in that order. In Section 2.9, the SMMR-derived SST's are compared with climatology and ship reports.

2.2 Year-1 Production—Version III

This version, given by Equations (1) to (4) below, is used for Year-1 PARM production:

$$(SST)_I = T_{II} + \Delta T; \tag{1}$$

$$T_{II} = T_I - 1.34 - 0.2\,[7.4 - T_I(1 - 0.025\,T_I)]; \tag{2}$$

$$\begin{aligned} T_I = {} & 1.7\,T_{6.6V} - 0.37\,T_{6.6H} + 56\,(285 - T_{10.7H}) / (285 - T_{10.7V}) \\ & - 245\,(285 - T_{18H}) / (285 - T_{18V}) - 326\,\ln(280 - T_{18V}) \\ & + 370\,\ln(280 - T_{18H}) - 11\,\ln(280 - T_{21H}) - 3\phi_{in} - 93.15 + 20; \end{aligned} \tag{3}$$

$$\begin{aligned} \Delta T = {} & 13.36456 - 0.09815\,(T_{10.7V} - T_{10.7H}) + 0.12460\,(T_{10.7V} - T_{10.7H}) \\ & - 0.20162\,(T_{18V} - T_{18H}) + 0.91644\,E(6) - 0.6688\,E(8) - 0.1982\,E(21) \\ & - 0.8040\,(\phi_{in} - 50) - 0.0927. \end{aligned} \tag{4}$$

where T_{fA} is the brightness temperature (in K) measured in the f GHz polarization channel, with f = 6.6, 10.7, 18, 21, or 37 and A = H or V, and ϕ_{in} is the incidence angle (in degrees), and E(k) with K - 6, 8, or 21 is the k-th housekeeping engineering value:

E(6) = 10.7-GHz Dicke Switch Temperature (Platinum),
E(8) = 21-GHz Dicke Switch Temperature (Platinum),
E(21) = 6.6- and 10.7-GHz Calibration Horn Temperature #1 (Platinum).

Table 2.1

Sea-Surface Temperature Algorithm History

Algorithm Version	Estimated Accuracy	Operational Production	Comments
I	Bias: 20 °C	N/A	Prelaunch, based on geophysical models alone. Used channels 6 V, 6 H, 10 V, 10 H, 18 V, 18 H, 21 H. Also used ϕ_{in}
II	rms: 2 °C	N/A	Bias removed, rain or bad data filtered; emissivity correction; modeled correlation between SST and water vapor.
III	rms: 1.5 °C	Yr 1	Three instrument temperatures included; eight coefficients tuned to fit climatology to account for latitudinal calibration drift and windspeed error.
IV	"	Yr 2	More prior data available to observe calibration drifts; 8 instrument temperatures and 1 crystal current used; 12 coefficients tuned to climatology as in Version III; 4 tuning periods.
IV.1	"	Yr 4	Eight instrument temperatures, 1 crystal current, 4 instrument temperature derivatives, and 2 brightness temperature ratios used; 21 coefficients; 6 tuning periods; improved calibration fit and windspeed performance.
IV.1*	"	Yrs 3, 5	Same as Version IV.1 except use of "corrected" 21 H; 5 tuning periods (Year 3) and 4 tuning periods (Year 5).
IV.2	"	Yr 6	Same as Version IV.1* except use of "corrected" 6 V and improved emissivity correction (see Version II); 5 tuning periods.
V	"	Yr 7	Similar in form to Version IV.2, but rederived from another prelaunch version that does not use 21-GHz radiometer data; 5 tuning periods.

The rationale leading to Equation (2) has been discussed in detail by Wilheit et al. (1984) and Gloersen et al. (1984). This method is an improvement over the retrieval techniques reported earlier (Chang and Wilheit, 1980; Wilheit, 1980) for use with the SMMR data. Briefly, the major source of the SST information is the 6.6 V channel, whereas the corrections for windspeed information come primarily from the 10.7 H and V channels, and the correction for atmospheric opacity is derived primarily from the 18.0 H and V channels. Equation (3), without the last constant term, is based entirely on atmospheric models which were available before launch. The constant

term italicized in Equation (3) corrects for a large bias which arises from instrument calibration errors. Equation (2) then corrects for small variations in the emissivities of the surface which are nonlinear in temperature, again based on prelaunch models. The correction term, ΔT, given by Equation (4), further corrects subtle errors in instrument calibration arising from changes in the instrument temperature.

2.3 Year-2 Production—Version IV

This version, given below by Equations (5) and (6), is used for Year-2 PARM production:

$$(SST)_2 = T_{II} + \Delta T, \tag{5}$$

where T_{II} is given by (2) and (3), and ΔT is given by

$$\begin{aligned}\Delta T \quad = \quad & -0.0968\,(T_{10.7V} + T_{10.7H}) - 0.1974\,(T_{18V} - T_{18H}) \\ & + C_1\,E(1) + C_2\,E(8) + C_3\,E(13) + C_4\,E(29) + C_5\,E(31) \\ & + C_6\,E(40) + C_7\,E(45) + C_8(48) + C_9\,E(53) + C_{10}\end{aligned} \tag{6}$$

Again, the E(k)'s appearing in Equation (6) are engineering values:

E(1): 6.6-GHz + XTL Current,
E(8): 21-GHz Dicke Switch Temperature (Platinum),
E(13): Antenna Feed Horn Temperature #1 Aperture (Platinum),
E(29): 6.6-GHz Chassis Bulkhead Temperature #1 (Platinum),
E(31): 37-GHz Calibration Horn Temperature #3 (Platinum),
E(40): Antenna Feed Horn Temperature #4 6.6-GHz-V Port (Platinum),
E(45): 6.6-GHz Calibration Horn Wave Guide Temperature #1 (Platinum),
E(48): Antenna Feed Horn Temperature #3 37-GHz Ortho (Platinum),
E(53): 10.7-GHz Calibration Horn Wave Guide Temperature #2 (Platinum).

The coefficients (C_k, k=1, 2, . . ., 10) appearing in the correction term of ΔT of Equation (6) are adjusted from one part of a year to another so that the difference between the SMMR-derived SST and climatological data should have the smallest variance for a chosen period. The process of periodic readjustment of the coefficients is called a "tuning procedure." The time period over which the coefficients are tuned is called a "tuning period." The idea of tuning was introduced to alleviate the apparent latitudinal dependence of retrieved SST's whose origin is ascribed to the instrument abnormality.

For the Year-2 production, the following choice of tuning periods has been made:

Period 1: October 1979–November 1979
Period 2: December 1979
Period 3: January 1980–March 1980
Period 4: April 1980–October 1980

Table 2.2 lists the tuning coefficients for each tuning period.

Table 2.2

Tuning Coefficients for Version IV SST Retrieval Algorithm—Used for Year-2 Production

	Days 274-223 1979	Days 336-365 1979	Days 1-90 1980	Days 91-273 1980
C_1	-7.819E - 02	-3.693E - 02	0.0	0.0
C_2	-9.783E - 01	-1.007E + 00	-7.224E - 01	9.567E - 01
C_3	-8.685E - 01	-7.818E - 01	-3.675E - 01	-9.965E - 01
C_4	8.553E - 01	1.107E + 00	6.896E - 01	-6.940E - 01
C_5	5.345E - 01	1.059E - 01	-3.620E - 01	8.268E - 01
C_6	1.053E - 01	1.585E + 00	9.889E - 01	-4.826E - 01
C_7	-1.626E + 00	-1.340E + 00	0.0	0.0
C_8	-3.679E - 01	-9.690E - 01	-9.243E - 01	-9.954E - 01
C_9	1.339E + 00	1.247E + 00	6.194E - 01	3.377E - 01
C_{10}	6.414E + 01	5.835E + 01	6.126E + 01	1.082E + 02

2.4 Year-4 Production—Version IV.1

This version, described below by Equations (7) through (11), is used for Year-4 production; with minor modifications, it is used also for Year-5 and Year-3 production:

$$(SST)_3 = T_{11} + \Delta T; \tag{7}$$

$$\Delta T = -0.0968\,(T_{10.7V} + T_{10.7H}) - 0.1974\,(T_{18V} - T_{18H}) - \Delta T_E - \Delta T_G - \Delta T_P; \tag{8}$$

$$\Delta T_E = C_1E(1) + C_2E(8) + C_5E(13) + C_6E(29) + C_7(31) + C_{10}E(40) + C_{11}E(45) + C_{12}E(48) + C_{13}E(53) + C_{19}; \tag{9}$$

$$\Delta T_G = C_3[(E_1(8) - E(8)] + C_4[E_2(8) - E(8)] + C_8[E_1(31) - E(31)] + C_9[E_2(31) - E(31)]; \tag{10}$$

$$\Delta T_P = 10C_{14}(T_{6.6H}/T_{6.6V}) + 100C_{15}(T_{6.6H}/T_{6.6V})^2 + 10C_{16}(T_{18H}/T_{18V}) + 100C_{17}(T_{18H}/T_{18V})^2 + 100C_{18}(T_{6.6H}/T_{6.6V})\,(T_{18H}/T_{18V}), \tag{11}$$

where T_{11} is given by Equations (2) and (3), E(k)'s are as explained in Section 2.3, and $E_1(k)$ and $E_2(k)$ are values of E(k) at times 4 and 8 minutes earlier, respectively.

The correction term ΔT_E of Equation (9) is the sum of the last 10 terms of Equation (6). The term ΔT_G of Equation (10) contains temporal increments of two engineering temperatures. The term ΔT_P of Equation (11) contains the ratios of brightness temperatures in two different polarizations. The reason for including additional terms, expressed by Equations (10) and (11), has been explained by Milman and Wilheit (1985).

The coefficients (C_k, k = 1, 2, . . ., 19) appearing in Equations (9) through (11) are tuned to climatology in the same way as the Year-2 production version. Their respective values are listed in Table 2.3. This time, the whole year—November 1981 though October 1982—is broken into six tuning periods:

Period 1: November 1981–December 1981
Period 2: January 1982
Period 3: February 1982–March 1982
Period 4: April 1982–July 1982
Period 5: August 1982
Period 6: September 1982–October 1982

Table 2.3

Tuning Coefficients for Year-4 SST Retrieval

	Nov. 81–Dec. 81 Night	Jan. 82 Night	Feb. 82–Mar. 82 Night	Apr. 82–July 82 Night	Aug. 82 Night	Sept. 82–Oct. 82 Night
C_1	2.98E - 01	-3.23E - 02	-5.49E - 02	-6.83E - 02	-1.03E - 01	-5.88E - 02
C_2	-8.85E - 01	-1.24E + 00	5.88E - 02	-6.41E - 03	4.64E - 02	-1.13E + 00
C_3	-1.04E + 00	-8.86E - 01	3.10E - 01	5.42E - 02	4.79E - 02	-6.08E - 01
C_4	-7.05E - 01	-7.97E - 01	-1.96E - 01	1.41E - 02	7.82E - 03	-9.54E - 01
C_5	1.14E + 00	1.50E + 00	3.87E - 02	2.36E - 01	7.62E - 03	2.74E - 01
C_6	4.20E - 01	1.17E + 00	7.32E - 01	4.47E - 01	3.22E - 01	1.44E + 00
C_7	5.31E - 01	1.49E + 00	-6.61E - 02	-7.57E - 01	-8.41E - 01	-6.08E - 01
C_8	5.14E - 01	6.26E - 01	3.23E - 02	-1.39E - 03	-7.48E - 03	1.38E - 01
C_9	6.17E - 01	1.98E + 00	6.92E - 03	-7.04E - 04	-3.55E - 03	-2.04E - 01
C_{10}	-7.62E - 01	-1.16E + 00	3.55E - 01	2.61E - 01	3.81E - 01	1.09E + 00
C_{11}	-6.96E - 01	-2.59E + 00	8.35E - 01	2.04E - 01	4.26E - 01	2.57E - 01
C_{12}	7.66E - 01	1.41E + 00	9.61E - 03	1.09E - 01	1.36E - 01	8.89E - 01
C_{13}	1.87E - 03	2.37E - 03	-1.28E + 00	-5.18E - 04	1.07E - 02	-1.51E + 00
C_{14}	-2.72E + 02	-3.02E + 02	-2.84E + 02	-2.69E + 02	-2.72E + 02	-2.10E + 02
C_{15}	3.44E + 01	3.67E + 01	3.70E + 01	3.49E + 01	3.50E + 01	2.77E + 01
C_{16}	7.82E + 01	7.97E + 01	7.77E + 01	8.28E + 01	8.24E + 01	7.57E + 01
C_{17}	1.94E + 00	1.66E + 00	2.98E + 00	2.17E + 00	2.07E + 00	1.17E + 00
C_{18}	-1.81E + 01	-1.76E + 01	-2.06E + 01	-1.94E + 01	-1.91E + 01	-1.58E + 01
C_{19}	3.00E + 02	3.91E + 02	3.16E + 02	3.31E + 02	3.27E + 02	1.16E + 02

2.5 Year-5 Production

The retrieval algorithm used for the Year-5 production is exactly the same in form as Version IV.1. The only difference is that corrected values of T_{21H} are substituted in computing the untuned SST's.

The algorithm is tuned with the following set of tuning periods:

Period 1: November 1982–February 1983

Period 2: March 1983–May 1983
Period 3: June 1983–August 1983
Period 4: September 1983–October 1983

The values of the tuning coefficients for each period are listed in Table 2.4.

Table 2.4

Tuning Coefficients for Year-5 SST Retrieval

	Nov. 82–Feb. 83	Mar. 83–May 83	June 83–Aug. 83	Sept. 83–Oct. 83
C_1	-3.53E - 03	2.65E - 01	-9.69E - 01	8.68E - 01
C_2	3.54E - 01	5.99E - 01	2.06E - 01	-3.50E - 01
C_3	-1.10E - 01	2.09E - 01	2.41E - 01	3.19E - 02
C_4	2.19E - 01	2.60E - 01	-4.14E - 01	1.19E - 03
C_5	5.88E - 01	2.34E - 01	6.79E - 01	2.94E - 01
C_6	8.74E - 02	6.14E - 02	1.09E + 00	1.05E - 01
C_7	-5.53E - 02	-6.24E - 01	-4.74E - 01	-1.24E + 00
C_8	1.14E - 01	-2.15E - 01	-2.45E - 01	-8.39E - 01
C_9	-6.85E - 02	-1.12E - 01	-1.08E - 01	-3.57E - 01
C_{10}	-5.83E - 01	1.96E - 01	7.52E - 01	1.72E - 01
C_{11}	5.81E - 01	-1.23E - 02	1.87E - 01	2.10E + 00
C_{12}	5.38E - 01	4.22E - 02	-1.04E - 01	3.21E - 01
C_{13}	-9.62E - 01	-2.16E - 03	-1.57E + 00	-1.30E + 00
C_{14}	-2.34E + 02	-3.29E + 02	-2.70E + 02	-2.21E + 02
C_{15}	3.24E + 01	4.47E + 01	3.50E + 01	3.48E + 01
C_{16}	7.51E + 01	9.64E + 01	8.23E + 01	9.36E + 01
C_{17}	3.15E + 00	4.55E + 00	2.13E + 00	3.75E + 00
C_{18}	-2.04E + 01	-2.74E + 01	-1.93E + 01	-2.54E + 01
C_{19}	2.16E + 02	4.10E + 02	3.19E + 02	1.52E + 02

2.6 Year-3 Production

Version IV.1 with corrected T_{21H} is used for Year-3 production. The procedures for correcting T_{21H} are described in Section 3.3. The latest T_{21H} correction method was used for Year-3 production. Three consecutive months are chosen for one single tuning period, starting September 1980:

Period 1: September 1980–November 1980
Period 2: December 1980–February 1981
Period 3: March 1981–May 1981
Period 4: June 1981–August 1981
Period 5: September 1981–November 1981

SST's are retrieved only for the 12-month period of November 1980 through October 1981. The values of the tuning coefficients for each tuning period are listed in Table 2.5.

Table 2.5

Tuning Coefficients for Year-3 SST Retrieval

	Sept. 80–Nov. 80	Dec. 80–Feb. 81	Mar. 81–May 81	June 81–Aug. 81	Sept. 81–Nov. 81
C_1	4.18E – 02	–1.36E – 01	4.00E – 01	–2.40E – 01	–4.34E – 02
C_2	–1.66E – 01	2.52E – 01	8.23E – 01	7.44E – 01	5.50E – 01
C_3	3.81E – 01	2.35E – 03	6.67E – 01	7.13E – 01	–2.01E – 01
C_4	–4.18E – 01	2.58E – 01	–3.05E – 01	–6.18E – 01	–6.14E – 01
C_5	2.84E – 01	9.84E – 01	–4.77E – 01	3.17E – 01	3.05E – 01
C_6	6.39E – 01	–3.53E – 01	–2.40E – 01	1.33E – 01	5.18E – 02
C_7	–4.97E – 02	1.33E + 00	5.08E – 01	1.01E + 00	–2.68E – 02
C_8	4.46E – 01	8.20E – 01	1.37E – 01	2.38E – 01	1.86E – 01
C_9	–9.20E – 02	3.85E – 01	2.42E – 01	–6.64E – 02	5.69E – 02
C_{10}	4.33E – 01	–2.19E + 00	6.90E – 01	3.61E – 01	4.81E – 02
C_{11}	2.93E – 01	–2.04E + 00	–6.15E – 01	–1.56E + 00	1.09E + 00
C_{12}	–1.29E – 01	9.74E – 01	3.71E – 02	1.39E – 01	–2.12E – 01
C_{13}	–1.09E + 00	1.21E + 00	–7.90E – 01	–1.10E + 00	–1.58E + 00
C_{14}	–2.70E + 02	–3.22E + 02	–2.91E + 02	–2.75E + 02	–2.52E + 02
C_{15}	3.34E + 01	3.69E + 01	3.57E + 01	3.13E + 01	3.19E + 01
C_{16}	7.47E + 01	7.22E + 01	7.77E + 01	6.40E + 01	7.14E + 01
C_{17}	1.53E + 00	1.11E + 00	1.57E + 00	4.82E – 01	1.66E + 00
C_{18}	–1.66E + 01	–1.52E + 01	–1.73E + 01	–1.23E + 01	–1.65E + 01
C_{19}	4.20E + 02	6.15E + 02	5.13E + 02	5.45E + 02	3.77E + 02

2.7 Year-6 Production

The overall structure of the Year-6 production version is essentially the same as that of Version IV.1. A slight modification of the untuned version [Equations (2) and (3)] was required to account for the long-term drift of $T_{6.6V}$, which is the major contribution term of SST retrievals.

Bias adjustment to T_I of Equation (3) is described as follows:

$$\hat{T}I = TI - B0 - B1*DAY - B2*(DAY)^2 \qquad (12)$$

where DAY is Julian day of year, and the values of B0, B1, and B2 are as follows:

	1983	1984
B0	–0.672	–1.89
B1	–0.00532	–0.023
B2	0.0	6.54×10^{-5}

The availability of ship reports for 1983 at the time of Year-6 production made it possible to redo the quadratic correction for surface emissivity; T_{II} of Equation (2) has been modified as follows (applicable only for the year 1983):

$$\tilde{T}_{II} = \tilde{T}_{I} + A0 + A1*\tilde{T}_{I} + A2*(\tilde{T}_{I})^2 \tag{13}$$

where the values of A0, A1, and A2 are as follows:

A0 = −.478
A1 = 0.168
A2 = −4.34E-03

The Year-6 production version, which will be termed Version IV.2, is obtained by adding ΔT of Equation (8) to T_{II}

Five tuning periods are chosen:

Period 1: September 1983–November 1983
Period 2: December 1983–February 1984
Period 3: March 1984–May 1984
Period 4: June 1984–August 1984
Period 5: September 1984–October 1984

Table 2.6 lists the tuning coefficients for each tuning period.

2.8 Year-7 Production

The 21-GHz radiometer was turned off on March 13, 1985, because of spacecraft power limitations. To account for this event, a new SST retrieval algorithm has been developed that does not use any brightness temperatures or engineering data measured in the 21-GHz radiometer.

Table 2.6

Tuning Coefficients for Year-6 SST Retrieval

	Sept. 83–Nov. 83	Dec. 83–Feb. 84	Mar. 84–May 84	June 84–Aug. 84	Sept. 84–Oct. 84
C_1	−1.68E − 01	5.54E − 01	7.18E − 01	4.51E − 01	−5.54E − 03
C_2	1.52E − 01	−8.12E − 01	1.25E + 00	1.53E − 01	1.59E − 01
C_3	1.10E − 02	−7.84E − 01	2.93E − 01	9.16E − 02	−6.22E − 02
C_4	6.19E − 02	−1.55E − 01	−8.97E − 01	6.64E − 02	4.78E − 02
C_5	2.43E − 01	7.21E − 01	1.62E − 01	8.16E − 02	4.44E − 01
C_6	−9.89E − 02	−1.78E + 00	3.60E − 01	7.34E − 01	6.69E − 01
C_7	−7.62E − 01	1.02E + 00	5.49E − 01	−4.26E − 01	6.07E − 03
C_8	−5.94E − 01	3.15E − 01	−8.94E − 03	−2.23E − 01	6.01E − 02
C_9	−9.57E − 02	5.79E − 01	3.65E − 01	2.62E − 03	7.89E − 02
C_{10}	−1.76E − 01	−4.70E − 02	−6.14E − 01	−2.46E − 02	−4.15E − 01
C_{11}	6.25E − 01	−2.40E + 00	−3.06E − 01	−4.05E − 01	−3.60E − 01
C_{12}	−1.08E − 01	1.23E + 00	2.00E − 01	4.24E − 03	−1.57E − 01
C_{13}	1.30E − 01	1.50E + 00	−1.43E + 00	2.66E − 01	−7.23E − 01
C_{14}	−2.09E + 02	−3.32E + 02	−3.82E + 02	−4.92E + 02	−3.83E + 02
C_{15}	2.95E + 01	4.12E + 01	4.67E + 01	5.34E + 01	4.72E + 01
C_{16}	7.72E + 01	9.24E + 01	1.10E + 02	9.28E + 01	1.01E + 02
C_{17}	1.86E + 00	2.04E + 00	1.74E + 00	1.17E + 00	2.44E + 00
C_{18}	−1.82E + 01	−2.10E + 01	−2.33E + 01	−1.90E + 01	−2.36E + 01
C_{19}	3.09E + 02	7.31E + 02	5.94E + 02	9.30E + 02	6.26E + 02

The new algorithm, which is termed Version V, is used for the Year-7 production. Its explicit expression is given by Equations (14) through (20):

$$T'_I = 1.62\,T_{6.6V} + 46(285 - T_{10.7H})/(285 - T_{10.7V}) - 0.58\,T_{10.7H} - 10\,\ln(280 - T_{18H}) - 0.37\phi_{in} - 2.15, \quad (14)$$

$$T'_{II} = -3.09 + 1.26\,T'_I - 0.00626\,(T'_I)^2, \quad (15)$$

$$(SST)_V = T'_{II} + \Delta T', \quad (16)$$

$$\Delta T' = 34.4 - 0.14\,(T_{10.7V} + T_{10.7H}) + 0.44\,(T_{10.7V} - T_{10.7H}) - 0.46\,(T_{18V} - T_{18H}) - C_{16} - \Delta T'_E - \Delta T'_G - \Delta T'_P, \quad (17)$$

$$\Delta T'_E = C_1\,E(1) + C_2\,E(13) + C_3\,E(29) + C_4\,E(31) + C_7\,E(40) + C_8\,E(45) + C_9\,E(48) + C_{10}\,E(53), \quad (18)$$

$$\Delta T'_G = C_5\,(E_1(31) - E(31)) + C_6\,(E_2(31) - E(31)), \quad (19)$$

$$\Delta T'_P = 10\,C_{11}\,(T_{6.6H}/T_{6.6V}) + 100\,C_{12}\,(T_{6.6H}/T_{6.6V})^2 + 10\,C_{13}\,(T_{18H}/T_{18V}) + 100\,C_{14}\,(T_{18H}/T_{18V})^2 + 100\,C_{15}\,(T_{6.6H}/T_{6.6V})\,(T_{18H}/T_{18V}), \quad (20)$$

where the symbols appearing in these equations are explained in Section 2.4.

Equation (14) is a prelaunch version developed by T. T. Wilheit. The main source of SST information is the brightness temperature measured in the 6.6 V channel; terms containing $T_{10.7V}$ and $T_{10.7H}$ correct for surface windspeed; and the logarithmic term involving T_{18H} corrects for atmospheric opacity.

Equation (13) shows the quadratic correction for changes in surface emissivity. Further corrections for surface windspeed and atmospheric effect are given in Equation (17) through linear terms containing the brightness temperatures measured by the 10.7- and 18-GHz radiometers.

Except for the E(8), the 21-GHz Dicke switch temperature and its time-lagged values, the expressions for $\Delta T'_E$ and $\Delta T'_G$ are exactly the same as the corresponding expressions of Version IV.1. The expression of $\Delta T'_P$ is exactly the same as that of Version IV.1.

The tuning coefficients (C_k, k = 1, . . ., 16) are determined in the same way as before, by minimizing the difference from climatology. Tuning periods are chosen on a seasonal basis, if possible:

Period 1: September 1984—November 1984
Period 2: December 1984—February 1985
Period 3: March 1985—May 1985
Period 4: June 1985—August 1985
Period 5: September 1985—October 1985

However, SST's are computed only for the period November 1984 through October 1985. Table 2.7 lists the values of the tuning coefficients for each tuning period. To account for the long-term drift in the 6.6 V channel, bias adjustment to the untuned Version II of Equation (12) was required prior to tuning:

$$T''_I = T'_I - B0 - B1*MON - B2*(MON)^2, \tag{21}$$

where

$$MON = 11(DAY - 15)/355 + 0.5, \tag{22}$$
$$DAY = \text{Day of year}$$

The values of B0, B1, and B2 are given below:

	1984	1985
B0	−10.93	−11.68
B1	−0.5779	−0.3790
B2	0.0466	0.0309

Table 2.7

Tuning Coefficients for Year-7 SST Retrieval

	Sept. 84–Nov. 84	Dec. 84–Feb. 85	Mar. 85–May 85	June 85–Aug. 85	Sept. 85–Oct. 85
C_1	−1.09E − 03	8.46E − 01	−2.23E − 01	−2.55E − 02	6.21E − 02
C_2	3.06E − 01	3.95E − 01	1.23E − 01	1.11E − 03	4.17E − 04
C_3	2.84E − 01	−1.05E − 01	−1.54E − 01	−2.12E − 01	2.02E − 01
C_4	1.03E − 01	4.41E − 01	9.63E − 02	2.57E − 02	5.07E − 01
C_5	−7.29E − 06	−2.20E − 03	2.59E − 04	−9.27E − 02	4.34E − 03
C_6	−5.87E − 03	9.27E − 02	2.40E − 03	−5.56E − 02	4.36E − 02
C_7	−6.33E − 01	−2.21E − 01	6.45E − 01	1.38E + 00	−1.38E + 00
C_8	2.39E − 01	−5.45E − 01	−7.20E − 01	−7.85E − 01	−8.23E − 01
C_9	8.22E − 01	2.38E − 01	9.53E − 02	−4.36E − 01	2.13E + 00
C_{10}	−7.58E − 01	−1.68E − 02	1.14E − 01	4.58E − 02	−2.73E − 01
C_{11}	−3.35E + 02	−2.83E + 02	−2.90E + 02	−4.70E + 02	−2.98E + 02
C_{12}	4.18E + 01	3.45E + 01	3.63E + 01	5.10E + 01	3.85E + 01
C_{13}	8.94E + 01	6.44E + 01	8.24E + 01	8.44E + 01	9.12E + 01
C_{14}	2.93E + 00	−2.72E + 00	2.38E + 00	1.99E + 00	2.80E + 00
C_{15}	−2.23E + 01	−1.75E + 01	−1.97E + 01	−1.90E + 01	−2.22E + 01
C_{16}	5.63E + 02	4.73E + 02	5.29E + 02	1.09E + 03	4.42E + 02

2.9 Validation

The SMMR-derived SST's are compared with the climatological and ship-reported values. Two types of SST differences are considered:

- SMMR-derived SST—Climatology
- SMMR-derived SST—Ship Reports

For each type of difference, monthly statistics are computed and tabulated. Climatological SST values are those of Robinson and Bauer, as described by Reynolds (1983).

Ship-reported values are extracted from "Surface Marine Observations" tapes (Tape Data Family 11) obtained from the National Weather Records Center, Asheville, North Carolina. SMMR SST's are computed only if:

- The correction term which has to be added to Version II SST is not greater than 5 °C in absolute value;
- The absolute value of the difference between SMMR SST and climatology is not greater than 7 °C;
- The ratio $(T_{6.6V} - T_{6.6H}/T_{6.6V} - T_{6.6H})$ is in the range 0.245 to 0.280.

The first two conditions are imposed to remove bad SMMR SST's; the third condition is to eliminate those SST's that are contaminated by high winds and unreliable brightness

temperatures measured in the 6.6-GHz radiometer. For point-by-point comparison of SMMR/Ship SST's, the following coincidence criteria are employed:

- Spatial separation must be less than 78 km, which is half of the Grid 1 CELL size;
- Temporal separation must be less than 12 hours;
- The difference, SMMR SST minus ship reports, must be less than or equal to 7.5 °C in absolute value.

The object of the third criterion listed above is to exclude bad SMMR and/or ship reports. Tables 2.8 through 2.14 list monthly averages and rms standard deviations of the difference, SMMR minus climatology, for Year 1 through Year 7, respectively. Figure 2.1 summarizes monthly standard deviations (or rms values) shown in these tables.

Tables 2.15 through 2.19 list monthly averages and rms standard deviations of the difference, SMMR minus ship reports, for Year 1 and Year 3 through Year 6, respectively. Figures 2.2 and 2.3 show scatter diagrams for ship SST versus SMMR SST for Year 3 and Year 5, respectively. The comparison between SMMR SST and ship reports may be summarized as follows:

- For point comparisons, the monthly standard deviations are about 2 °C;
- If the ship reports are smoothed by monthly averaging over 2° x 2° grids, the monthly standard deviations are about 1.5 °C.

Table 2.8

Monthly Statistics of SMMR Minus Climatology for Year 1 (Nighttime)

Month	Average	rms	N. Data*
78 Dec.	0.4	1.34	5889
79 Jan.	0.0	1.38	5350
Feb.	–0.3	1.27	5502
Mar.	–0.2	1.26	5548
Apr.	–0.3	1.35	5572
May	–0.3	1.28	5713
June	–0.3	1.29	5391
July	–0.3	1.34	5685
Aug.	–0.1	1.27	5209
Sept.	–0.3	1.28	5482
Oct.	–0.4	1.43	5488

* Cell 3; 50° S to 45° N

Table 2.9

Monthly Statistics of SMMR Minus Climatology for Year 2 (Nighttime)

Month	Average	rms	N. Data*
78 Nov.	0.0	1.30	15217
Dec.	0.0	1.29	15034
80 Jan.	–0.1	1.33	15749
Feb.	–0.1	1.37	13852
Mar.	0.0	1.31	16522
Apr.	0.1	1.25	15623
May	–0.1	1.25	15730
June	–0.2	1.23	16638
July	–0.1	1.26	16394
Aug.	0.1	1.23	14401
Sept.	0.1	1.28	15146
Oct.	0.0	1.27	16303

* Cells 2, 3, and 4; 50° S to 50° N

Table 2.10

Monthly Statistics of SMMR Minus Climatology for Year 3 (Nighttime)

Month	Average	rms	N. Data*
80 Nov.	0.06	1.27	14773
Dec.	0.03	1.34	18824
81 Jan.	0.04	1.32	20828
Feb.	–0.08	1.44	18813
Mar.	–0.01	1.38	20021
Apr.	0.08	1.27	19817
May	–0.07	1.32	21053
June	–0.01	1.34	19744
July	–0.03	1.31	19937
Aug.	0.06	1.32	16108
Sept.	–0.03	1.36	19102
Oct.	0.01	1.34	18839

* Cells 2, 3, and 4; 50° S to 50° N

Table 2.11

Monthly Statistics of SMMR Minus Climatology for Year 4 (Nighttime)

Month	Average	rms	N. Data*
81 Nov.	0.06	1.26	15917
Dec.	–0.06	1.32	16802
82 Jan.	–0.01	1.32	15392
Feb.	0.04	1.37	14772
Mar.	–0.04	1.40	16538
Apr.	0.13	1.44	16506
May	0.22	1.37	14958
June	0.13	1.35	16122
July	0.02	1.28	15131
Aug.	–0.06	1.34	12304
Sept.	0.13	1.42	16733
Oct.	–0.10	1.46	15028

* Cells 2, 3, and 4; 50° S to 50° N

Table 2.12

Monthly Statistics of SMMR Minus Climatology for Year 5 (Nighttime)

Month	Average	rms	N. Data*
82 Nov.	0.04	1.65	15444
Dec.	–0.08	1.71	14378
83 Jan.	–0.07	1.68	17131
Feb.	0.14	1.63	16313
Mar.	0.12	1.55	18616
Apr.	–0.06	1.62	20228
May	–0.04	1.60	21528
June	–0.05	1.61	19264
July	0.05	1.66	19309
Aug.	0.01	1.56	20849
Sept.	0.07	1.44	19383
Oct.	–0.12	1.44	17939

* Cells 2, 3, and 4; 50° S to 50° N

Table 2.13

Monthly Statistics of SMMR Minus Climatology for Year 6 (Nighttime)

Month	Average	rms	N. Data*
83 Nov.	0.06	1.46	12043
Dec.	1.24	1.41	12486
84 Jan.	–1.00	1.52	16270
Feb.	–0.00	1.54	16306
Mar.	0.05	1.54	16806
Apr.	0.22	1.53	12998
May	–0.39	1.48	15561
June	–0.13	1.44	15310
July	0.03	1.43	15043
Aug.	–0.11	1.40	8908
Sept.	0.04	1.35	15567
Oct.	–0.03	1.36	15549

* Cells 2, 3, and 4; 50° S to 50° N

Table 2.14

Monthly Statistics of SMMR Minus Climatology for Year 7 (Nighttime)

Month	Average	rms	N. Data*
84 Nov.	–0.23	1.45	14992
Dec.	–0.15	1.47	16051
85 Jan.	–0.02	1.51	15992
Feb.	0.09	1.55	14935
Mar.	–0.22	1.53	17371
Apr.	0.17	1.44	14856
May	0.03	1.40	15604
June	–0.12	1.35	14518
July	–0.02	1.37	16133
Aug.	0.05	1.33	14463
Sept.	0.11	1.41	15512
Oct.	–0.15	1.41	16723

* Cells 2, 3, and 4; 50° S to 50° N

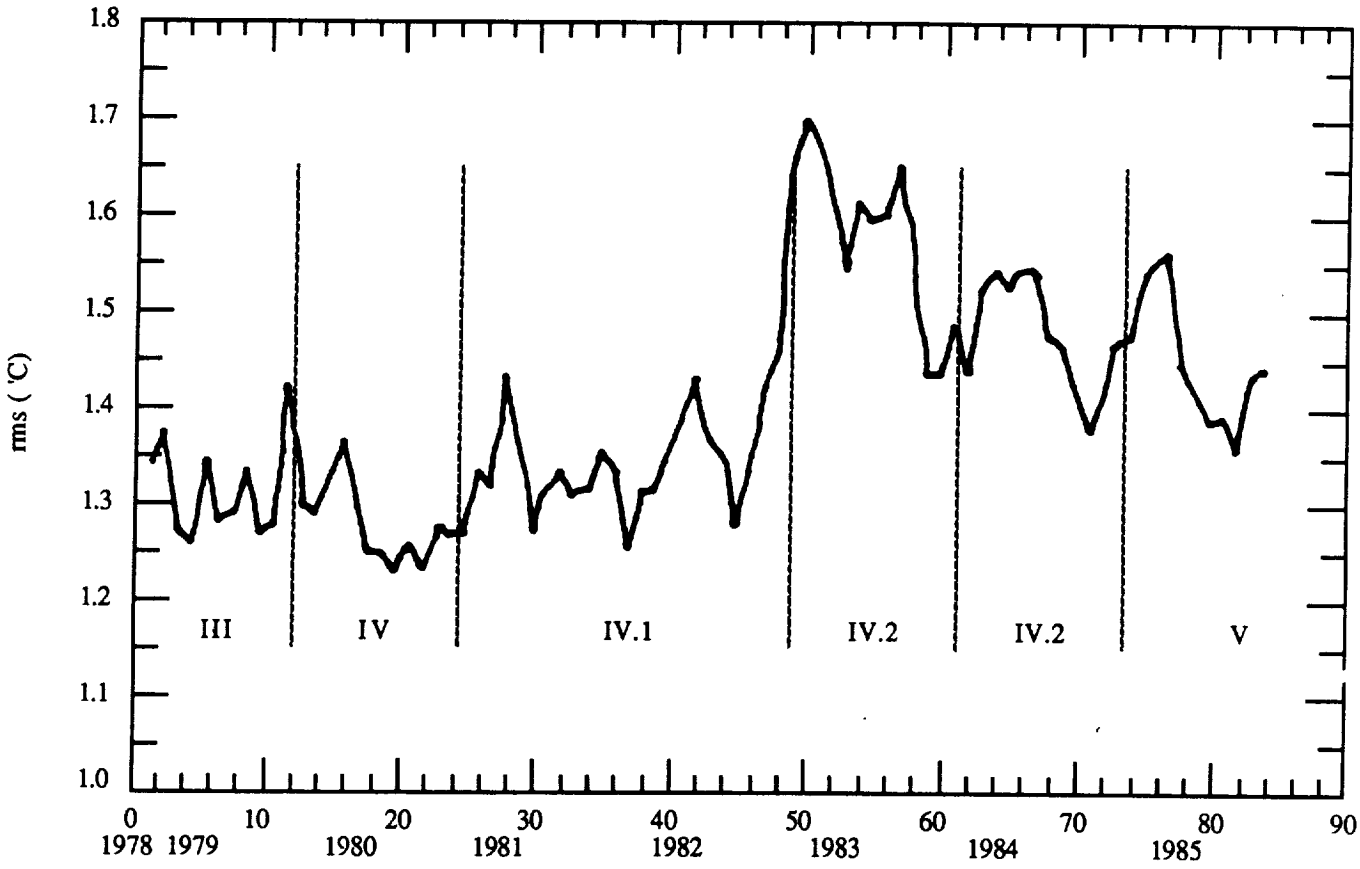

Figure 2.1. Monthly rms values of SMMR SST minus climatology vs. time.

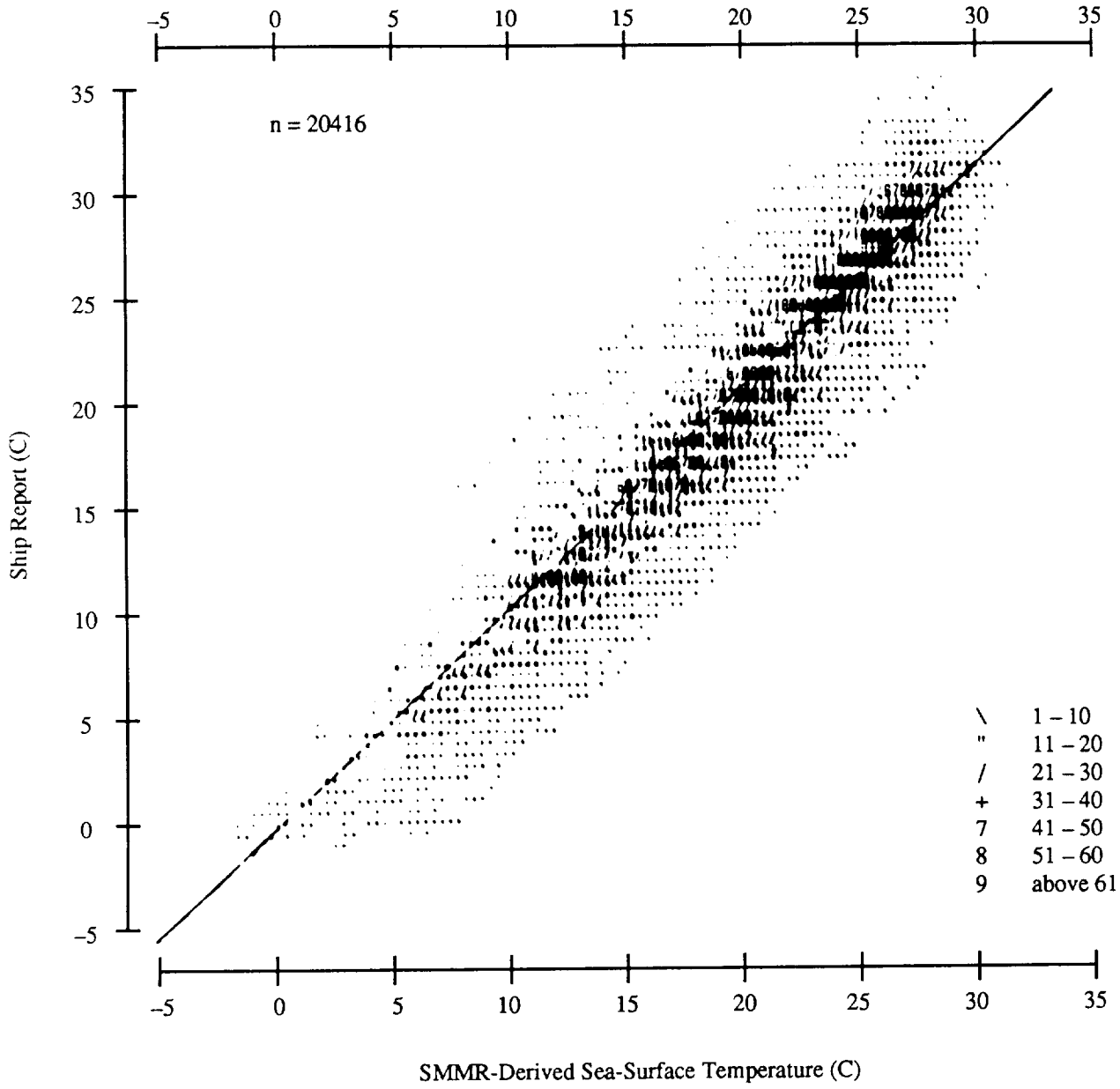

Figure 2.2. Scatter diagram for ship SST vs. SMMR-derived SST for year 3.

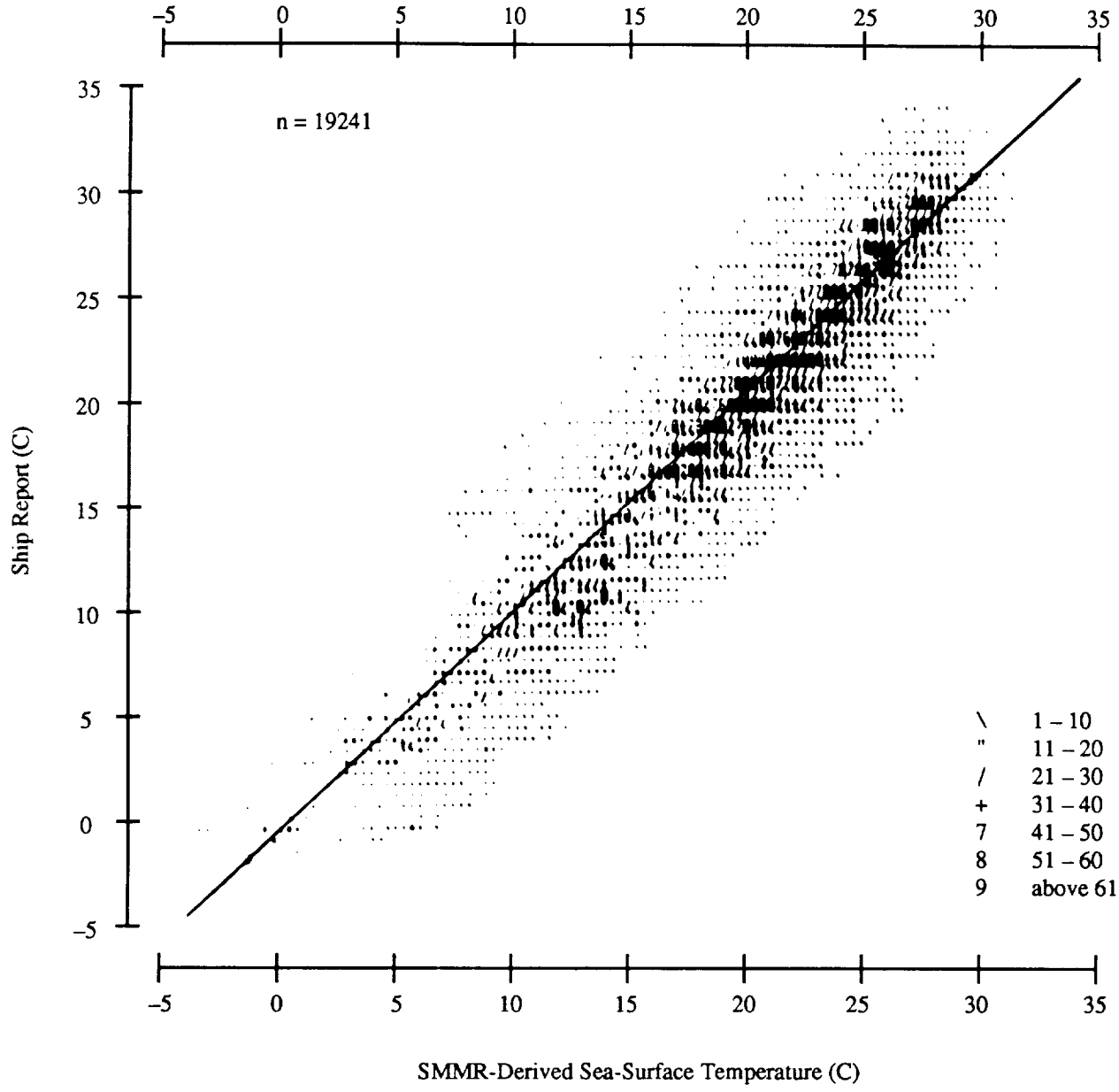

Figure 2.3. Scatter diagram for ship SST vs. SMMR-derived SST for year 5.

Table 2.15

Monthly Statistics of SMMR Minus Ship Reports for Year 1 (Nighttime)

Month	Average	rms	N. Data*
79 Jan.	–0.1	1.51	11281
Feb.	–0.2	1.56	10691
Mar.	–0.2	1.43	10680
Apr.	–0.3	1.58	10671
May	–0.1	1.42	11564
June	–0.2	1.37	11568
July	–0.4	1.41	10654
Aug.	–0.4	1.30	9897
Sept.	–0.3	1.55	10016
Oct.	–0.4	1.52	9487
Nov.	–0.3	1.51	7879
Dec.	–0.4	1.72	5452

*Number of data points in this column refers to the sum of the number of SMMR data points that fall into 2° x 2° grid points where a valid average of ship data exists.

Table 2.16

Monthly Statistics of SMMR Minus Ship Reports for Year 3 (Nighttime)

Month	Average	rms	N. Data*
80 Nov.	0.78	2.31	1453
Dec.	0.85	2.19	1625
81 Jan.	0.33	1.97	1698
Feb.	–0.24	2.11	1752
Mar.	0.55	2.23	1924
Apr.	0.26	2.01	1962
May	–0.17	1.88	1793
June	0.13	1.97	1816
July	0.15	1.92	1760
Aug.	0.33	1.94	1358
Sept.	–0.17	1.96	1732
Oct.	0.32	2.00	1543
Total	0.25	2.07	20416

*Number of data points in this column refers to the sum of the coincidence points defined on page 15.

Table 2.17

Monthly Statistics of SMMR Minus Ship Reports for Year 4 (Nighttime)

Month	Average	rms	N. Data*
81 Nov.	0.21	1.47	12198
Dec.	0.02	1.57	12812
82 Jan.	0.15	1.50	10771
Feb.	0.30	1.51	10865
Mar.	0.23	1.74	11912
Apr.	0.43	1.57	12387
May	0.42	1.62	11308
June	0.21	1.53	11572
July	0.04	1.55	10506
Aug.	0.00	1.52	8628
Sept.	0.41	1.66	11957
Oct.	–0.01	1.61	11070

*Number of data points in this column refers to the sum of the number of SMMR data points that fall into 2° x 2° grid points where a valid average of ship data exists.

Table 2.18

Monthly Statistics of SMMR Minus Ship Reports for Year 5 (Nighttime)

Month	Average	rms	N. Data*
82 Nov.	0.54	2.29	1380
Dec.	0.77	2.20	1322
83 Jan.	0.32	2.12	2733
Feb.	0.07	2.20	1488
Mar.	0.84	2.23	815
Apr.	0.66	2.34	1706
May	0.22	2.11	1638
June	0.33	2.34	1607
July	0.53	2.05	1641
Aug.	0.37	2.11	1593
Sept.	0.11	2.00	1596
Oct.	0.38	2.14	1722
Total	0.40	2.18	19241

*Number of data points in this column refers to the sum of the coincidence points defined on page 15.

Table 2.19

Monthly Statistics of SMMR Minus Ship Reports for Year 6 (Nighttime)

Month	Average	rms	N. Data*
83 Nov.	0.61	2.23	1348
Dec.	1.95	2.15	1346
84 Jan.	–0.49	2.19	1847
Feb.	0.04	2.17	1725
Mar.	0.24	2.07	2077
Apr.	0.63	2.14	1280
May	–0.14	2.03	1420
June	0.25	2.13	1663
July	0.30	2.10	1611
Aug.	0.34	2.12	709
Sept.	0.10	2.08	1605
Oct.	0.11	2.21	1664
Total	0.28	2.21	18295

*Number of data points in this column refers to the sum of the coincidence points defined on page 15.

3. WATER VAPOR

3.1 Introduction

This section describes the retrieval of water vapor from SMMR radiances. Atmospheric water vapor content is defined as the depth of water which would accumulate if all the water vapor in an atmospheric column with a 1-cm^2 cross-section were precipitated out. It is expressed in cm or equivalently gm/cm^2. SMMR water vapor retrievals typically range from 0 to 7 cm. Since microwave remote sensing can be done in the presence of nonprecipitating clouds, global water vapor coverage can be obtained on a timescale of about a week. This is valuable in tropical ocean areas where radiosonde data is limited and infrared retrieval techniques suffer from problems arising from persistent cloudiness near the intertropical convergence zone (ITCZ). Chang et al. (1984) provide a good review of the retrieval of water vapor with the SMMR as well as a summary of the results from the 1st year of SMMR data. Chang and Wilheit (1979) have described the theory behind the microwave remote sensing of atmospheric water vapor.

There are two basic water vapor retrieval algorithms. For the first 6 years of SMMR production, only the tuned Staelin-Rosenkranz algorithm, described in Section 3.2, was used. The first 2 years of retrievals showed a steady increase of about 0.6 cm in water vapor. This increase was caused by an increase of about 10 K in the 21-GHz H brightness temperature. To remedy this situation, several versions of 21-GHz correction were used for the next 4 years of production. These corrections are considered in Section 3.3. The water vapor retrieval values appearing on the PARM tapes may be adjusted to obtain a retrieved water vapor that is equivalent to that of the best currently available correction of the 21-GHz radiances (Version IV). Section 3.4 shows how these adjustments can be made. However, after May 1983, even Version IV is not satisfactory because of a change in the long-term drift behavior of the 21-GHz channels. An algorithm without the 21-GHz channels was used for the 7th year because the 21-GHz radiometer was turned off in March 1985. This algorithm is discussed in Section 3.5. A short description of the production water vapor algorithm versions appears in Table 3.1. Section 3.6 presents the results of comparisons between SMMR retrievals and coincident radiosonde reports.

3.2 Staelin-Rosenkranz Algorithm

This water vapor algorithm is based on work done by Rosenkranz and Staelin (1976, 1978, 1982). It has been derived from theoretical modeling and experience with data from the multispectral microwave radiometers on the Nimbus–5 and Nimbus–6 satellites. It is designed to minimize the effect of cloud liquid water on retrieved water vapor. The algorithm uses the 18, 21, and 37 GHz SMMR channels in both polarizations as follows:

$$WV' = 2.0 + 0.1V + 0.0011V^2 \text{ (cm)}, \tag{23}$$

Table 3.1

Water Vapor Retrieval Algorithm Production Versions

	Version	Years Used
I	No 21 GHz correction	Years 1 and 2
II	Different long-term 21 H corrections for day and night	Year 4
III	New long-term 21 H correction + time-of-day correction	Year 5
IV	Version III with cross-track gradient correction to both 21 H and 21 V	Years 3 and 6
V	New algorithm using 18- and 37-GHz channels after 21-GHz turn-off	Year 7

where

$$\begin{aligned} V = {} & -0.405\,(T18H - 105.5) - 0.165(T18V - 173.3) \\ & +0.489\,(T_{21H} - 139.8) + 0.382\,(T_{21V} - 195.7) \\ & -0.225\,(T_{37H} - 141.0) + 0.250\,(T_{37V} - 204.0). \end{aligned} \tag{24}$$

This algorithm was tuned by comparing selected radiosonde observations from ships with coincident SMMR data for the period February 15–27, 1979 (Chang et al., 1984). This comparison yielded the following offset and sensitivity adjustments to the theoretical expression in Equation (23):

$$WV = 1.085\,WV' - 0.288\ (cm) \tag{25}$$

A scatter plot of this tuning comparison appears in Figure 3.1. A further comparison, consisting of 30 coincident points from March 1–17, 1979, is shown in Figure 3.2. In most of these cases there was more than one coincident SMMR value for a given radiosonde report. This yielded an rms difference between SMMR retrievals and radiosonde reports of 0.21 cm, which is comparable to the values (about 0.25 cm) reported by Wilheit and Chang (1980) and Prabhakara et al. (1982).

Global distributions of monthly averaged water vapor over ocean areas have been derived using Equations (23) and (24). The general characteristics of these distributions are in qualitative agreement with other independent studies (Chang et al., 1984). These studies have revealed features associated with ocean currents and the general circulation of the atmosphere. Relatively dry zones with low water vapor have been found to be associated with cold currents, such as the California and Peru currents, while humid zones were found over warm currents, such as the Kuroshio and the Gulf Stream. The SMMR results also have revealed a meridional dependence in the water

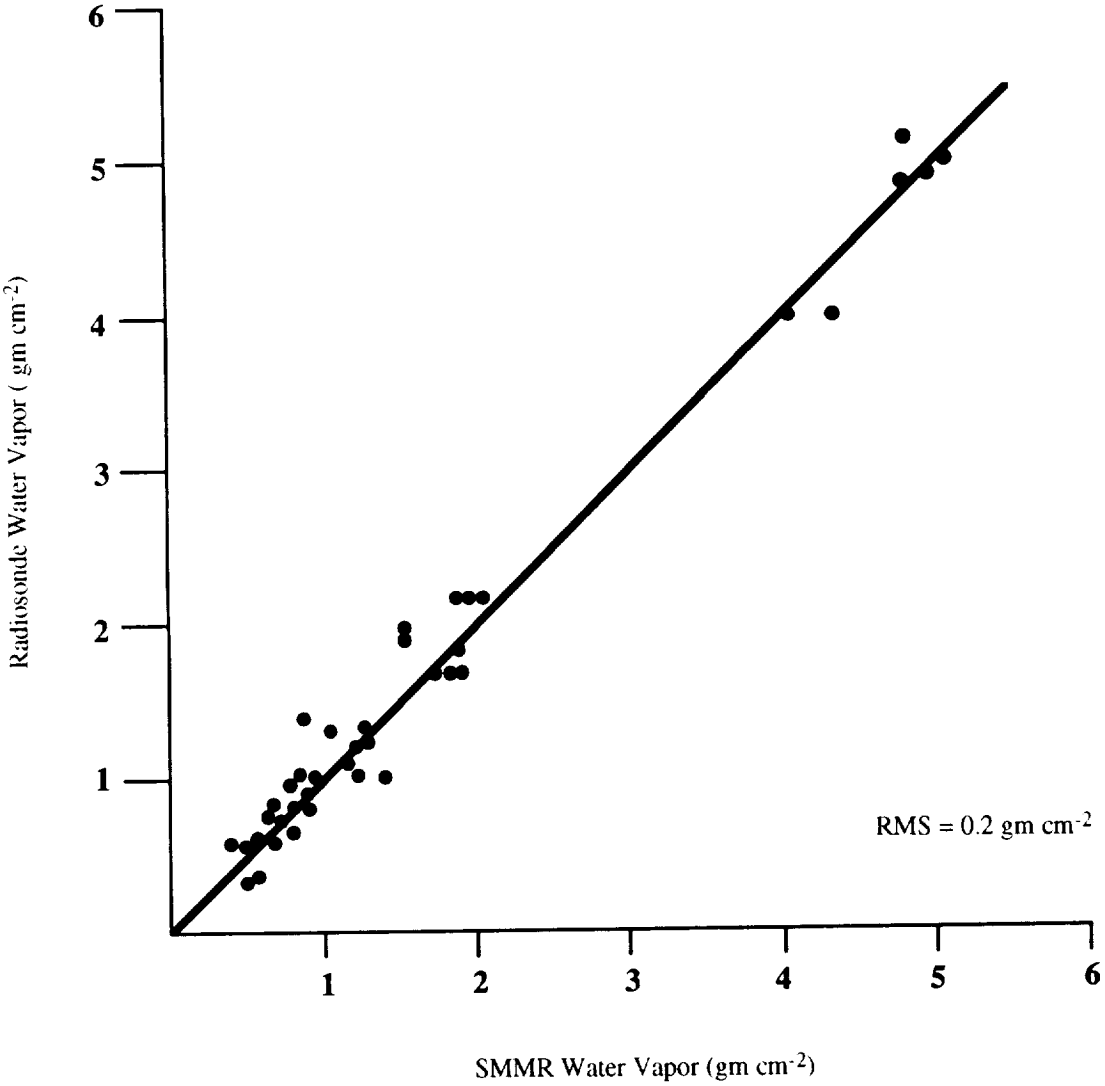

Figure 3.1. Comparison of SMMR water vapor with radiosonde water vapor for Feb. 15–27, 1979.

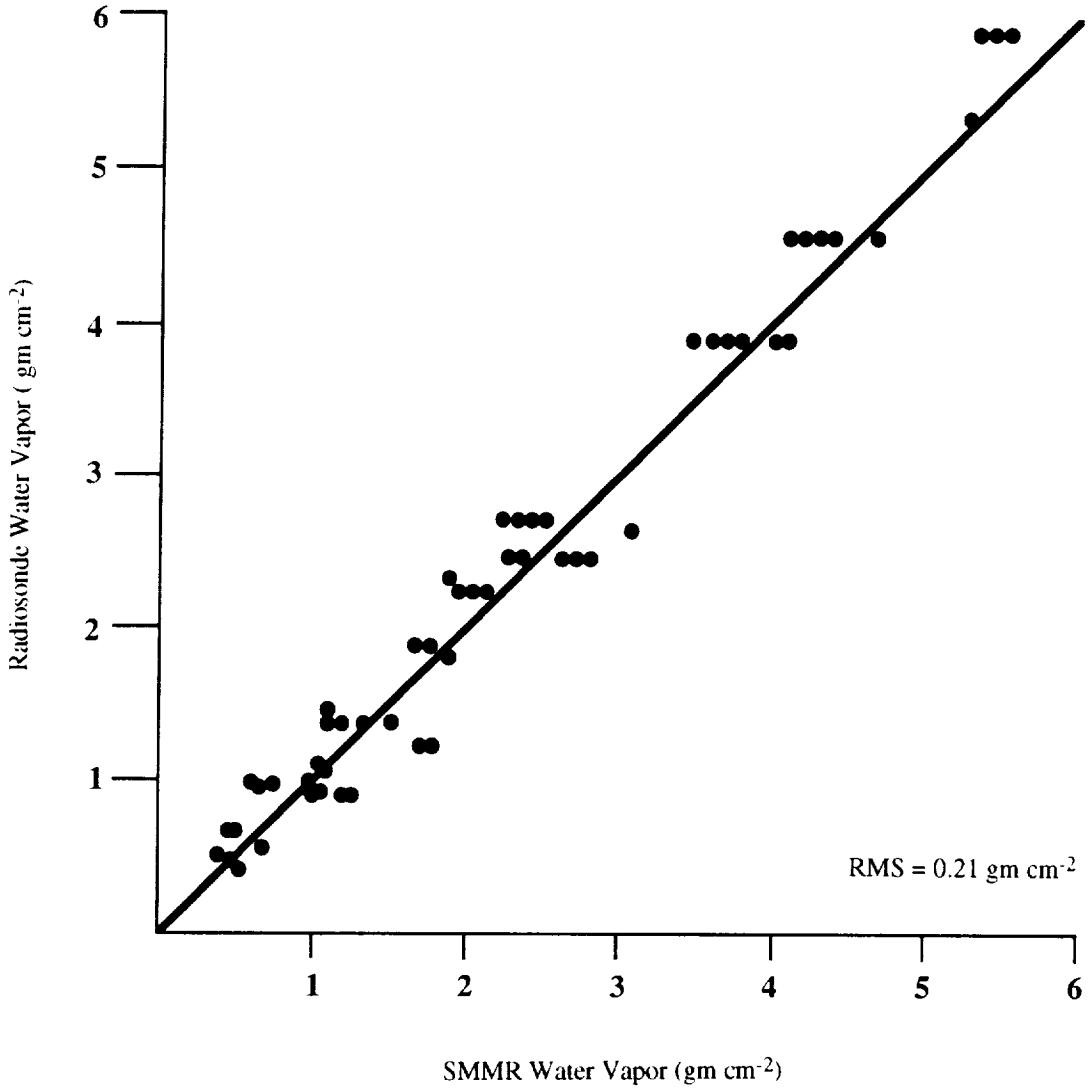

Figure 3.2. Comparison of SMMR water vapor with radiosonde water vapor for March 1–17, 1979.

vapor distribution over the equatorial Pacific. There is a humid zone in the western Pacific and a dry zone in the eastern Pacific. The distribution of water vapor in the equatorial Pacific region is in good agreement with earlier studies using satellite data as well as with conventional measurements.

3.3 Correction of 21-GHz Channels

3.3.1 Correction for Year-4 Production

The first 21 H correction (Version II) was used only for Year-4 production. Based on brightness temperatures from the first 4 years, separate, long-term drift corrections were made for the day and night 21 H brightness temperatures (Chang, 1983). The brightness temperatures are adjusted as follows:

$$T'_{21H} = T_{21H} - 0.15t - \Delta T_1 - \Delta T_2 \text{ (day)}; \tag{26}$$

$$T'_{21H} = T_{21H} - 0.11t \text{ (night)}, \tag{27}$$

where T_{21H} is the measured 21 H brightness temperature and t is the number of weeks from January 1, 1979. The correction term ΔT_1 was used to account for the large annual oscillations in the difference between day and night brightness temperatures. The difference was approximated by the Fourier series

$$\Delta T_1 = \sum_{n=0}^{4} (a_n \cos(n\pi t/L) + b_n \sin(n\pi t/L)), \tag{28}$$

where L = 26, and the values of the coefficients a_n and b_n are

n	a_n	b_n
0	0.103	0.0
1	2.459	0.302
2	–0.564	–0.054
3	0.319	–0.151
4	0.224	0.332

The residual day/night difference was then fitted by the polynomial

$$\Delta T_2 = -1.3994 \times 10^{-5} (t-53)^3 + 0.249 \times 10^{-2} (t-53)2 - 0.113 (t-53) + 0.9495. \tag{29}$$

3.3.2 Correction for Year-5 Production

For Year-5 production, a new 21 H correction was developed (Kim et al., 1984). The slope of the 21 H drift was found by a statistical analysis of 6-day averages of T_{21H} over the 4-year period from January 1979 to December 1982. To minimize the effect of polarization mixing, only the center cell of each scan was used. Analysis showed that the 21 H slope had both a long-term and a short-term component. This slope was a function of the time from instrument turn-on. Retrieved liquid water, which depends strongly on the 21-GHz channels, was unusually high over areas covered by the first or second orbit after the SMMR instrument was turned on. This observation led to the idea of using an exponentially decreasing term to compensate for the short-term warmup behavior. As a function of the number of minutes (t_m) from instrument turn-on, the slope (deg. K/6-day period) of the long-term orbit was fitted with the expression

$$S(t_m) = a_1 + a_2[1 - \exp(-a_3 t_m)], \tag{30}$$

where

$$a_1 = 0.0366,\ a_2 = 0.0954, \text{ and } a_3 = 0.00247.$$

The corrected 21-GHz H brightness temperature is then

$$T'_{21H} = T_{21H} - \Delta T_H, \tag{31}$$

where

$$\Delta T_H = S(t_m)\, t_w \tag{32}$$

T_{21H} is the uncorrected 21 H brightness temperature, and t_w is the number of 6-day periods from January 1, 1979.

3.3.3 Correction for Year-3 and Year-6 Production

Years 3 and 6 used the best available correction for the 21-GHz channels. This version includes a cross-track gradient correction to both the 21 H and 21 V channels. Such a correction is necessary because there is polarization mixing between the horizontal and vertical channels. This mixing is described by a rotation matrix which tells how the measured antenna counts T_x and T_y are transformed from the actual radiances T_{21H} and T_{21V} of the observed scene:

$$T_x = T_{21H} \cos^2(\phi + \delta\phi_x) + T_{21V} \sin^2(\phi + \delta\phi_x), \tag{33}$$

$$T_y = T_{21H} \sin^2(\phi + \delta\phi_y) + T_{21V} \cos^2(\phi + \delta\phi_y). \tag{34}$$

At each scan angle ϕ, the vertical and horizontal polarization axes have been rotated by an angle (equal to the scan angle) with respect to the fixed antenna axes. (The scan angle ranges from −25° to 25° from left to right across the orbital track.) However, this transformation is not

symmetrical about the zero scan angle. Offset angles $\delta\phi_x$ and $\delta\phi_y$ are needed to describe the asymmetry. These angles were determined by averaging the antenna temperatures at each scan angle over many scans. This averaging procedure was performed to remove scan-angle dependence arising from geophysical variation. The remaining scan-angle dependence was then fitted to determine the offset angles. For the 21-GHz channels, these angles are $\delta = -2.8°$ and $\delta\phi_y = 10°$. Gloersen (1980, 1983) and Han (1980) have described the polarization mixing and the derivation of the offset angles for all channels. In addition, Han (1980) provides a model that shows how the additional polarization rotation by the offset angles can be caused by leakages in the ferrite polarization selector switches.

This correction was developed by assuming that the radiance counts measured in the 21 H channel have a systematic bias ΔT_x, which is independent of scan angle, but that $\Delta T_y=0$. Then, inversion of the polarization mixing equations in Equations (33) and (34) yields the bias terms

$$T_{21H} = \Delta T_x [\cos^2 (\phi + \delta\phi_y/D(\phi)], \tag{35}$$

$$T_{21V} = -\Delta T_x [\sin^2 (\phi + \delta\phi_y)/D(\phi)], \tag{36}$$

where $D(\phi)$ is the determinant of the matrix in Equations (33) and (34):

$$D(\phi) = 1 - \sin^2(\phi + \delta\phi_x) - \sin^2(\phi + \delta\phi_y). \tag{37}$$

Since the 21 H correction given in Equation (34) above was found for center cells, it can be expressed as

$$\Delta T_H = \Delta T_{21H}(\phi=0).$$

Therefore, Equations (35) and (36) yield the systematic bias

$$\Delta T_x = \Delta T_H [D(0)/\cos^2(\delta\phi_y)]. \tag{38}$$

The corrected 21-GHz brightness temperatures are then

$$T'_{21H} = T_{21H} - \Delta T_{21H}, \tag{39}$$

$$T'_{21V} = T_{21V} - \Delta T_{21V}, \tag{40}$$

where T_{21H} and T_{21V} are the uncorrected brightness temperatures that appear on the CELL tapes.

After May 1983, this correction is no longer satisfactory because the long-term drift behavior of the 21-GHz channels changed.

3.4 Adjustments of Water Vapor Retrievals

It is possible to adjust the water vapor retrieval values (Years 1–2 and 4–5) appearing on the PARM tapes up to May 1983 in order to account for the drift behavior of the 21-GHz H channel. These adjustments will yield a retrieved water vapor equivalent to that using the best available correction of the 21-GHz radiances (Version IV).

An adjusted value V_c for the quantity in Equation (24) is found in terms of the 21-GHz correction. We first consider Version I, which had no 21-GHz correction. Equations (23) and (25) are first solved for the V that was used to calculate the water vapor WV(PARM) (in cm) given on the PARM tape.

$$V = 45.45 \{-1 + [.2125 + .4055\ WV(PARM)]^{1/2} - 1\} \tag{41}$$

The corrected value V_c differs from V by an amount dependent upon the corrections (Version IV) to the 21-GHz channels given by Equations (32), (35), (36), and (38):

$$V_c = V - \Delta V \tag{42}$$

where

$$\Delta V = 0.489\ \Delta T_{21H} + 0.382\ \Delta T_{21V} \tag{43}$$

The expressions (35) and (36) are evaluated at the scan angles corresponding to each cell in a band of gridded PARM data. For Grid 3, the 13 scan angles are: 0.0, ±3.736, ±7.488, ±11.272, ±15.105, ±19.008, and ±23.003 deg. Then the adjusted water vapor is found using Equations (23) and (25) by replacing V by V_c.

This correction requires the number of minutes (t_m) that the instrument has been on to compute ΔT_{21} in expression (32). This can be found from the UTC (expressed in integer seconds of the day) corresponding to the center of each band of PARM values:

$$t_m = [UTC(current) - UTC(turn\text{-}on)]/60. \tag{44}$$

The UTC(turn-on) is approximately the first UTC recorded on the PARM tape for each day of operation. [The fact that there is a gap of about 24 hours between SMMR operation days can be used to determine this UTC(turn-on).]

For Versions II and III, whatever 21-GHz correction was used must be removed and replaced with the correction (Version IV) described above. In Version II, the 21-GHz H correction described in Section 3.3.1 was made. Removing this and making the above adjustment, we replace expression (42) by:

$$V_c = V + 0.489(0.15\ t + \Delta T_1 + \Delta T_2) - \Delta V \quad (day) \tag{45}$$

$$V_c = V + (0.489)0.11\ t - \Delta V \quad (night). \tag{46}$$

In Version III, the center-cell correction was applied to the 21 H radiances for all scan angles. This must be replaced by the scan-angle dependent correction to both the 21 H and 21 V radiances. The expression in (43) becomes

$$V_c = V + 0.489\,\Delta T_{21H}(\phi=0) - \Delta V, \tag{47}$$

where

$\Delta T_{21H}(\phi=0) = \Delta T_H$ is given by (32).

3.5 18- and 37-GHz Algorithm

A new algorithm using only the 18- and 37-GHz channels was developed because the 21-GHz radiometer was turned off in March 1985. The accuracy of this algorithm was expected to be significantly less than for the Staelin-Rosenkranz algorithm. This is because the-21 GHz channels are two to three times as sensitive to water vapor as the 18- and 37-GHz channels. Additionally, the 37-GHz channels are very sensitive to cloud liquid water. This algorithm was used only for Year-7 production. It is based on the brightness temperature model of Wilheit and Chang (Wilheit, 1979; Wilheit and Chang, 1980), which predicts the radiances at each frequency as a function of the geophysical parameters: sea-surface temperature, sea-surface windspeed, and the atmospheric contents of water vapor and liquid water. A multilinear regression was performed on a statistical sampling of the model to express water vapor content in terms of functions of the radiances:

$$\begin{aligned} V = {} & 23.92\,\ln(285 - T_{37H}) - 16.52\,\ln(285 - T_{37V}) \\ & - 26.6\,\ln(285 - T_{18H}) + 0.1007\,T_{18H} + 98.23. \end{aligned} \tag{48}$$

This expression was tuned using a set of coincident SMMR and radiosonde measurements from the period 1979–1980:

$$WV = -10.14 + 0.8815\,V - 0.008385V^2\ (\text{cm}). \tag{49}$$

As yet, this algorithm has not been validated for Year-7 SMMR data. However, comparisons of retrievals with coincident radiosonde data for the first 6 years yield yearly rms differences ranging from 0.54 cm to 0.65 cm.

3.6 Comparison With Radiosonde Measurements

Water vapor retrievals for the first 6 years have been compared with coincident radiosonde observations. The radiosonde reports were taken from National Meteorological Center (NMC) Upper Air Observation tapes obtained from the National Climatic Data Center in Asheville, North Carolina. These reports are mostly north of 20° south in the Pacific and north of the equator in the Atlantic. They include data from island stations, research ships, and fixed weather ships.

The criteria for the coincidence of an SMMR observation and a radiosonde report are that their temporal separation be within 3 hours and that the spatial separation between the center of

the SMMR field-of-view and the radiosonde be within 0.5° in latitude and longitude. An SMMR retrieval was not made if there was rain in the SMMR field-of-view. Upper limits of 184 K for the 37-GHz horizontal radiance and 148 K for the 18-GHz horizontal radiance were used to filter out the rain cases.

Comparisons with SMMR retrievals for 6 years of production are shown in Tables 3.2 through 3.7. The comparisons were made with the production Versions I through IV of the algorithm. These tables give the average difference (bias) and the standard deviation of the differences between SMMR retrievals and radiosonde measurements. Coincidences with SMMR/radiosonde water vapor differences greater than 1.5 cm were not kept. Such large differences are usually associated with bad radiosonde reports (e.g., a sign error in the location) or bad SMMR data. This upper limit is about three times the standard deviation of the differences. The numbers of points that were eliminated by this limit are also shown in these tables. It can be seen that when the behavior of the 21-GHz channels changed after May 1983, the numbers of eliminated points increased. The bias from these tables for each year of water vapor production has been plotted for Years 1 through 6 in Figure 3.3. Roman numerals refer to the algorithm version described in Table 3.1. Two notable features of this plot are the increase of retrieved water vapor in the first 2 years before any corrections were applied and the abnormal behavior after about May 1983, when the behavior of the 21-GHz channels changed. In Figure 3.4, the bias is plotted for day and night separately. Aside from Year 6, there is a significant difference between day and night biases in both Years 4 and 5. In Year 4, the correction to the 21-GHz horizontal radiance did not properly account for the drift in that channel. Figure 3.5 shows the variation of the standard deviation of the error of the retrievals. This error is reasonably constant during the first 3 years and then becomes progressively worse. It is clear that even with Version IV of this algorithm water vapor retrievals after May 1983 are not reliable.

In Figures 3.3 and 3.5, the bias and standard deviation is also shown using Version IV for each year. It is clearly better to use this version, which has the best available corrections of the 21-GHz channels. Section 3.4 describes the adjustments that can be made to the PARM production retrievals to obtain this version. However, in order to improve water vapor retrievals after May 1983 using the Staelin-Rosenkranz algorithm, the behavior of the 21-GHz channels has to be further studied.

The comparison between radiosonde reports and SMMR retrievals depends upon the magnitude of the water vapor retrieval. Comparisons for each year from 1979 to 1982 using Version IV are shown in Figures 3.6 through 3.9. Coincident data were averaged for each 0.2 cm interval of radiosonde water vapor when there were at least five coincidences in the interval. The average coincident SMMR-retrieved water vapor is plotted versus the average radiosonde water vapor for each interval.

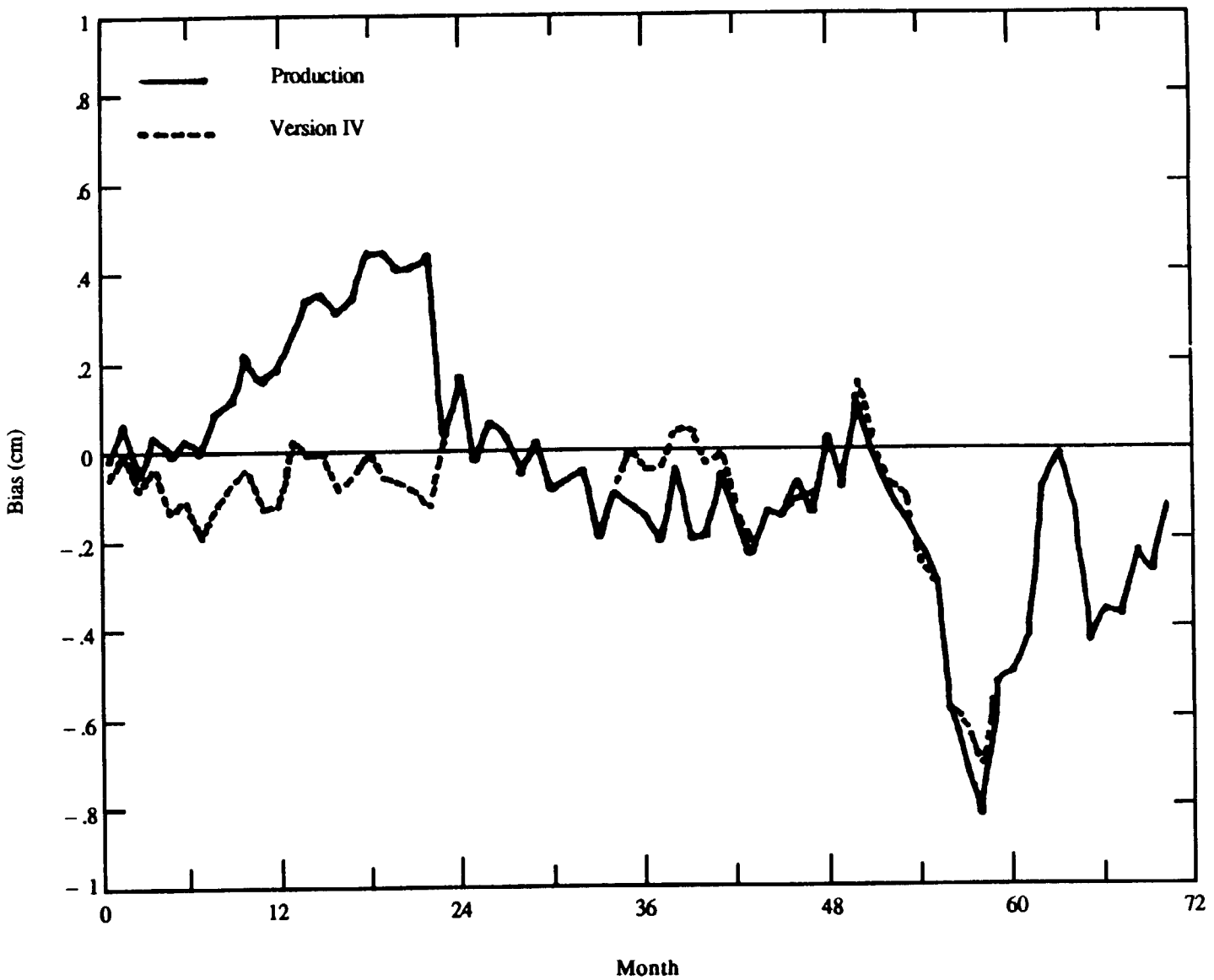

Figure 3.3. Average difference (bias) between SMMR water vapor and coincident radiosonde measurements (production versions compared to Version IV separately).

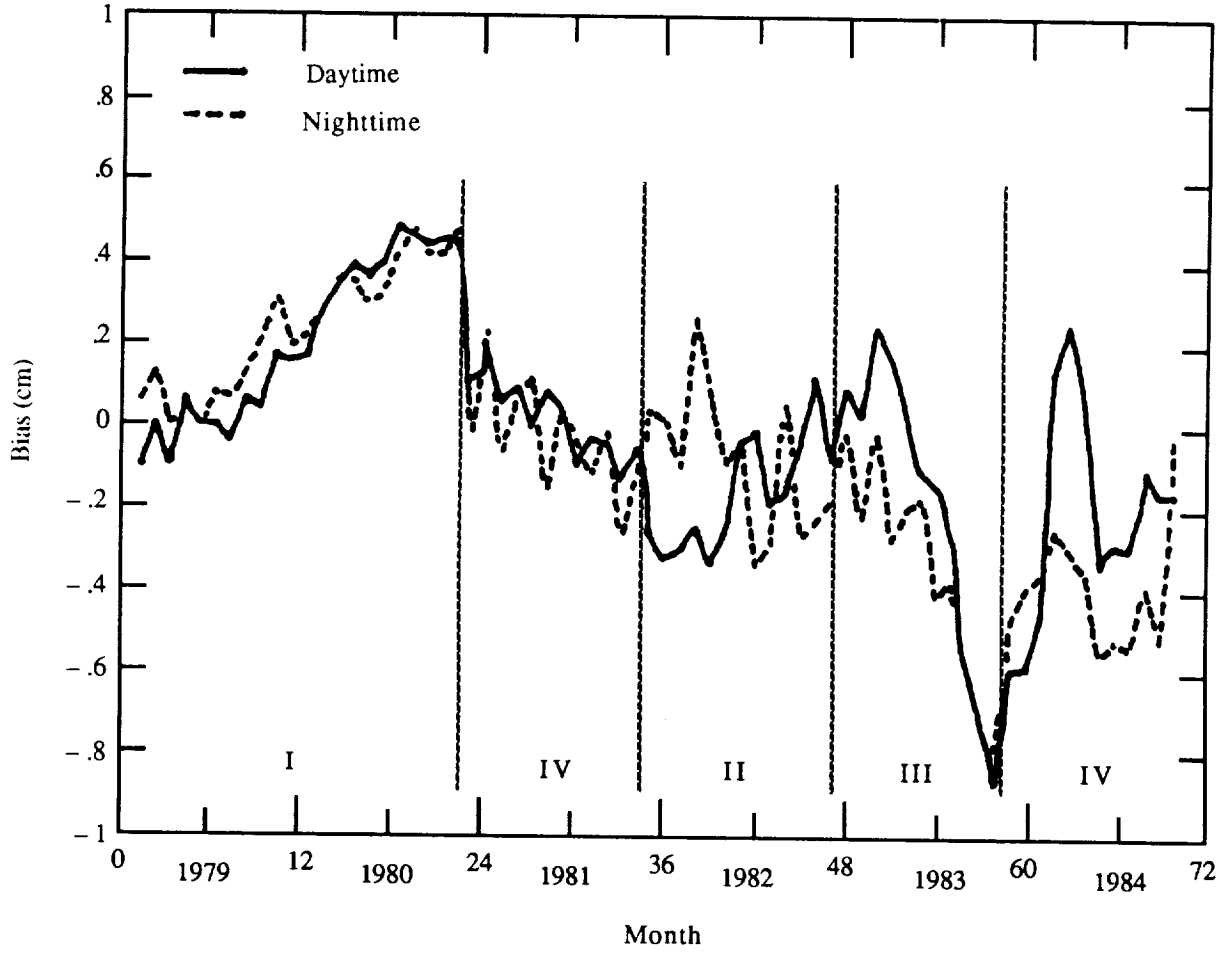

Figure 3.4. Average difference (bias) between SMMR water vapor and coincident radiosonde measurements for day and night retrievals separately.

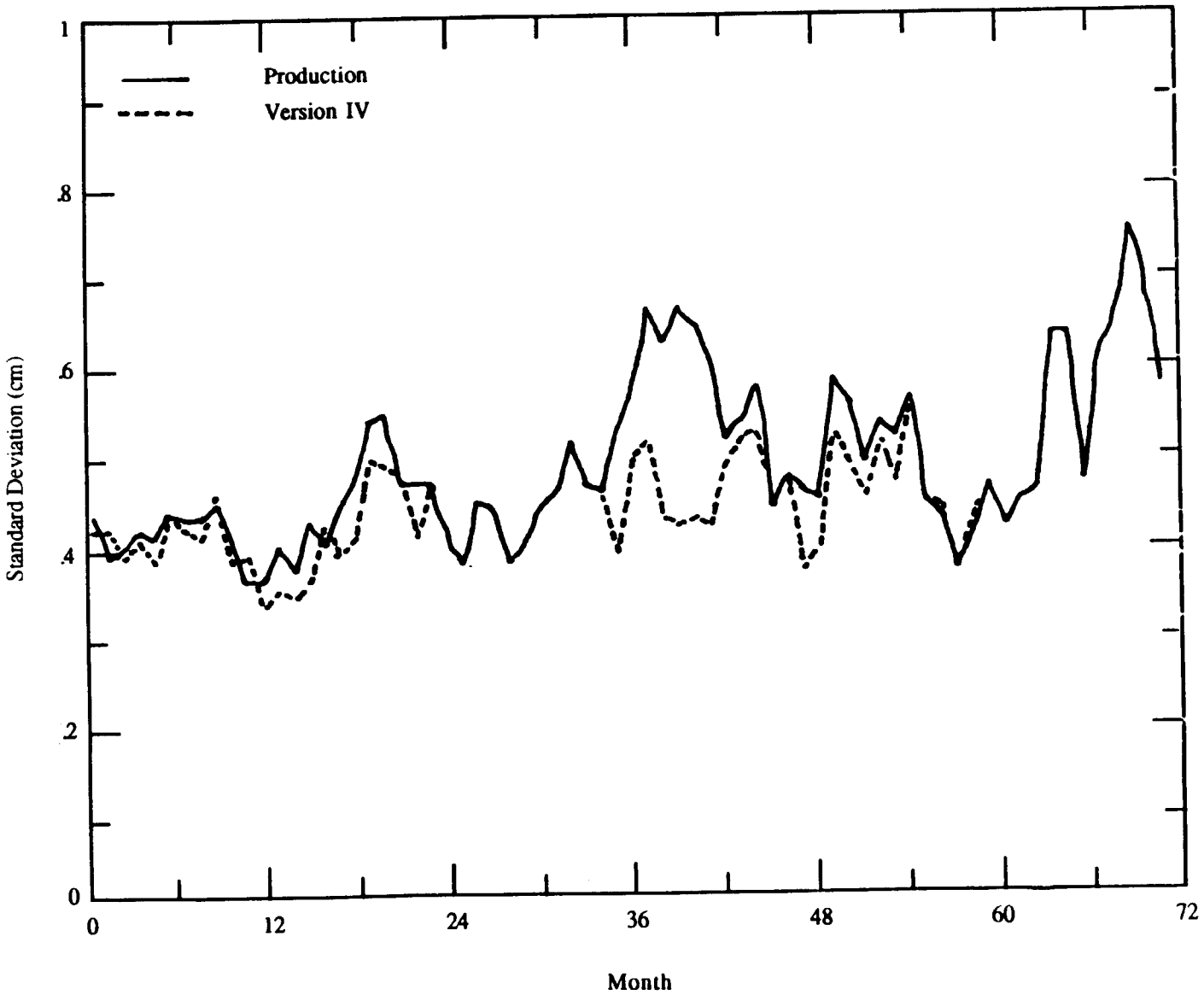

Figure 3.5. Variation of the standard deviation of the retrieval errors (production versions compared to Version IV separately).

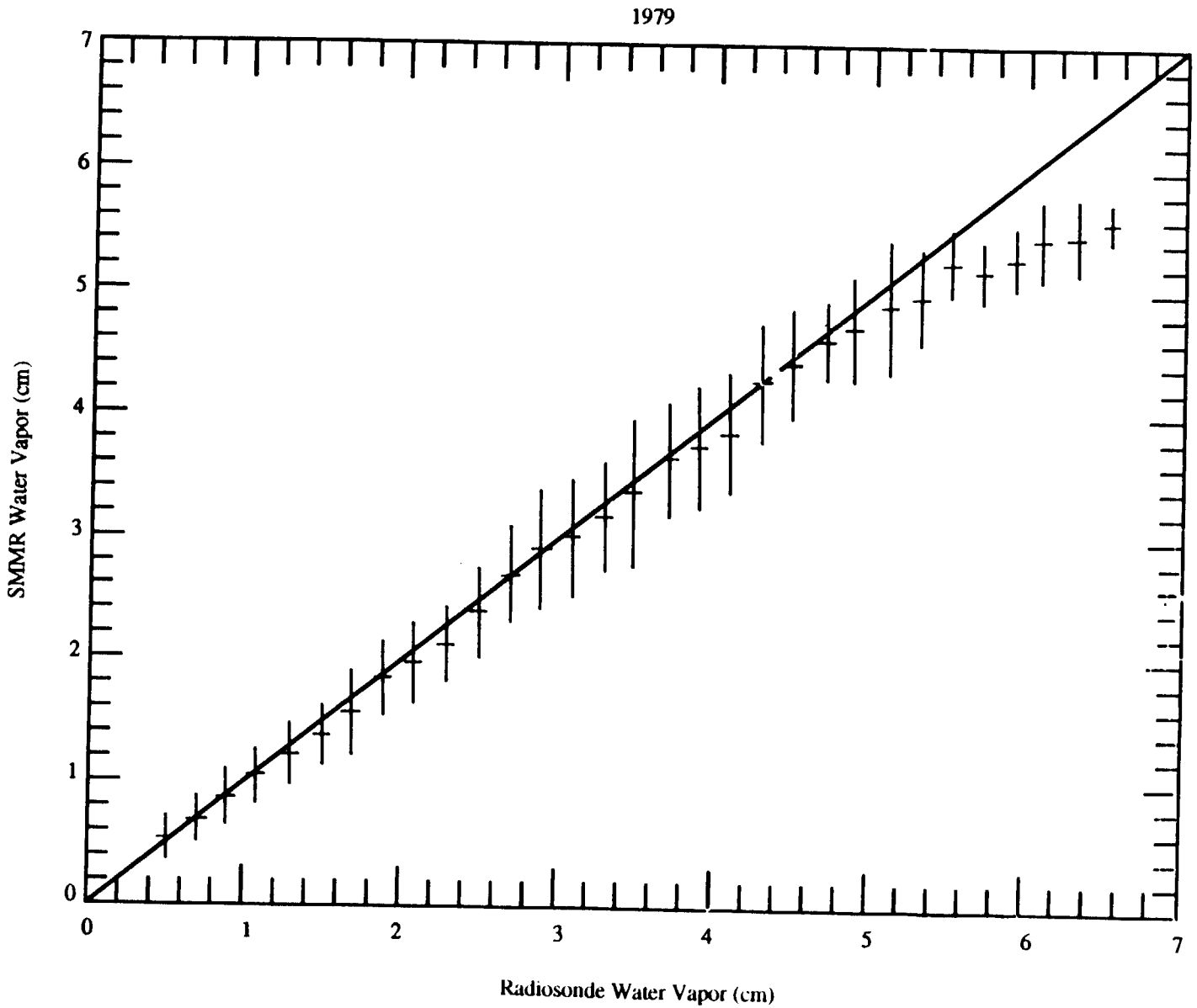

Figure 3.6. Comparison between SMMR water vapor (Version IV) and radiosonde data (1979).

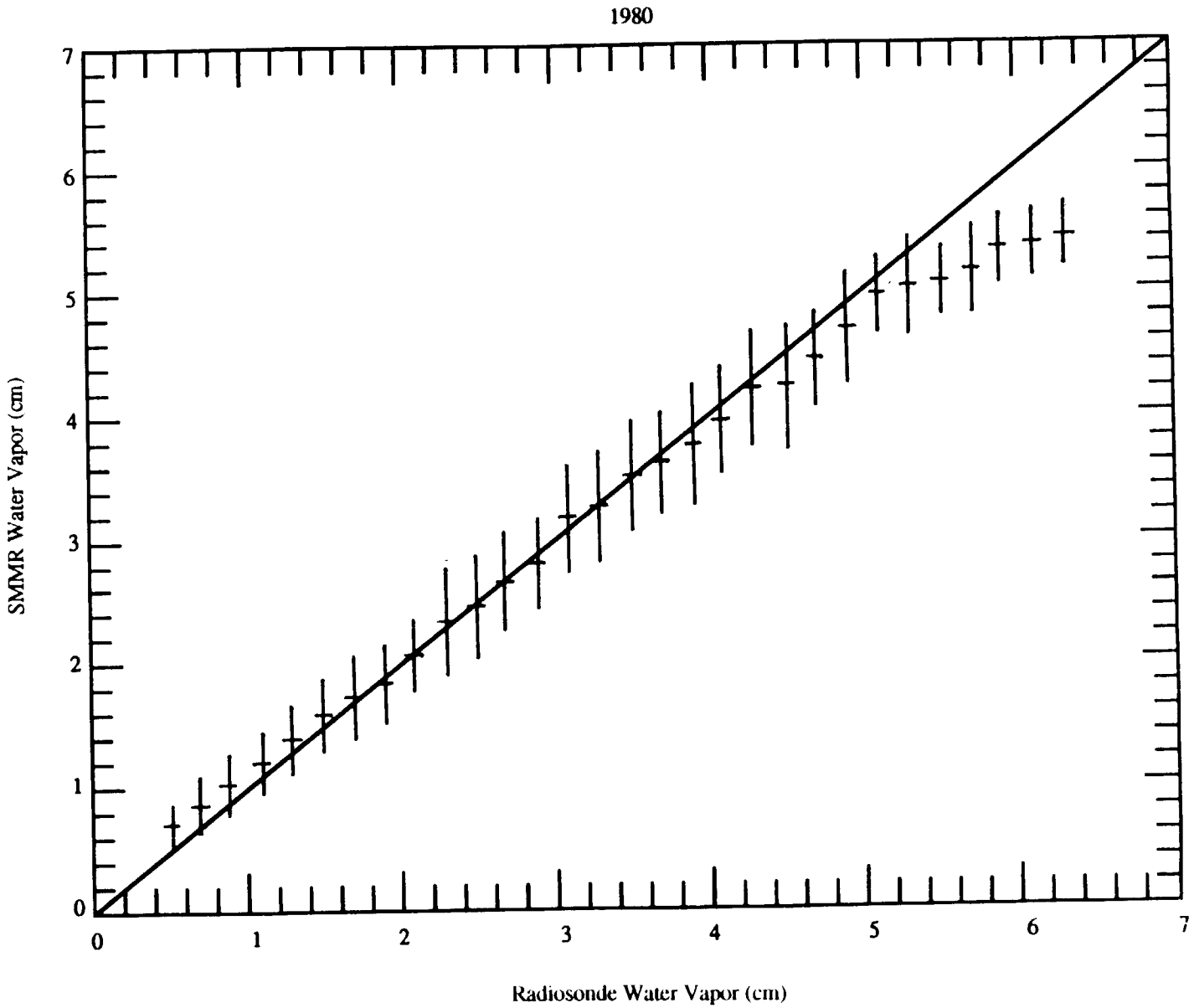

Figure 3.7. Comparison between SMMR water vapor (Version IV) and radiosonde data (1980).

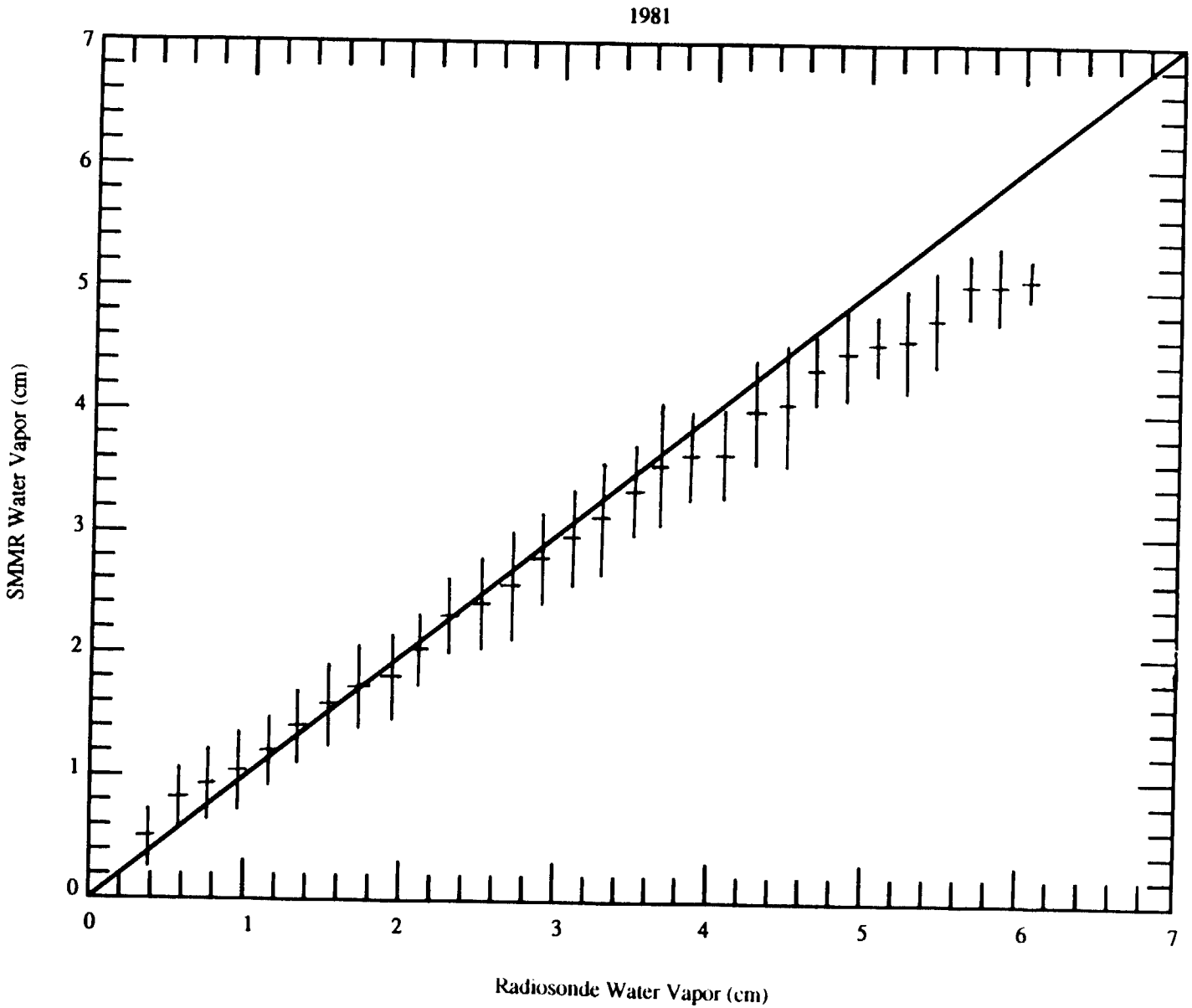

Figure 3.8. Comparison between SMMR water vapor (Version IV) and radiosonde data (1981).

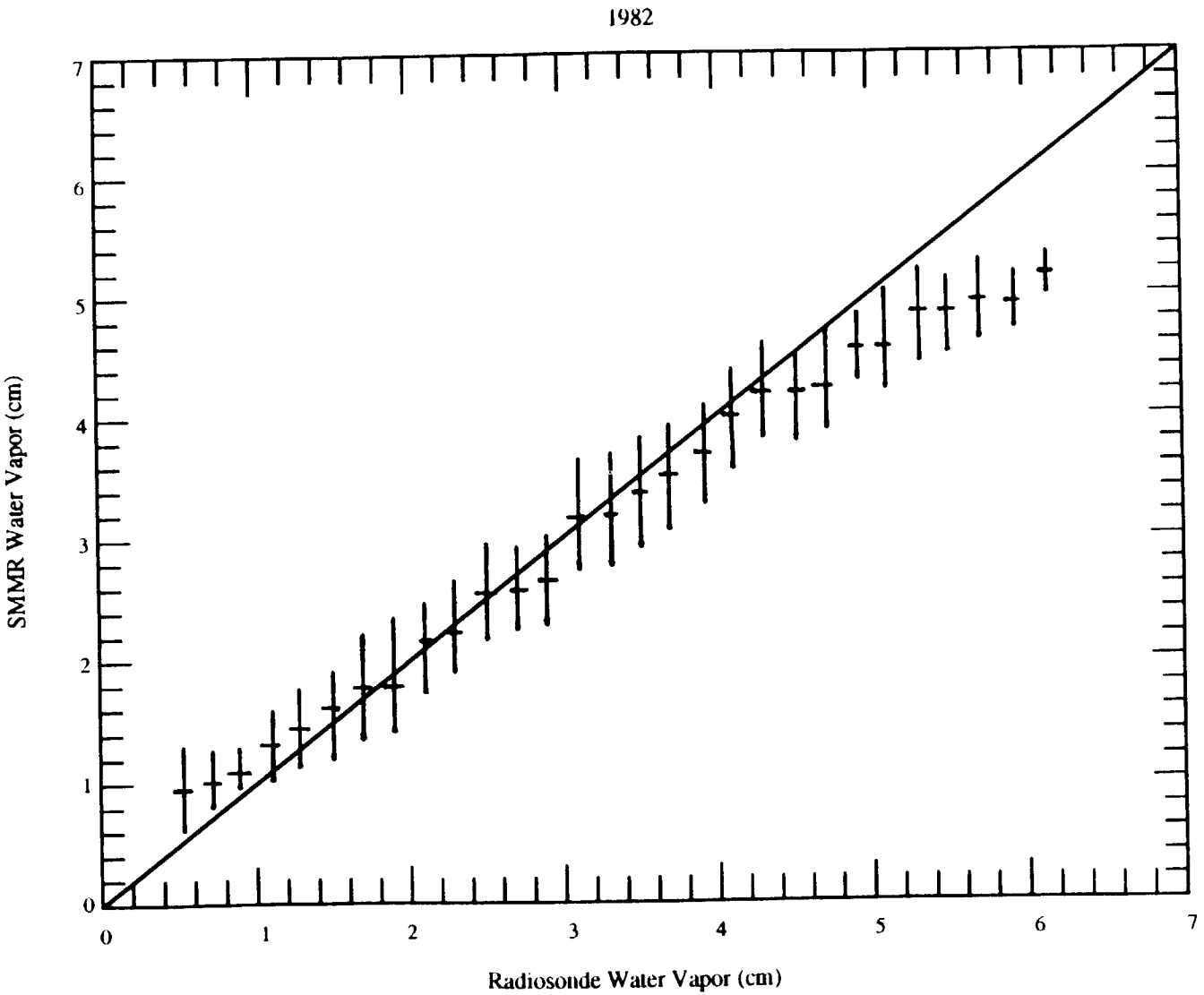

Figure 3.9. Comparison between SMMR water vapor (Version IV) and radiosonde data (1982).

Table 3.2

Comparisons With Radiosonde Data: Year 1

	Bias			Standard Deviation			Number of Points		
Month	D/N	D	N	D/N	D	N	D/N	D	N
Jan. 79	–0.01	–0.11	0.06	0.44	0.50	0.37	78(0)	33(0)	45(0)
Feb. 79	0.08	0.01	0.13	0.39	0.34	0.42	82(2)	33(1)	49(1)
Mar. 79	–0.05	–0.10	0.00	0.40	0.42	0.38	73(0)	34(0)	39(0)
Apr. 79	0.05	0.07	0.03	0.42	0.34	0.49	83(0)	44(0)	39(0)
May 79	0.00	0.01	–0.01	0.41	0.40	0.41	130(1)	67(1)	63(0)
June 79	0.04	–0.00	0.08	0.44	0.44	0.44	147(1)	84(0)	63(1)
July 79	0.01	–0.04	0.07	0.43	0.40	0.45	119(0)	63(0)	56(0)
Aug. 79	0.10	0.07	0.13	0.43	0.41	0.46	106(1)	57(0)	49(1)
Sept. 79	0.13	0.04	0.21	0.45	0.44	0.45	85(1)	39(1)	46(0)
Oct. 79	0.24	0.18	0.32	0.40	0.32	0.47	78(1)	42(0)	36(10)

NOTE: In this table and the following five tables, D/N refers to day and night comparisons taken together. D or N refers to day or night comparisons separately. The tables give the number of points that satisfy the coincidence criteria in Section 3.6. The number of points that were eliminated because |SMMR WV - Radiosonde WV| > 1.5 appear in parentheses.

The error bar for each point is the standard deviation of the SMMR retrievals for an interval. One can see a degradation of the retrievals over the 4-year period. This is evident at both the high end and low end of the water vapor range. It is likely that SMMR retrievals underestimate the water vapor at the high end because SMMR averages the water vapor content over the field-of-view.

The rms difference between SMMR retrievals and coincident radiosonde reports includes effects from the following:

a) the actual error of the SMMR measurement
b) the error in the radiosonde measurement or in its report
c) the radiosonde/SMMR coincidence time and spatial difference

Table 3.3

Comparisons With Radiosonde Data: Year 2

	Bias			Standard Deviation			Number of Points		
Month	D/N	D	N	D/N	D	N	D/N	D	N
Nov. 79	0.17	0.16	0.19	0.36	0.32	0.42	36(0)	21(0)	15(0)
Dec. 79	0.20	0.17	0.22	0.36	0.33	0.37	66(2)	27(0)	39(2)
Jan. 80	0.29	0.29	0.29	0.40	0.39	0.40	90(0)	38(0)	52(0)
Feb. 80	0.36	0.35	0.36	0.37	0.34	0.40	63(1)	37(0)	26(1)
Mar. 80	0.38	0.40	0.36	0.43	0.34	0.52	106(1)	58(0)	48(1)
Apr. 80	0.33	0.36	0.30	0.40	0.40	0.39	104(1)	58(0)	46(1)
May 80	0.6	0.40	0.33	0.45	0.40	0.49	113(1)	56(1)	57(0)
June 80	0.47	0.49	0.43	0.48	0.46	0.52	109(1)	66(1)	43(0)
July 80	0.47	0.47	0.48	0.54	0.49	0.60	120(2)	72(0)	48(2)
Aug. 80	0.43	0.44	0.42	0.55	0.56	0.54	113(4)	56(2)	57(2)
Sept. 80	0.44	0.45	0.42	0.47	0.50	0.43	99(4)	62(0)	37(4)
Oct. 80	0.47	0.45	0.48	0.47	0.50	0.45	111(1)	60(1)	51(0)

d) the pointlike radiosonde measurement compared with the field-of-view-averaged SMMR measurement. (At 18 GHz, this area is about 60 km in diameter.)

By model considerations and the introduction of radiance noise (1 K rms), Chang and Wilheit (1979) gave a theoretical estimate of 0.15 cm for the retrieval error. This error is a combination of the noise error and the error in fitting their radiance model with a regression function for water vapor. The effect (a) includes these errors, inaccuracies of the model itself, and radiance calibration errors. However, the effect of calibration errors is diminished because the algorithm has been tuned to ground truth data. Hogg et al. (1983) estimated that the rms difference between actual water vapor and that measured by operational radiosondes was 0.21 cm at Sterling, Virginia (where the mean water vapor amount was 3.5 cm), and 0.15 cm at Denver, Colorado (with a mean of 1.5 cm).

Table 3.4

Comparisons With Radiosonde Data: Year 3

	Bias			Standard Deviation			Number of Points		
Month	D/N	D	N	D/N	D	N	D/N	D	N
Nov. 80	0.05	0.09	–0.03	0.47	0.38	0.58	51(0)	32(0)	19(0)
Dec. 80	0.19	0.16	0.23	0.41	0.47	0.29	66(1)	39(0)	27(1)
Jan. 81	–0.01	0.05	–0.08	0.38	0.34	0.41	79(0)	40(0)	39(0)
Feb. 81	0.08	0.10	–0.07	0.45	0.45	0.44	100(0)	50(00	50(0)
Mar. 81	0.05	–0.01	0.12	0.44	0.48	0.38	71(0)	42(0)	29(0)
Apr. 81	–0.04	0.09	–0.18	0.38	0.37	0.33	102(0)	55(0)	47(0)
May 81	0.04	0.03	0.06	0.40	0.42	0.35	80(1)	54(1)	26(0)
June 81	–0.08	–0.11	–0.04	0.44	0.49	0.47	111(1)	62(0)	49(1)
July 81	–0.06	–0.03	–0.12	0.46	0.47	0.44	77(0)	50(0)	27(0)
Aug. 81	–0.03	–0.04	–0.01	0.52	0.56	0.48	80(2)	46(2)	34(0)
Sept. 81	–0.19	–0.14	–0.28	0.47	0.45	0.50	61(1)	39(0)	22(1)
Oct. 81	–0.08	–0.05	–0.12	0.46	0.44	0.48	80(1)	49(1)	31(0)

Considering the spatial and temporal variability of water vapor, we have estimated that the rms coincidence errors due to the spatial and temporal coincidence windows may each be as large as 0.2 cm. Introducing rms errors of 0.2 cm for each of effects (a) through (c) would produce a net rms SMMR/radiosonde difference of 0.4 cm, assuming that these effects are not correlated. This exercise is intended to show that the rms difference between SMMR retrievals and coincident ground truth data is not unreasonable in light of the possible contributing errors. Another important factor is that our algorithm is tuned over the whole range of water vapor amounts and is applied globally. For local area studies, it is likely that results would be improved if the algorithm was tuned for that region.

Table 3.5

Comparisons With Radiosonde Data: Year 4

	Bias			Standard Deviation			Number of Points		
Month	D/N	D	N	D/N	D	N	D/N	D	N
Nov. 81	–0.11	–0.27	0.04	0.53	0.49	0.53	69(4)	35(4)	34(0)
Dec. 81	–0.14	–0.32	0.01	0.58	0.60	0.51	61(8)	28(8)	33(00
Jan. 82	–0.20	–0.30	–0.10	0.67	0.71	0.61	64(4)	31(4)	33900
Feb. 82	–0.02	–0.24	0.27	0.63	0.65	0.44	57(7)	33(7)	24(0)
Mar. 82	–0.19	–0.34	0.07	0.67	0.69	0.55	47(2)	30(2)	17(0)
Apr. 82	–0.19	–0.26	–0.09	0.65	0.66	0.61	78(4)	47(3)	31(1)
May 82	–0.03	–0.04	–0.03	0.61	0.64	0.57	83(5)	46(5)	37(0)
June 82	–0.14	–0.01	–0.34	0.52	0.50	0.47	85(3)	52(2)	33(1)
July 82	–0.23	–0.19	–0.28	0.54	0.58	0.46	79(2)	48(1)	31(1)
Aug. 82	–0.12	–0.16	0.07	0.58	0.62	0.31	50(1)	41(0)	9(1)
Sept. 82	–0.14	–0.04	–0.27	0.44	0.45	0.39	59(0)	34(0)	25(0)
Oct. 82	–0.05	0.13	–0.23	0.48	0.42	0.47	78(2)	39(0)	39(2)

In our comparisons, we have used both ship and island data from the NMC tapes. To avoid possible land contamination of radiances, reports from large islands were not used. The upper limit on the SMMR/radiosonde difference filters out some of the bad radiosonde reports. In addition, if radiosonde data were reported only to the 400 mbar level, that report was rejected because the amount of water vapor above 400 mbar is significant. To improve the comparison results, one would need to examine in detail each radiosonde report (pressure, height, temperature, and dew point temperature at each level) to find any possible errors in the report: location errors, transmission errors, or lapse rate inconsistencies.

Table 3.6

Comparisons With Radiosonde Data: Year 5

	Bias			Standard Deviation			Number of Points		
Month	D/N	D	N	D/N	D	N	D/N	D	N
Nov. 82	–0.14	–0.10	–0.18	0.46	0.53	0.37	51(1)	25(1)	26(0)
Dec. 82	0.05	0.10	0.00	0.45	0.41	0.48	57(0)	31(0)	26(0)
Jan. 83	–0.08	0.02	–0.24	0.59	0.65	0.44	66(1)	40(1)	26(0)
Feb. 83	0.13	0.25	–0.00	0.56	0.58	0.50	96(1)	53(1)	43(0)
Mar. 83	0.01	0.16	–0.28	0.49	0.42	0.50	73(0)	48(0)	25(0)
Apr. 83	–0.07	0.03	–0.20	0.54	0.56	0.49	81(1)	47(1)	34(0)
May 83	–0.13	–0.11	–0.17	0.52	0.51	0.55	43(1)	27(1)	16(0)
June 83	–0.21	–0.14	–0.41	0.57	0.58	0.48	94(2)	69(0)	25(2)
July 83	–0.29	–0.26	–0.37	0.45	0.42	0.50	87(4)	59(3)	28(1)
Aug. 83	–0.58	–0.59	–0.56	0.43	0.43	0.45	97(13)	63(4)	34(9)
Sept. 83	–0.71	–0.71	–0.73	0.37	0.32	0.43	62(13)	37(9)	25(4)
Oct. 83	–0.84	–0.87	–0.80	0.42	0.33	0.50	39(22)	21(13)	18(9)

Table 3.7

Comparisons With Radiosonde Data: Year 6

	Bias			Standard Deviation			Number of Points		
Month	D/N	D	N	D/N	D	N	D/N	D	N
Nov. 83	–0.52	–0.58	–0.47	0.47	0.43	0.50	65(6)	29(1)	36(5)
Dec. 83	–0.50	–0.58	–0.39	0.42	0.41	0.40	74(3)	41(0)	33(3)
Jan. 84	–0.41	–0.46	–0.36	0.45	0.45	0.45	70(5)	36(4)	34(10
Feb. 84	–0.06	0.12	–0.25	0.46	0.47	0.36	86(1)	44(0)	42(1)
Mar. 84	0.01	0.26	–0.30	0.64	0.64	0.48	94(8)	52(2)	42(6)
Apr. 84	–0.12	0.05	–0.36	0.64	0.64	0.55	89(4)	52(0)	37(4)
May 84	–0.43	–0.34	–0.55	0.47	0.41	0.52	108(11)	61(7)	47(4)
June 84	–0.35	–0.29	–0.51	0.61	0.63	0.53	64(6)	46(4)	18(2)
July 84	–0.37	–0.29	–0.54	0.66	0.69	0.55	87(8)	60(5)	27(3)
Aug. 84	–0.21	–0.10	–0.37	0.76	0.82	0.64	49(8)	29(3)	20(5)
Sept. 84	–0.27	–0.17	–0.52	0.70	0.70	0.63	61(8)	43(4)	18(4)
Oct. 84	–0.11	–0.16	–0.02	0.58	0.64	0.42	70(7)	47(1)	23(6)

4. SEA-ICE PARAMETERS

The dual-polarized, multifrequency radiances available from the Nimbus–7 SMMR permit the determination of several sea-ice parameters. These include: (1) the total sea-ice concentration, (C), defined as the fraction of ocean surface covered by sea ice within the field-of-view of the instrument; (2) the multiyear ice fraction, (C_M), defined as the fraction of ice cover that has survived at least one summer's melt; and (3) the first-year ice, (C_F). The sum of C_M and C_F is the total ice concentration, C.

4.1 Algorithm

The algorithm designed for use with the Nimbus–7 SMMR to compute sea-ice concentrations has been described previously by Cavalieri et al. (1984), Gloersen et al. (1984), and Gloersen and Cavalieri (1986). The SMMR algorithm calculates C, C_F, and C_M from the microwave polarization ratio PR at 18-GHz and from a spectral gradient ratio, GR, which utilizes vertically polarized 18-GHz and 37-GHz radiances. These ratios are defined as follows:

$$PR = (T_{18V} - T_{18H}) / (T_{18V} + T_{18H}), \tag{50}$$

$$GR = (T_{37V} - T_{18V}) / (T_{37V} + T_{18V}). \tag{51}$$

Following the method of Cavalieri et al. (1984), the radiative transfer equation can be written as

$$T = T_W(1 - C_F - C_M) + T_F C_F + T_M C_M, \tag{52}$$

where T is the radiance observed at the satellite; T_W, T_F, and T_M are the radiances chosen as typical for open ocean, first-year ice, and multiyear ice, respectively. This equation holds for each SMMR frequency and polarization and neglects contributions from both atmospheric and cosmic radiations. Upon the substitution of Equation (52) into Equations (50) and (51) for each of the three channels, the resulting equations can be solved simultaneously for C_F and C_M. The result is

$$C_M = [M_0 + M_1 PR + M_2 GR + M_3(PR)(GR)]/D \tag{53}$$

$$C_F = [F_0 + F_1 PR + F_2 GR + F_3(PR)(GR)]/D \tag{54}$$

where

$$D = D_0 + D_1 PR + D_2 GR + D_3(PR)(GR) \tag{55}$$

$$M_0 = A_0 B_4 - A_4 B_0 \tag{56}$$

$$M_1 = A_1 B_4 - A_5 B_0 \tag{57}$$

$$M_2 = A_0 B_5 - A_4 B_1 \tag{58}$$

$$M_3 = A_1 B_5 - A_5 B_1 \tag{59}$$

$$F_0 = A_0B_2 - A_2B_0 \quad (60)$$

$$F_1 = A_1B_2 - A_3B_0 \quad (61)$$

$$F_2 = A_0B_3 - A_2B_1 \quad (62)$$

$$F_3 = A_1B_3 - A_3B_1 \quad (63)$$

$$D_0 = A_2B_4 - A_4B_2 \quad (64)$$

$$D_1 = A_3B_4 - A_5B_2 \quad (65)$$

$$D_2 = A_2B_5 - A_4B_3 \quad (66)$$

$$D_3 = A_3B_5 - A_5B_3 \quad (67)$$

$$A_0 = -T_{W,18V} + T_{W,18H} \quad (68)$$

$$A_1 = T_{W,18V} + T_{W,18H} \quad (69)$$

$$A_2 = T_{M,18V} - T_{M,18H} - T_{W,18V} + T_{W,18H} \quad (70)$$

$$A_3 = -T_{M,18V} - T_{M,18H} + T_{W,18V} + T_{W,18H} \quad (71)$$

$$A_4 = T_{F,18V} - T_{F,18H} - T_{W,18V} + T_{W,18H} \quad (72)$$

$$A_5 = -T_{F,18V} - T_{F,18H} + T_{W,18V} + T_{W,18H} \quad (73)$$

$$B_0 = -T_{W,37V} + T_{W,18V} \quad (74)$$

$$B_1 = T_{W,37V} + T_{W,18V} \quad (75)$$

$$B_2 = T_{M,37V} - T_{M,18V} - T_{W,37V} + T_{W,18V} \quad (76)$$

$$B_3 = -T_{M,37V} - T_{M,18V} + T_{W,37V} + T_{W,18V} \quad (77)$$

$$B_4 = T_{F,37V} - T_{F,18V} - T_{W,37V} + T_{W,18V} \quad (78)$$

$$B_5 = -T_{F,37V} - T_{F,18V} + T_{W,37V} + T_{W,18V} \quad (79)$$

Noting that $C = C_F + C_M$ and using observed SMMR radiances for each of the three channels typical of open water, first-year ice, and multiyear ice (Cavalieri et al., 1984) obtained from the SMMR CELL tapes (Gloersen et al., 1984), Equations (53) and (54) become

$$C = [1721 - 5452(PR) - 6380(GR) + 791.7(PR)(GR)]/D, \quad (80)$$

$$C_M = [-550.1 + 15559(PR) - 22397(GR) - 38507(PR)(GR)]/D, \quad (81)$$

where

$$D = 1422 + 8643(PR) - 4123(GR) + 9032(PR)(GR). \quad (82)$$

The concentrations calculated from Equations (80) and (81) have an inherent spatial resolution of 60 km because of the footprint size of the 18-GHz SMMR channels. The polarization at 37 GHz is also used to obtain concentration (using different A coefficients obtained from the 37-GHz H and V channels) at an improved spatial resolution, but at the expense of greater atmospheric interference.

The effects of weather on the microwave emissive properties of the open ocean are well known (Swift, 1980; Wilheit and Chang, 1980). The microwave emission from a specular ocean surface is a function of frequency, viewing angle, and polarization. Early work by Nordberg et al. (1971), has shown an association between an increase of windspeed over the open ocean and an increase in microwave emission at 19.35 GHz. They found an increase of about 1–1.5 K for each meter per second increase in windspeed, depending on the angle of incidence. This work was extended to cover a range of frequencies from 1.4 to 37 GHz viewing at an angle of 38° providing information at both horizontal and vertical polarizations (Webster et al., 1976). Theoretical models extending the emissive properties of the ocean surface to SMMR frequencies and polarizations as well as observational results show the horizontal polarizations to be almost twice as sensitive as the vertical polarizations to near-surface winds (NSW) (Gloersen and Barath, 1977). As a consequence, an increase of 6 m/s in surface windspeed results in an increase of about 16 percent in calculated ice concentration when using the 18-GHz dual-polarized radiances (Cavalieri et al., 1984).

Variations in atmospheric water vapor and cloud liquid water at microwave wavelengths are also important considerations. While contributions due to atmospheric water vapor fluctuations can be neglected in polar regions, they are important at lower latitudes. A typical midlatitude fluctuation in columnar atmospheric water vapor is about 2 cm, which results in a computed ice concentration change of 5 percent. Cloud liquid water contributes more significantly to increased microwave emission over open ocean. Atmospheric radiative transfer model calculations show that the 37-GHz channels are substantially more sensitive to variations in cloud liquid water than are the 18-GHz channels. For example, an increase of 0.04 cm in columnar cloud liquid water will increase the computed ice concentration by 1 percent at 18 GHz and by 8 percent at 37 GHz (Cavalieri et al., 1984).

Weather interference in the calculation of sea-ice concentration has also been observed using single-channel instruments. For example, single-day averages of Electrically Scanning Microwave Radiometer (ESMR) radiances (1.55-cm wavelength) show strong indications of weather effects over the open ocean. Three-day averages show somewhat less, and 1-month averages display greatly reduced effects over the open seas, because of the transient nature of weather disturbances. Even for the monthly average, computed sea-ice concentrations less than or equal to 14 percent were set to zero to eliminate any residual weather effects (Zwally et al., 1983). Obviously, the use of averaging is not viable for studying short-term variations of sea ice. Unfortunately, except for averaging and using threshold concentrations, no other means for reducing weather interference is apparent for single-channel data.

Fortunately, there is a simple method for reducing these weather effects over open ocean (Gloersen and Cavalieri, 1986). This technique also provides a means for simultaneously displaying the position of the ice edge in areas of first-year sea ice on images of multiyear sea-ice concentration. A filter to reduce the effects of weather over the open oceans and near the ice edge

is part of the SMMR sea-ice algorithm. It consists simply of designating all oceanic areas for which GR ≥ 0.08 (50) as ice-free. In order to understand this selection, it is useful to examine a plot of the spectral gradient ratio (GR) versus the polarization ratio (PR) at 18 GHz defined by Equations (50) and (51) in the north polar region. This distribution is given in Figure 4.1. Superimposed on this plot is a graphical depiction of the relations used to calculate sea-ice concentration and multiyear fraction, defined as $F = C_M/C$ [see Equations (53) and (54)]. Values for C and F calculated with the algorithm lie on or within the triangle defined by three points representing first-year sea ice (C = 1, F = 0), multiyear sea ice (C = 1, F = 1), and open ocean (C = 0). These points are used in the algorithm to define the microwave character of each surface (algorithm tie points). Thus the computed total concentrations of pure multiyear ice should lie along the lower leg of the triangle, those for pure first-year sea ice along the upper leg, and those for first-year/multiyear mixtures within the triangle, as is depicted by the short lines (along which multiyear fraction varies with constant total concentration) connecting the 20 percent concentration interval points on these two legs.

Also superimposed on this distribution are some points calculated on the basis of the radiative transfer equation (e.g., Gloersen and Barath, 1977) for a specular ocean (no winds, clouds, or atmospheric water vapor) near the freezing point (271,0,0,0 in Figure 4.1) and extreme values of each of the parameters: sea-surface temperature (SST) of 306 K near-surface winds (NSW) of 36 m/sec, water vapor W of 8 cm, and cloud droplet liquid water content of 0.08 cm. First, it should be noted that the ice-free ocean tie point and the specular ocean point do not coincide. This results from a decision to use a tie point more typical of ocean/atmosphere conditions near the ice margin (Cavalieri et al., 1984). As can be seen in Figure 4.1, increasing atmospheric water vapor to 8 cm in the column (a high value rarely observed: 1.5 cm is closer to the maximum value in the marginal ice zone, with 0.5 cm being more typical) decreases the polarization greatly, but the spectral gradient ratio only slightly. Increasing NSW also decreases PR but not GR, and increasing L decreases PR but increases GR. In fact, the only parameter that by itself decreases GR below the 0.08 level is SST for values of SST not found in polar regions.

The points of extreme values of SST, NSW, atmospheric water vapor, and cloud liquid water shown in Figure 4.1 can be used to interpret the cluster of points around the open ocean tie point (C=0) as being reasonable variations in these four parameters, since the observed points lie within these extremes. At intermediate values of ice concentrations, most of the points are distributed on either side of the upper leg of the triangle. As mentioned earlier, the points within the triangle represent mixtures of first-year ice, multiyear ice, and open water. The departure of the points outside of the triangle along the upper leg decreases with increasing ice concentration.

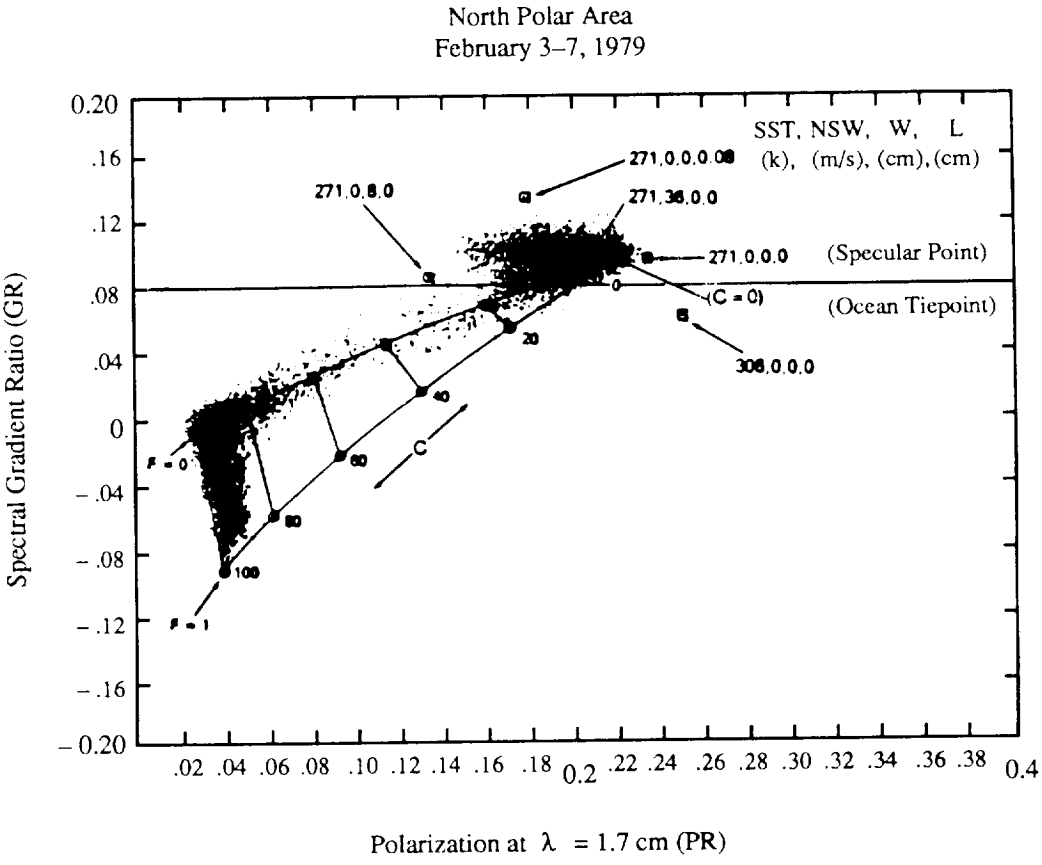

Figure 4.1. Spectral gradient ratio (GR) versus polarization ratio (PR) at 1.7 cm (18 GHz) for the polar area shown in Figure 4.7. The curved triangle is a representation of the algorithm used to calculate sea-ice concentration and age. The arrows indicate model calculations of GR and PR deviations from cold, specular oceanic conditions (see text) (from Gloersen and Cavalieri, 1986).

This is consistent with the interpretation that these departures result from high winds and/or heavy clouds (including rain) near the ice margin and with the fact that the atmospheric effects are more apparent against a low-emissive background of the open ocean. By the same token, some of the points inside the triangle also result partly from weather effects that decrease in importance with increasing ice concentration. The high density of points slightly outside the triangle near the C = 1, F = 0 tie point may result from selecting as the first-year tie point an area with radiometrically significant snow cover, so that areas with lower snow cover fall outside. Alternatively, they may result from the significant presence of radiometrically different ice types (e.g., Cavalieri et al., 1983, 1984). The points above the triangle between F = 0 and C = 0 all result in negative values of multiyear concentration C_M upon application of Equation (81).

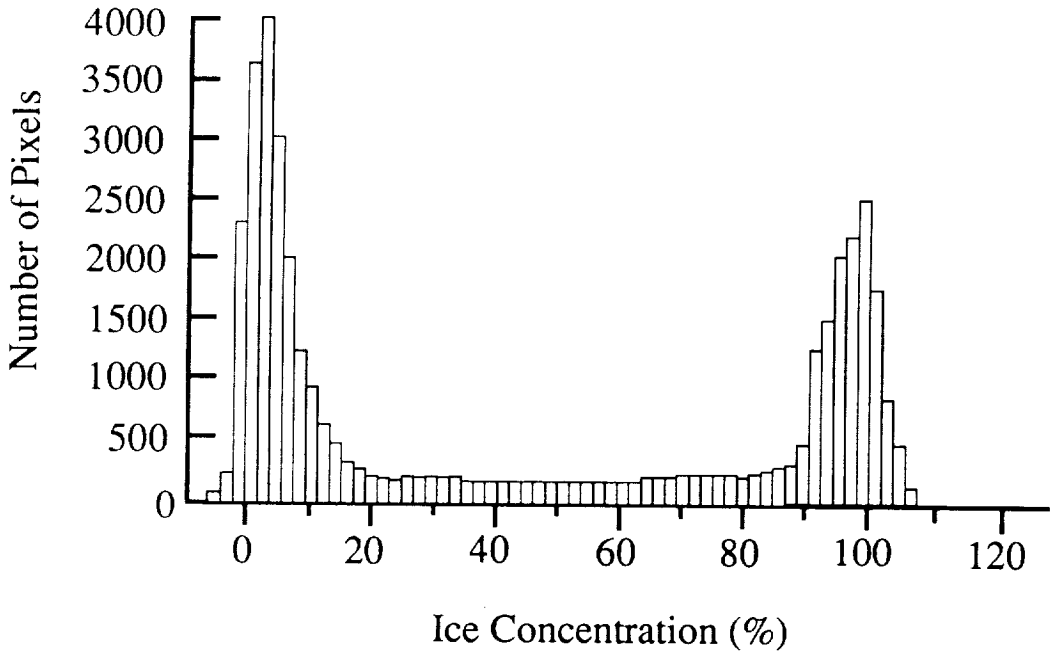

Figure 4.2. Histogram of the SMMR sea-ice concentration computed over the Northern Hemisphere from approximately 50° N to 84° N for the period February 3–7, 1979 (from Cavalieri et al., 1984).

4.2 Total Ice Concentration—Accuracy Estimates

The accuracy of the sea-ice algorithm described here depends largely on the validity of the underlying assumptions and on the degree to which the spatially and temporally varying microwave radiances of the two sea-ice types and of ice-free ocean match the chosen tie-points. Algorithm sensitivity studies show that a random error of 1 K in the radiances results in errors of about 3 percent in the ice concentration and 6 percent in the multiyear fraction. As outlined below, histograms of both the total ice concentration and ice fractions show that the results fall within reasonable bounds (see Figures 4.2 and 4.3). In Figure 4.4, the data shown in Figure 4.2 are replotted on a logarithmic scale. For comparison, a similar plot of February 1985 data is shown in Figure 4.5. This comparison indicates that there was no drift outside the estimated accuracy of the algorithm for the period 1979–1985.

Monitoring the average total radiance for each of the 10 channels over the global oceans has shown that all except the 21-GHz channels have changed less than 2 K over the 7-year lifetime

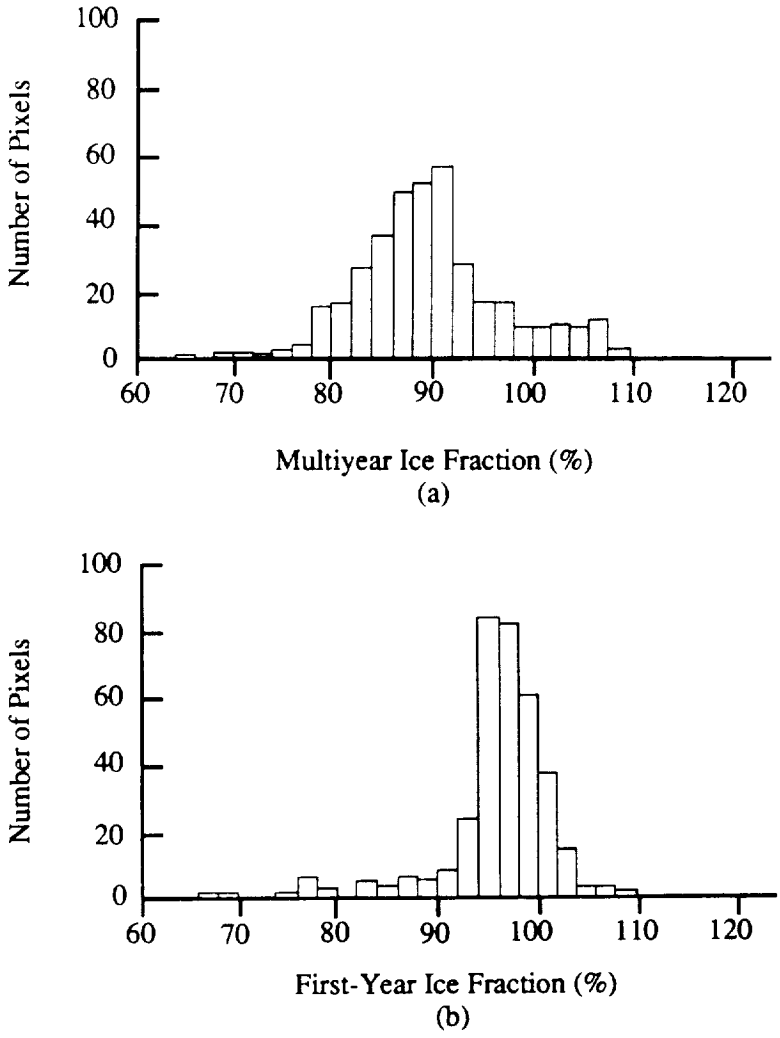

Figure 4.3. Histogram of SMMR (a) multiyear ice fraction for a region in the Canadian Basin and (b) first-year ice fraction for a region in the Kara Sea (from Cavalieri et al., 1984).

of the SMMR. The algorithm does not use the 21-GHz channels. Furthermore, the drift of the warm reference signal has been shown to be less than 1 K for all channels, and so the effects on the algorithm outputs will vary depending on the total or multiyear concentrations—the errors being less at the high-concentration end of the scale, which corresponds to the high-radiance regime, than at the low end, where the instrument drifts have been noted. It should be noted that the algorithm makes use of ratios of differences and sums of radiances, which also may help ameliorate the effects of any long-term drift. Also, the weather filter included in this algorithm cuts off the lowest 8–12 percent concentrations, so that any drifts may not be detectable.

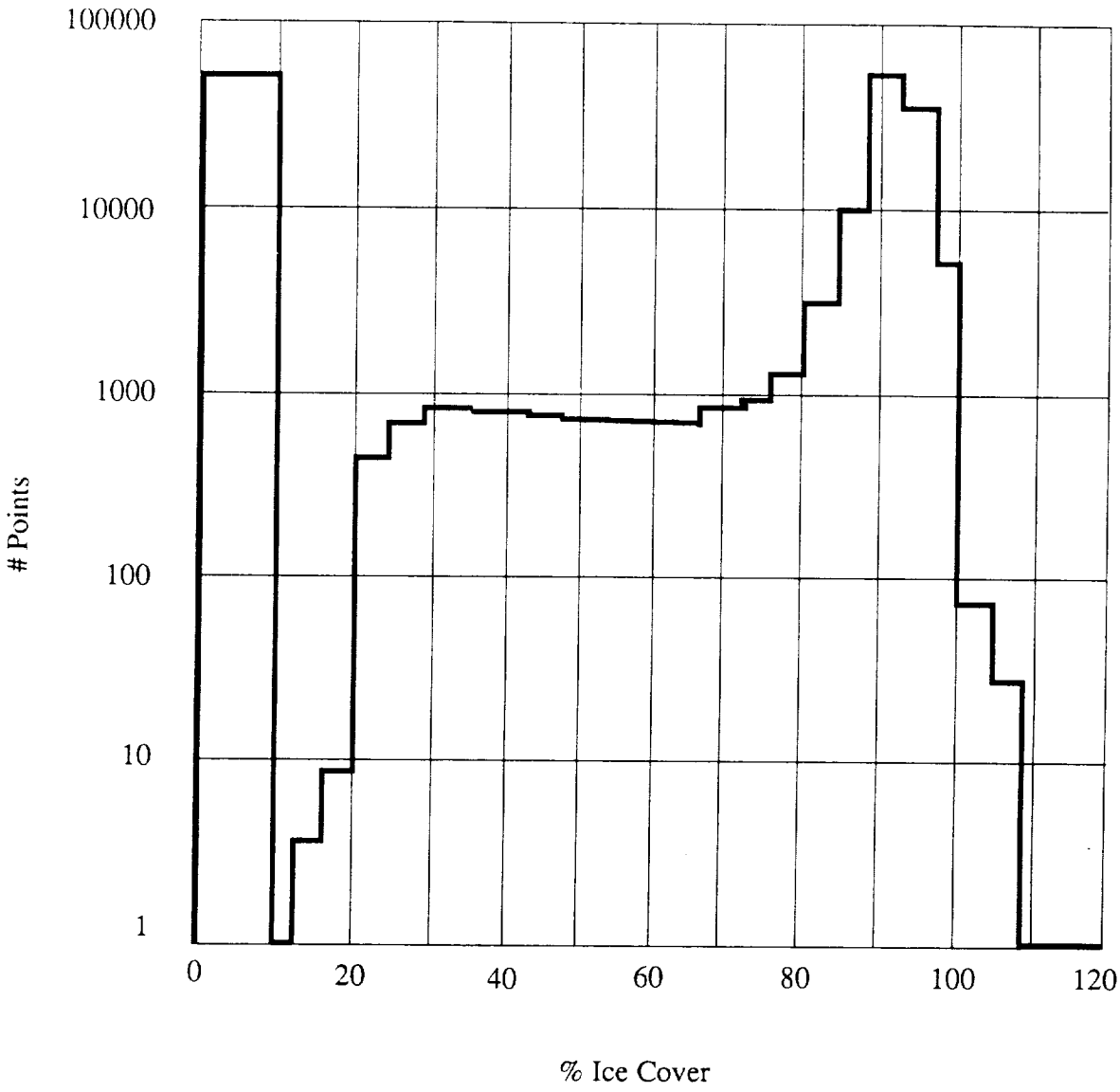

Figure 4.4. Histogram of the SMMR sea-ice concentration computed over the Northern Hemisphere from approximately 50° N to 84° N for the entire month of February 1979. Number of samples are presented on a logarithmic scale in order to emphasize the lower portions of the distribution.

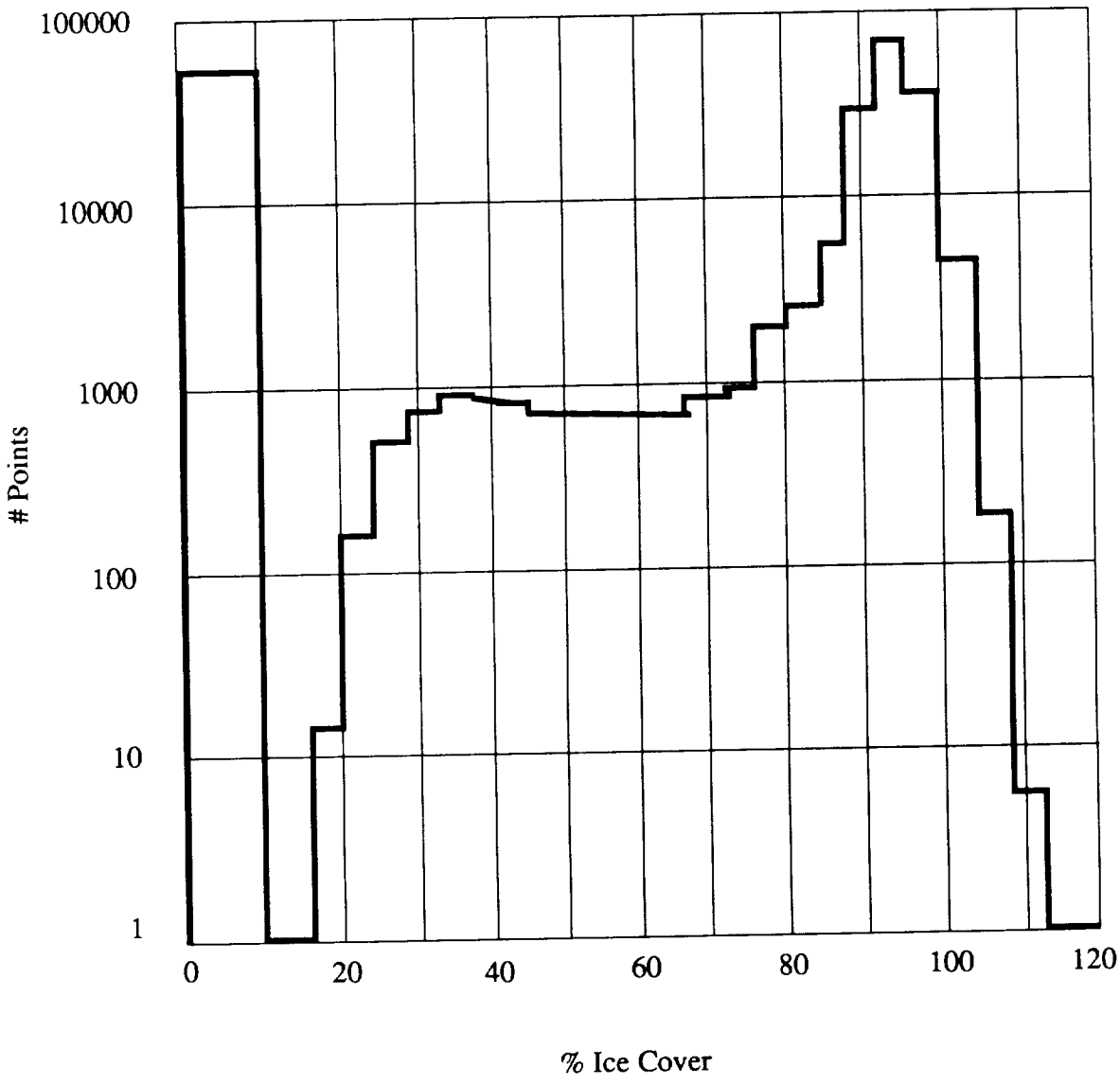

Figure 4.5. Histogram of the SMMR sea-ice concentration computed over the Northern Hemisphere from approximately 50° N to 84° N for the entire month of February 1985. Number of samples are presented on a logarithmic scale in order to emphasize the lower portions of the distribution.

Another test of the effects of instrument drift on the algorithm was to produce a scatter diagram similar to the one in Figure 4.1 for each of the winter months since launch up to 1986.

Rather than plotting individual points on these scatter diagrams as was done in Figure 4.1, the data were collected into (PR18, GR) bins and then plotted as the truncated natural logarithm of the number of observations minus one. By drawing a contour around the "3s" (representing at least 50 observations) in each of the diagrams on transparent material and superimposing the results (not shown), it can be seen that there is no perceptible shift in the two sea-ice tie points, and a barely discernable shift at the open ocean tie points.

A similar analysis, but instead utilizing monthly mean radiances mapped onto a polar projection grid down to 50°, was also used to produce histograms of sea-ice concentrations for four winter months—December, January, February, and March—this time in 2 percent bins. From these histograms, a time series of the histogram peak, the high-concentration toe-in (25 or more occurrences), and maximum values of ice concentration were obtained. The results are plotted in Figure 4.6 for these four winter months for each of the eight SMMR years. While there is considerable interannual variability for each of the four winter months examined, no pattern emerges which would suggest a clear long-term trend attributable to calibration drift.

Next, the monthly mean parameters and their standard deviations for specified regions in the Arctic over the 8 years of SMMR operation were examined. For this purpose, the Arctic region was subdivided into an 8 by 8 grid (64 elements of approximately equal area) and statistics obtained for each element. This Arctic Analysis Grid is shown in Figure 4.7. Each element is approximately 600 by 600 km on a side corresponding to about 100 18-GHz footprints. Monthly mean sea-ice concentration statistics have been generated for each of the 64 elements, and time series of these elements have been plotted for 8 years: 1978–86.

Time series of the calculated monthly mean sea-ice concentration and standard deviation are given in Figure 4.8 for grid element (3, 4). Similar time series are plotted in because each is representative of a surface having different microwave characteristics. These grids then are classified as follows:

(3, 4) Canadian Basin—Multiyear (MY) ice
(3, 7) Baffin Bay—First-year (FY) ice
(6, 3) Kara Sea—Central Arctic FY ice
(7, 7) Norwegian Sea—Ice-free ocean

For the Canadian Basin—Grid (3, 4) (Figure 4.8), the calculated ice concentrations are close to 100 percent. The standard deviation is typically on the order of a few percent. Again, we find no long-term trend.

For Baffin Bay—Grid (3, 7) (Figure 4.9), the range of variation of the mean is not very different for Baffin Bay than it was for the Canadian Basin, but the standard deviations are considerably greater for each year. This is particularly true for December and January, the times of ice growth. Most of the variability in the ice concentration results again from ice growth during the months of December and January. For the midwinter months of February and March, there is no apparent long-term trend in the ice concentrations.

For the Kara Sea—Grid (6, 3) (Figure 4.10), the ice concentration curves are quite reasonable, with large standard deviations for some months, but these may be due to a few spurious data points.

In the Norwegian Sea—Grid (7, 7) (Figure 4.11), because of the weather filter in the algorithm, there is no information on sea ice concentration variability which, if present, would be presumably due to weather-related effects.

The approach used to compute the sensitivity coefficients follows that of Swift and Cavalieri (1985) and uses simulated radiometric brightness temperature data. Simulated brightness temperatures were generated using representative values of surface emissivities and ice temperatures. The computed brightness temperatures were varied by ± 1 K and the calculation repeated to observe the effect on the computed ice parameters. Results from this simulated data approach are given in Table 4.1. The sensitivity coefficients in Table 4.1 give the error associated with the computed sea-ice parameters, first-year ice concentration (C_{FY}), multiyear ice concentration (C_{MY}), and open water amount (C_W) for an error of 1.0 K in brightness temperature. Values are given for each channel used by the algorithm under conditions of both multiyear ice and first-year ice cover. The total root-sum-squared sensitivity is also given for each parameter. These coefficients may also be used to obtain an estimate of the errors incurred by variations in the radiometric properties of the ice surface, for example, variations in first-year or multiyear ice types.

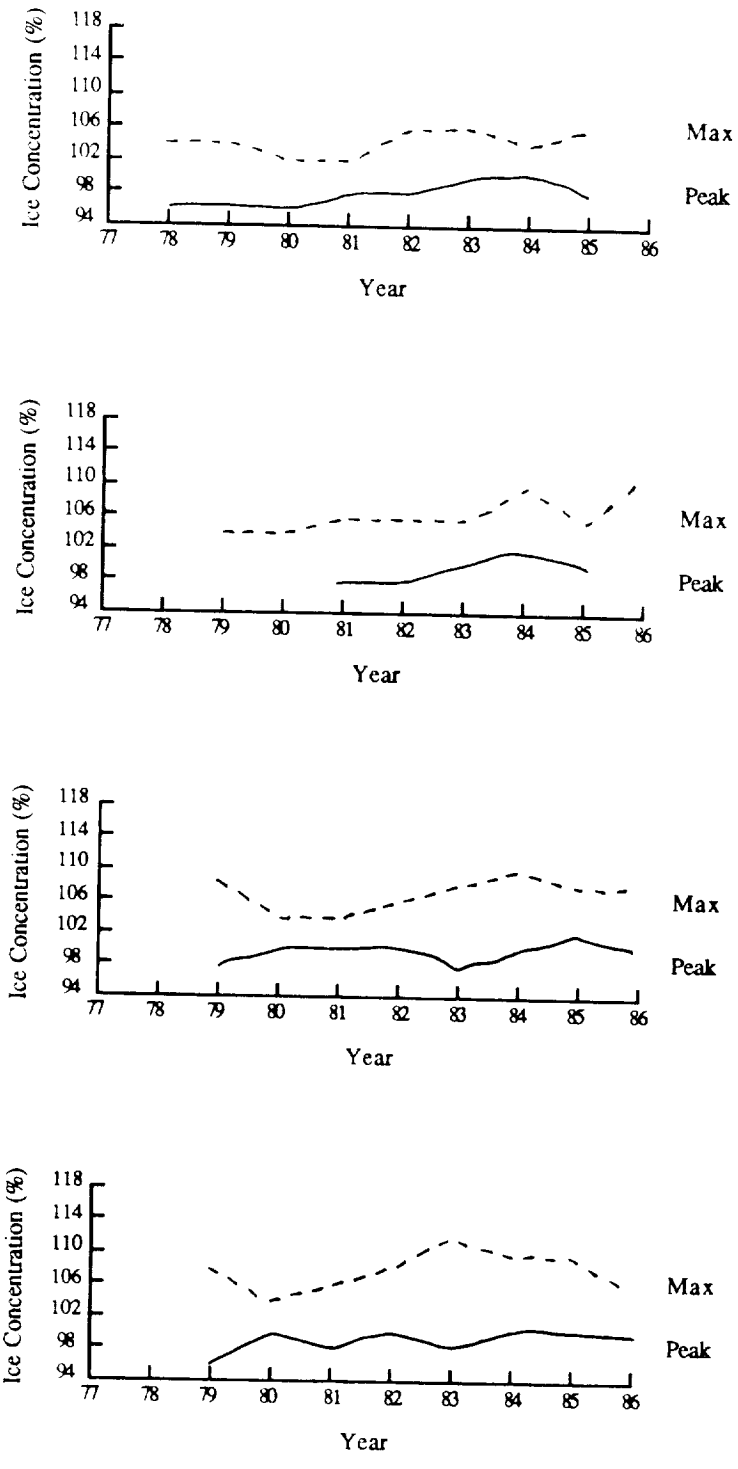

Figure 4.6. Histogram statistics based on monthly averaged sea-ice concentrations.

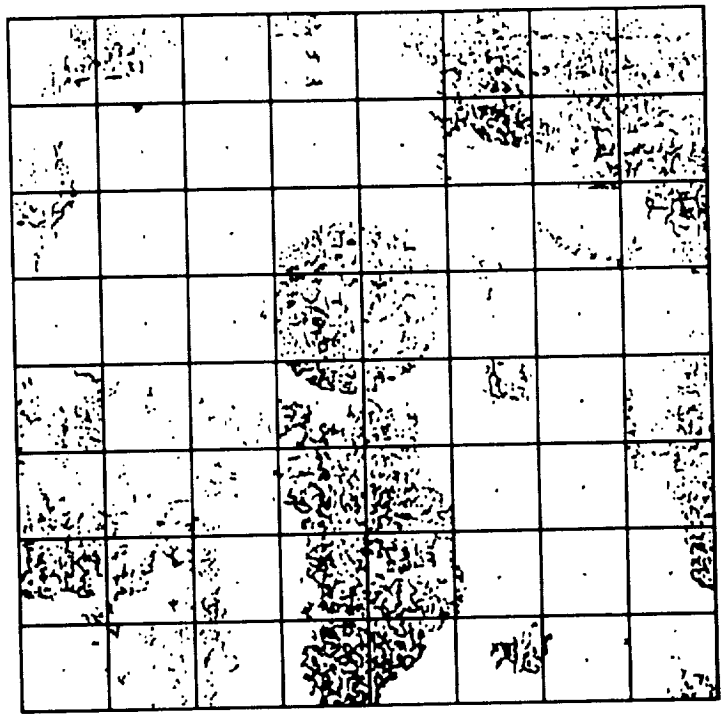

Figure 4.7. Arctic analysis grid.

Table 4.1

Algorithm Sensitivity Coefficients Calculated Using the Simulated Data Approach With an Assumed Error of ± 1 K for T_B

	δC_{FY}	δC_{MY}	δC_W
Goddard Algorithm			
	First-Year Ice		
δT_{18H} (±1.0K)	±0.040	±0.020	±0.020
δT_{18V} (±1.0K)	±0.067	±0.050	±0.017
δT_{37V} (±1.0K)	±0.029	±0.031	±0.002
$[\Sigma(\delta T_B)^2]^{1/2}$	±0.083	±0.062	±0.026
	Multiyear Ice		
δT_{18H} (±1.0K)	±0.030	±0.011	±0.019
δT_{18V} (±1.0K)	±0.049	±0.033	±0.016
δT_{37V} (±1.0K)	±0.025	±0.027	±0.002
$[\Sigma(\delta T_B)^2]^{1/2}$	±0.063	±0.044	±0.025

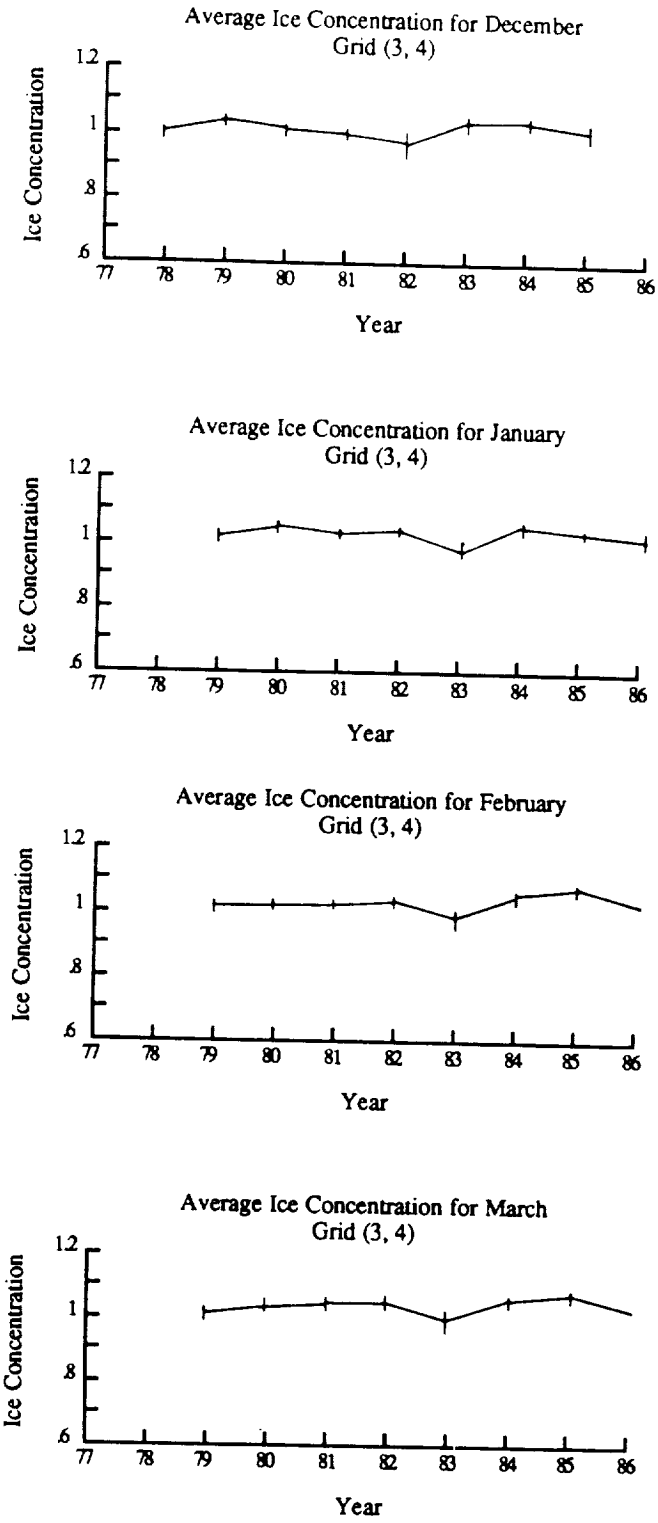

Figure 4.8. Time series of calculated monthly mean sea-ice concentrations and standard deviations for grid element (3, 4).

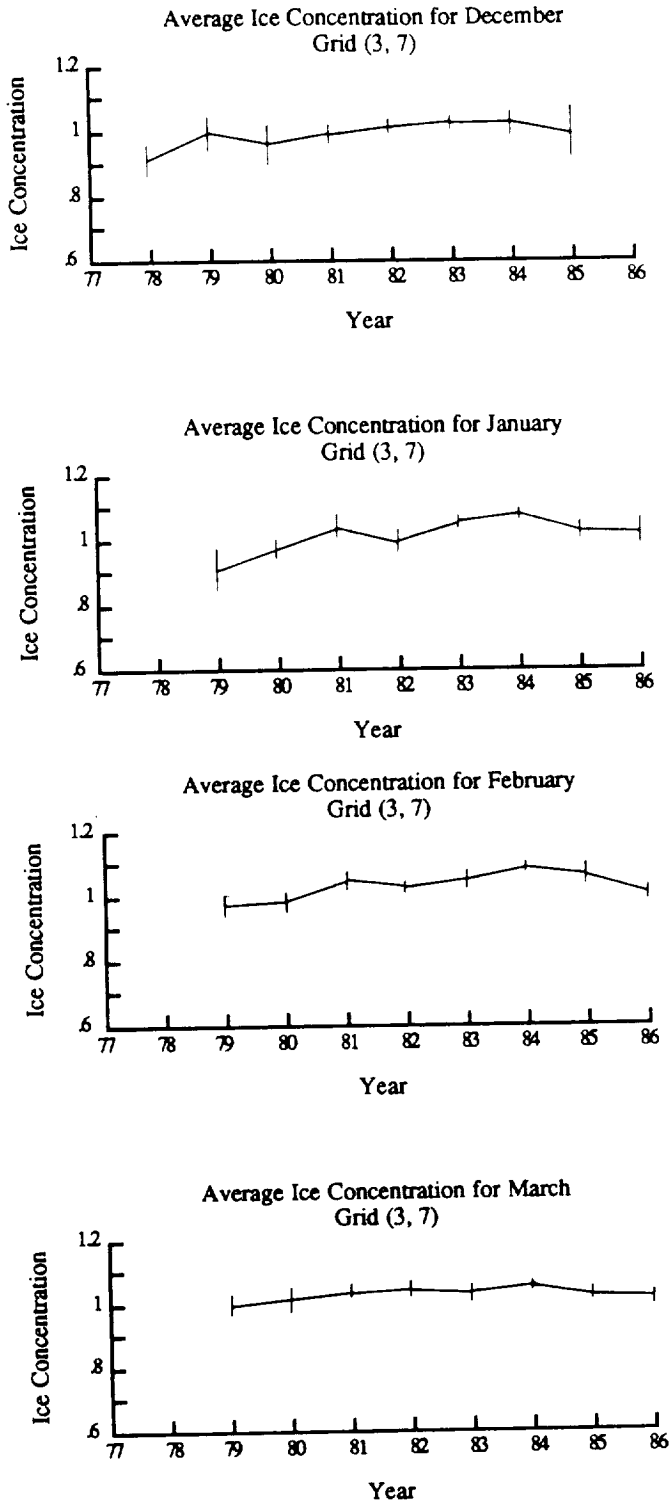

Figure 4.9. Time series of calculated monthly mean sea-ice concentrations and standard deviations for grid element (3, 7).

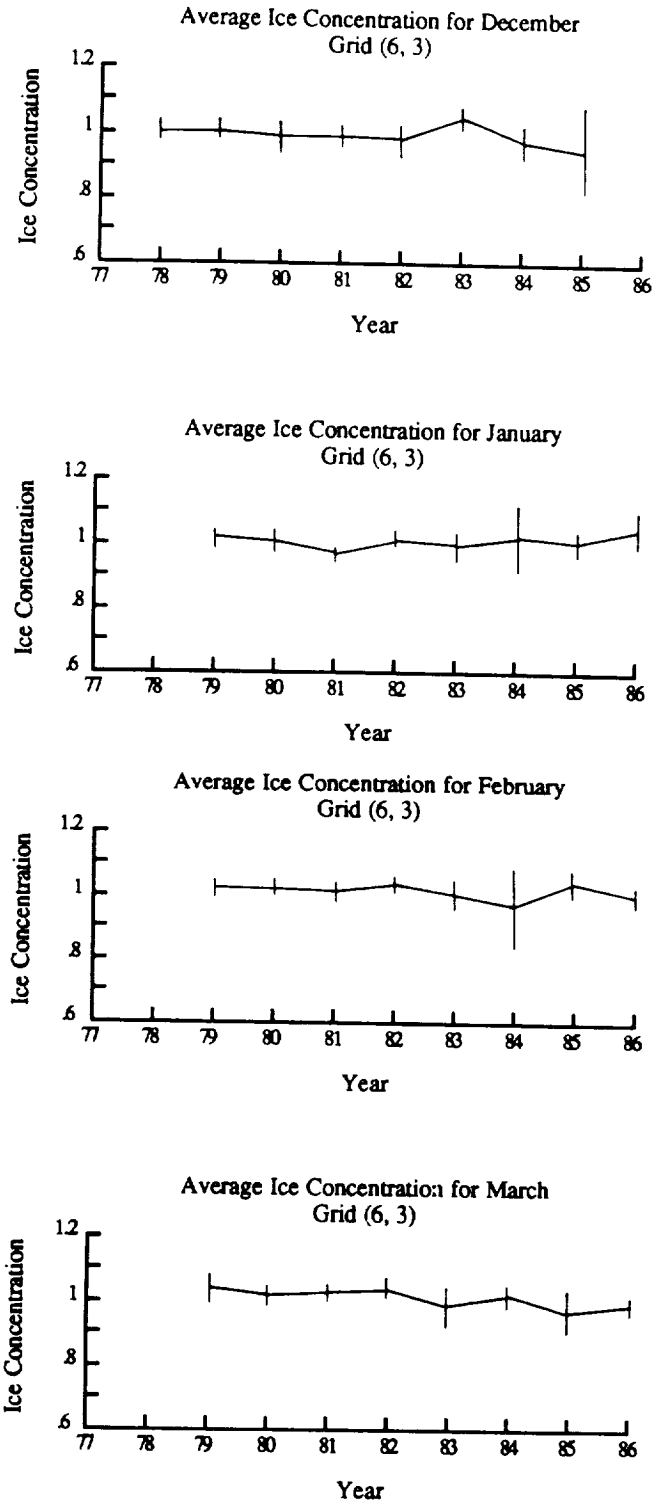

Figure 4.10. Time series of calculated monthly mean sea-ice concentrations and standard deviations for grid element (6, 3).

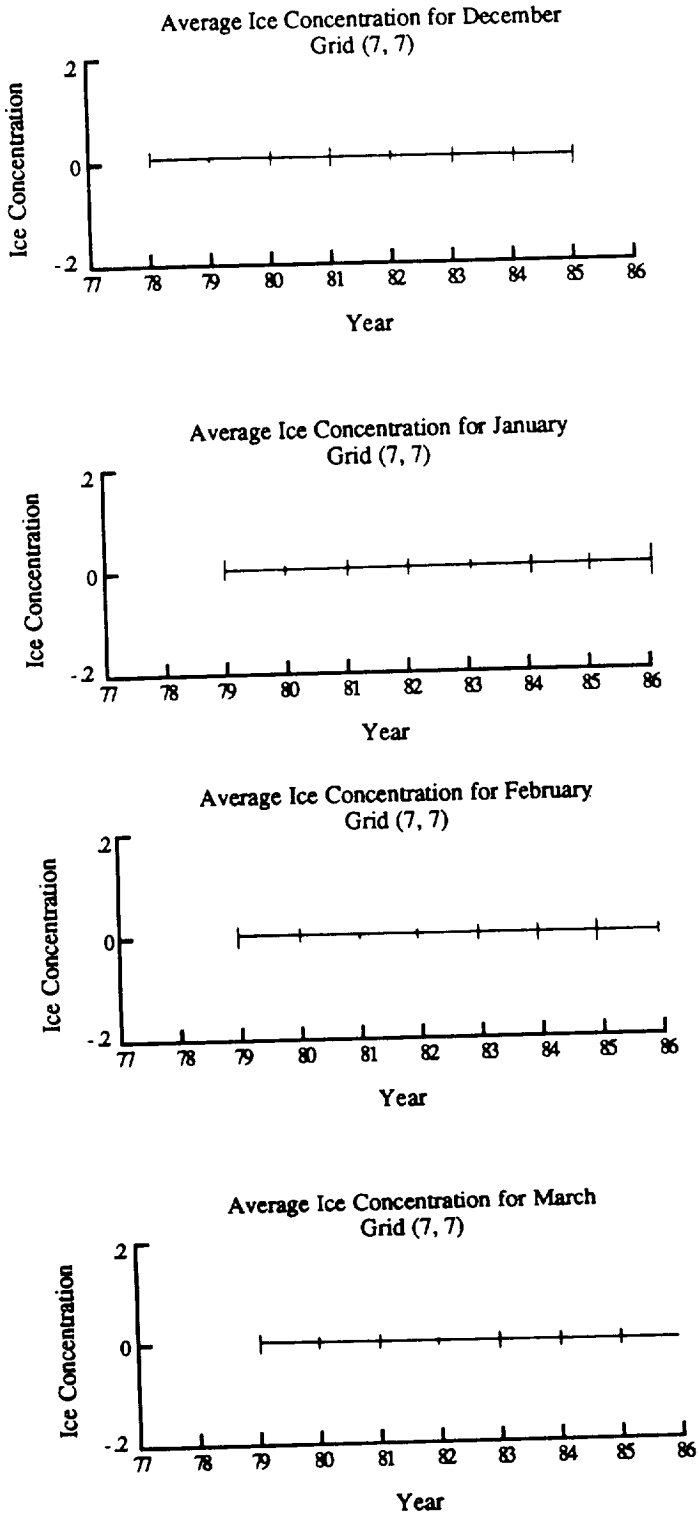

Figure 4.11. Time series of calculated monthly mean sea-ice concentrations and standard deviations for grid element (7, 7).

The sea-ice concentration is calculated at a spatial resolution of 60 km, based primarily on the 18.0-GHz polarization. Analysis of the total ice-concentration histograms for the first 11 months of SMMR operation shows that for winter months the ice peak is generally centered within 2 percent of the 100 percent concentration point. The half-width at half-maximum of the ice peaks range from 4 percent to 6 percent. During the summer months, the peak concentrations are lower and the width broader.

The ocean peak is centered at about 4 percent and is broader than the ice peak because of atmospheric and ocean surface roughness effects. Both from an analysis of the variance of ice concentration across the central Arctic and from the measured width of the histogram ice peak, an estimate of 5 to 9 percent is obtained for the relative accuracy of total ice concentration (Cavalieri et al., 1984).

4.3 Multiyear Ice Concentration—Accuracy Estimates

Although histograms of the multiyear fraction are more difficult to assess because of the greater spatial variability of this parameter in the central Arctic, some limits on the relative accuracy of the retrievals may be obtained from a comparison of histograms from two regions. The first is a region in the Canadian Arctic known to have a high fraction of multiyear ice cover; the second is a region in the Kara Sea, an area known to be largely free of multiyear ice. The histograms of ice fractions for these two regions are shown in Figures 4.12 and 4.13. The distribution of the Canadian Arctic multiyear ice fraction shown in Figure 4.12 is centered at 90 percent, has a mean value of 89 percent, and a standard deviation of 8 percent. The 8 percent standard deviation implies that 95 percent of the population will be within about 13 percent of the mean, assuming a normal distribution.

The first-year ice distribution shown for the Kara Sea in Figure 4.13 has a mean of 94 percent, which implies a multiyear ice fraction of 6 percent. Also, extensive regions in seasonal sea-ice zones (where first-year ice predominates) exhibit, at times, multiyear ice fractions as great as 15 percent. Less extensive areas, such as in Hudson and Baffin bays, regions known to be free of multiyear ice, do occasionally show values as large as 25 percent, probably due to strong variability in the amount of snow cover as well as to the metamorphosis of the snow crystals themselves. On the basis of these data, we estimate that the precision or relative accuracy of the multiyear fraction is 15–25 percent. As previously noted, only independent observations can provide a measure of the absolute accuracy of these retrievals.

4.4 Sea-Ice Temperature

The quality of the calculated sea-ice temperature is difficult to assess at this time, primarily because the set of measurements of sea-ice temperature corresponding to the radiating portion of the ice is extremely limited. Until coincident observations become available, the best we can do is to compare the calculated sea-ice temperatures with in situ surface air temperatures obtained from meteorological stations and with in situ temperatures obtained from the Arctic Ocean Buoy Program (Thorndike and Colony, 1979). The calculated SMMR ice temperatures and the surface

temperatures obtained from the Arctic Ocean Buoy data set, which combine temperatures from both stations and buoys, are presented in Figures 4.14 and 4.15, respectively, for February 1–5, 1979.

Comparison of the two temperature fields shows similarities in the large-scale features. Both maps show minimum temperatures located in the Canadian Archipelago region. Both maps also show the warmest temperatures located in the Greenland and Norwegian seas' marginal ice zones as well as in the Chukchi Sea. The SMMR data show a band of relatively warm (250 K) temperatures stretching across the pole along the 0°–180° meridian with a branch following the 75° N latitude circle in the Beaufort Sea. These regions of relatively warm SMMR ice temperatures are associated with relatively low ice concentrations (Cavalieri et al., 1984).

The SMMR temperatures are generally warmer and do not exhibit as great a range across the Arctic as do those from the buoy data set. Since the SMMR temperatures represent values close to the snow/ice interface temperature or to some weighted mean portion of the ice, it is not surprising that these temperatures are 10–15 K greater than the in situ temperatures, which presumably reflect more closely the surface temperature.

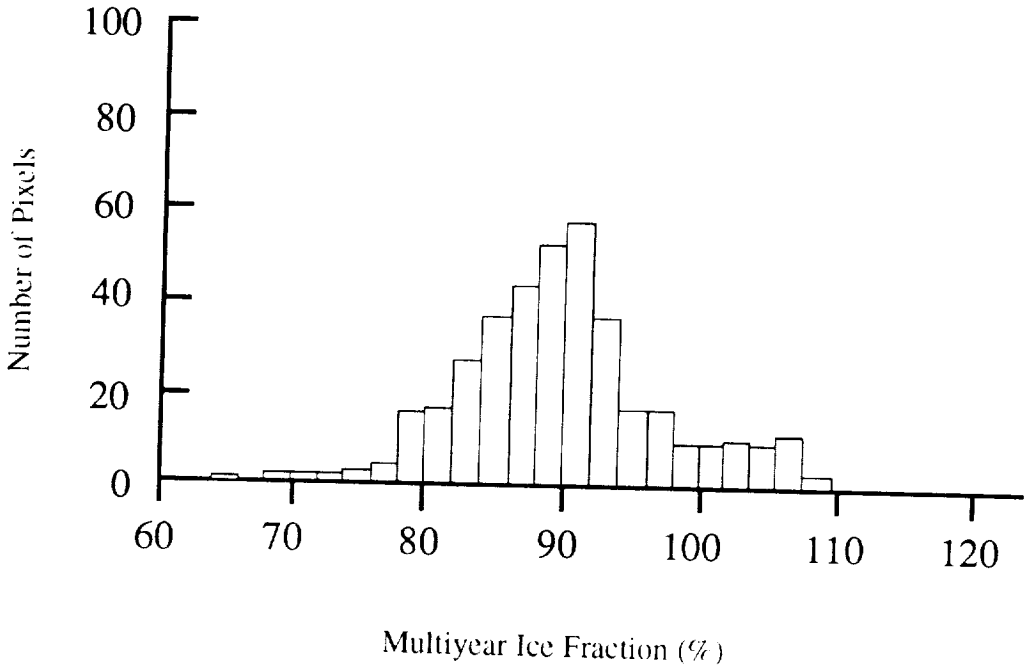

Figure 4.12. Histogram multiyear ice fraction for Canadian Arctic.

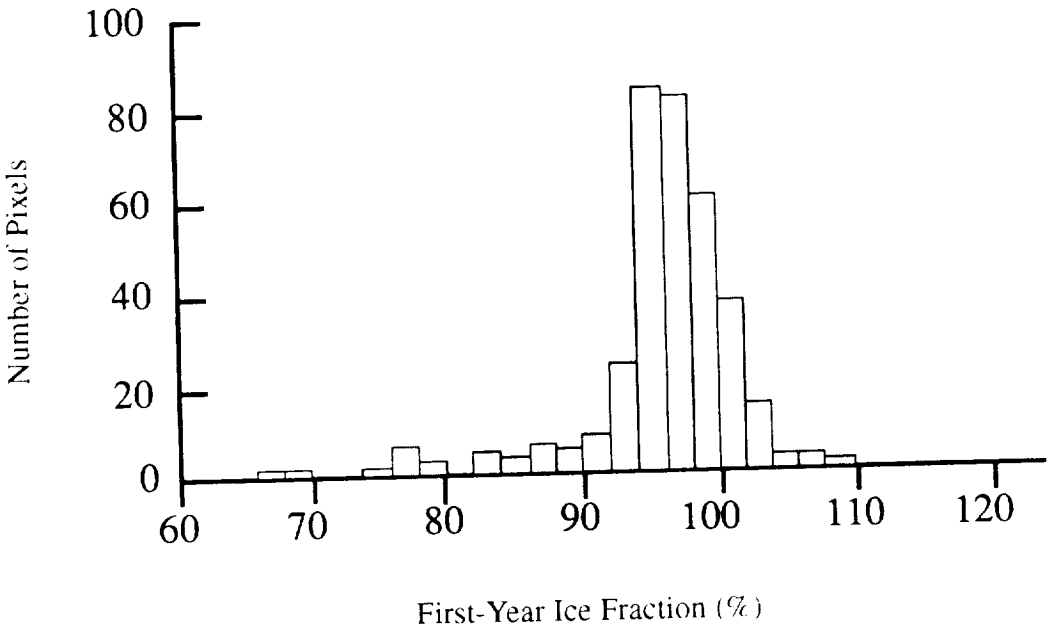

Figure 4.13. Histogram of multiyear ice fraction for Kara Sea.

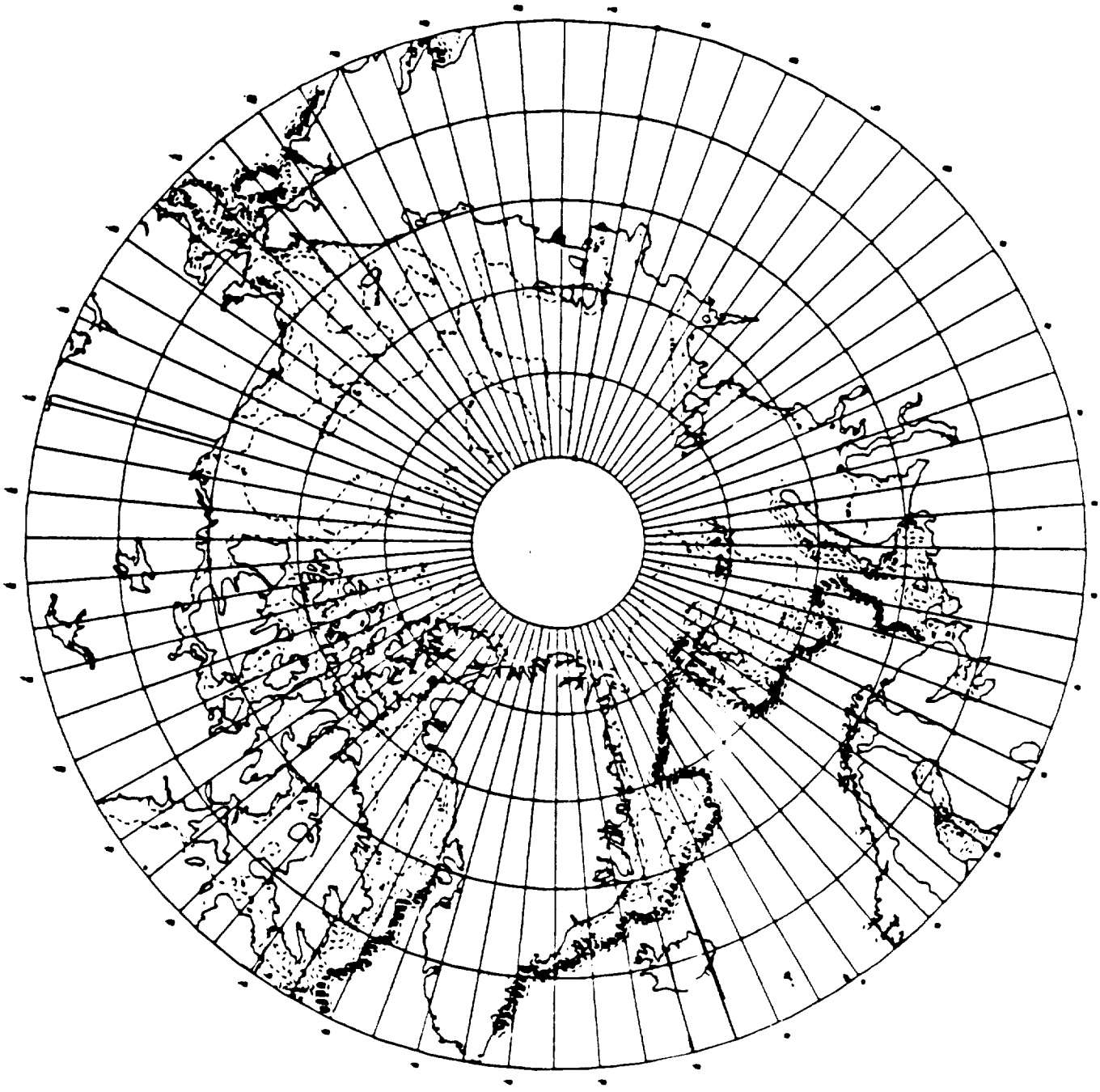

Figure 4.14. SMMR calculated ice temperature, February 1–5, 1979.

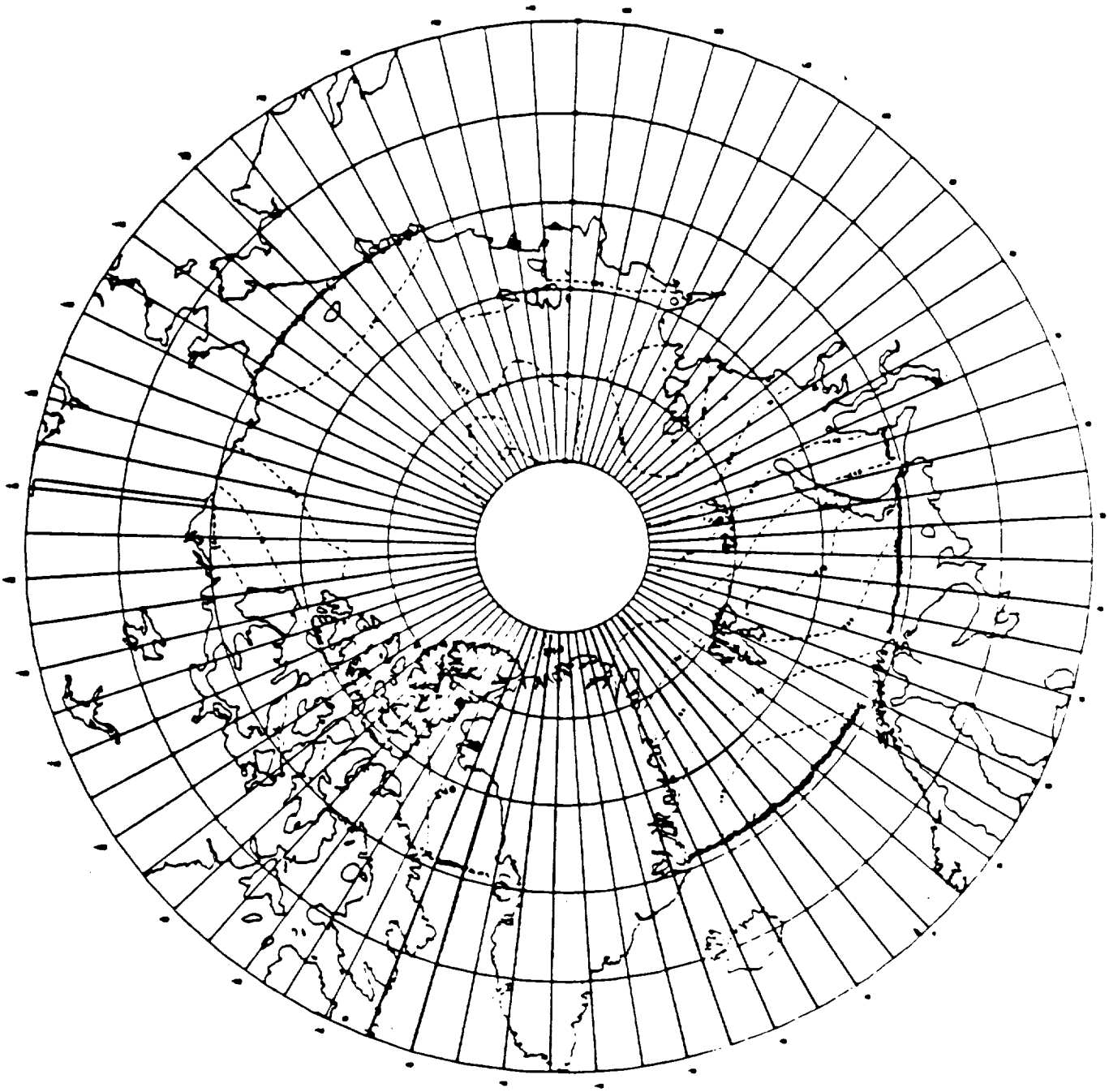

Figure 4.15. Arctic buoy reported surface temperature, February 1–5, 1979.

5. SEA-SURFACE WINDSPEED

5.1 Algorithm

A statistical approach similar to the one developed by Wilheit and Chang (1980) was used to derive the sea-surface wind retrieval algorithm. It started with a statistical ensemble of geophysical parameter sets of atmospheric temperature profile, relative humidity profile, surface temperature, surface windspeed, and column density of cloud liquid water contents. Each parameter in the set was chosen randomly within reasonable limits. For example, the temperature lapse rate was chosen between 5 and 7 °C/km, and the relative humidity was chosen between 0 and 100 percent. The instrument field-of-view was assumed to be partially filled with cloud. The fraction of field-of-view being covered with cloud was also randomly chosen. For each set of geophysical parameters, brightness temperatures at frequencies of SMMR observation were calculated using the same radiative transfer models as used by Wilheit (1978, 1979).

A multiple linear regression technique was employed to derive the equations relating windspeed and brightness temperature from the ensemble of simulated brightness temperatures. The 10.7-GHz and 37-GHz channel brightness temperatures and ratios of these brightness temperatures were chosen to be the independent variables in the regression. The resulting retrieval equation is as follows:

$$\begin{aligned} W \;=\; & -23.74\,(T_{10.7H} - 285) / (T_{10.7V} - 285) - 6.055\,(T_{37H} - 285) / (T_{37V} - 285) \\ & - 73.57\,(T_{10.7V} - T_{10.7H}) / (T_{10.7V} + T_{10.7H}) + 0.5142\,T_{10.7H} - 0.2308\,T_{37V} + 66.57, \end{aligned} \tag{83}$$

where

T_{fV} and T_{fH} are the vertical and horizontal component of the brightness temperatures at frequency f.

This algorithm was used to derive the SMMR windspeed from Year-2 through Year-7 (no Year-1 windspeed data were generated). The retrieval was performed only when there was no rain or ice in the field-of-view of SMMR. No windspeed was derived in areas within 600 km from land because of possible contamination of the radiances from land mass through the antenna side lobes. However, it was later determined that only the data very close to land were affected by the land contamination. The SMMR windspeed was, therefore, generated for all ocean areas from Year 6 on, but the user should use discretion in using data from areas close to land.

The retrieved windspeed W must be adjusted to compensate for the discrepancy between the observed and the predicted characteristics of SMMR brightness temperatures. Using the coincident ship and buoy reports of Year 1979 as the ground truth for the SMMR retrievals, the adjusted windspeed W' was derived to be

$$W' = 1.71\,W - 7.52. \tag{84}$$

It should be noted that the above correction formula was not applied in the derivation of SMMR windspeeds.

5.2 Comparison With Surface Reports

The retrieved windspeeds were compared with the coincident windspeed reports from ships and buoys. The criteria for an SMMR observation and a surface report to be coincident were that the observation and the report time be within 1.5 hours and that the distance between the location of the report and the center of the SMMR footprint be within 50 km. The retrieval was performed only when there was no rain in the field-of-view of SMMR. A threshold value of 37-GHz horizontal brightness temperature (184 K) was used as a filter to screen the raining cases. SMMR data within 600 km from land were not used because of the contamination of the brightness temperatures from land mass through antenna side lobes. More than 8,000 pairs of coincident data each year were used for comparison. The majority of the surface reports came from merchant ships, most of which were located in the Northern Hemisphere. There were two anchored buoys and two stationary weather ships that were located more than 600 km away from land, and these four stations reported windspeed regularly for every hour or 3 hours, depending on the station reporting frequency. Since these station reports were provided continuously from fixed locations, it was possible to filter out questionable reports of large rates of change in windspeed. The four stations were all located in the Northern Hemisphere: three in the Pacific Ocean and one in the Atlantic Ocean. The latitudes and longitudes of these four stations are 41° N, 138° W; 50° N, 145° W; 52° N, 156° W; and 47° N, 17° W. For SMMR Year-1 and Year-2 data, a total of 517 pairs of coincident SMMR and buoy data were available for comparison. The retrieved windspeeds and their coincident buoy reports are plotted in Figure 5.1. Data were also averaged into bins of 2 m/sec intervals of buoy-reported windspeed. These averages and standard deviations are plotted in Figure 5.2. If there were fewer than 10 sample pairs in the interval, the representative point in the plot is circled. The average difference between the SMMR and the buoy windspeeds is close to zero; the standard deviation of the difference is under 2.5 m/sec. There are three cases where the difference is larger than 10 m/sec, due to possibly bad SMMR data. If these three cases are excluded, the standard deviation of the difference is reduced to 2.1 m/sec. Details of the statistics of the comparison are listed in Table 5.1.

Similar comparisons were performed for the SMMR-derived and the ship-reported windspeeds. The 10 m/sec upper limit of the difference of the two windspeeds, which was about three times the standard deviation of the difference, was used to eliminate possibly bad ship or SMMR data. Approximately 1 percent of the total sample population was excluded from the comparison. Separate statistics of the comparison were also computed for the 1979 and 1980 data. The results are very similar to one another, which show that the algorithm tuned to the 1979 data applied equally well to the 1980 data. The average windspeeds in 2 m/sec intervals are plotted in Figures 5.3 and 5.4 for 1979 and 1980 data, respectively. The standard deviation of the difference between the retrieved and the reported windspeeds is about 3 m/sec. The poorer quality of the ship data is believed to be the main reason for the larger standard deviation of difference between SMMR and ship windspeeds. The detailed statistics of comparison are described in Table 5.1.

The algorithm was further tested for its validity on data within different latitude bands. The total sample was divided according to location in latitude. Separate statistics were derived from data in each group of data. The results of comparison in various latitude zones are listed in Table 5.2. The variation of the average difference of windspeeds in different zones is within 1 m/sec. The

average SMMR windspeed and average difference of windspeeds in each 5-degree latitude band are plotted against latitude in Figure 5.5. It should be noted that most of the ship reports used for tuning of the algorithm came from the Northern Hemisphere, which may explain some of the difference in retrievals derived from Northern and Southern hemispheres.

Table 5.1

Comparison of SMMR-Retrieved Windspeeds With Ship and Buoy Reports of 1979 and 1980

	$\bar{S}$	σ_S	$\bar{G}$	σ_G	$\bar{D}$	σ_D	N
All coincident data	8.04	4.38	8.05	4.33	–0.01	3.38	16766
All data without $\|D\| > 10$	7.98	4.28	7.98	4.20	–0.00	3.04	16581
1979 data without $\|D\| > 10$	7.94	4.28	7.90	4.21	0.04	3.02	6971
1980 data without $\|D\| > 10$	8.01	4.28	8.04	4.19	–0.03	3.05	9610
Buoy data	8.33	4.21	8.33	3.72	–0.00	2.35	517
Buoy data without $\|D\| > 10$	8.24	4.06	8.33	3.73	–0.08	2.10	514

$\bar{S}$: Mean SMMR windspeed

$\bar{G}$: Mean-surface-reported windspeed

$\bar{D}$: $\bar{S} - \bar{G}$

σ : Standard deviation

N : Number of samples

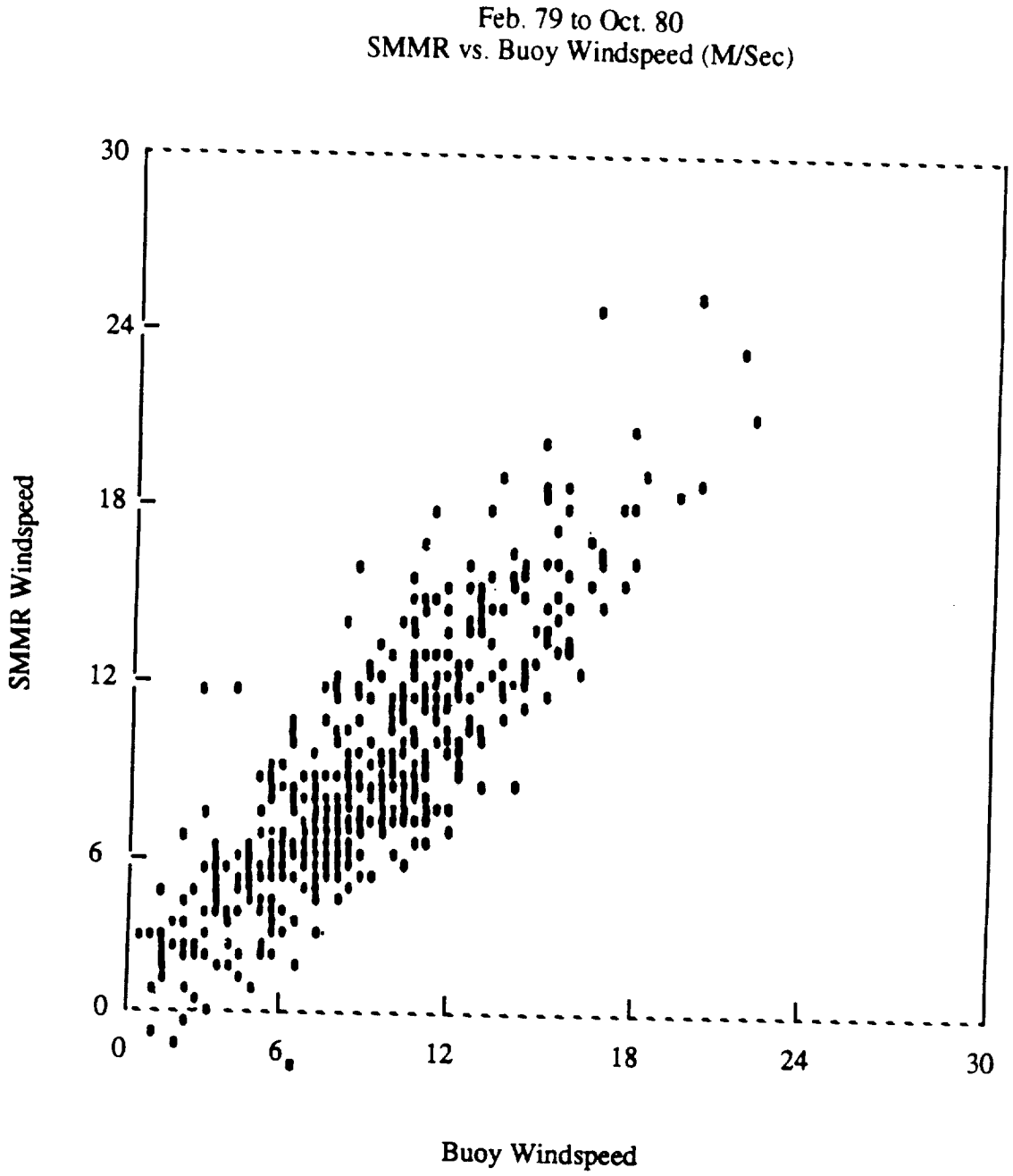

Figure 5.1. SMMR windspeed vs. buoy data (Feb. 1979–Oct. 1980).

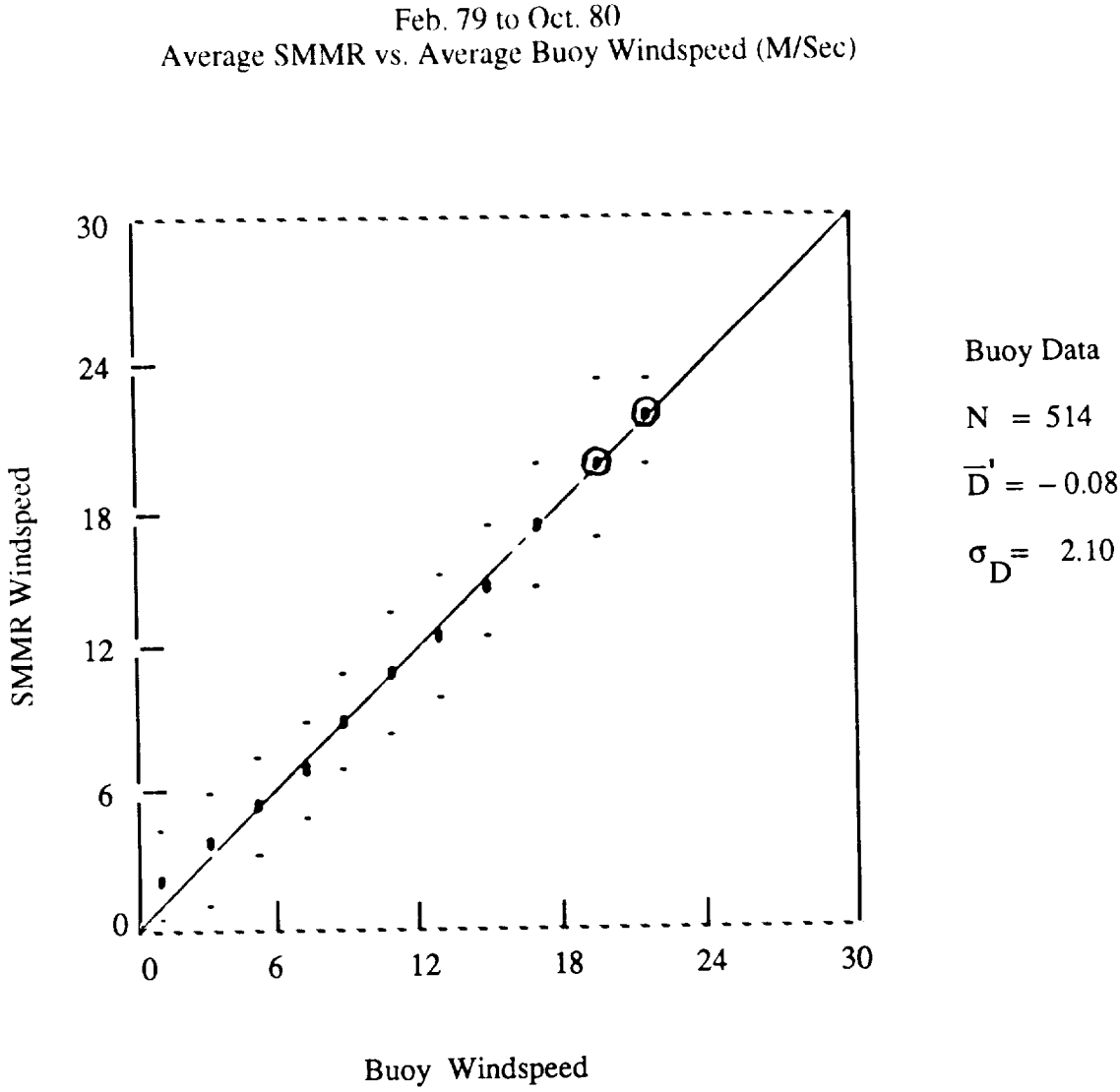

Figure 5.2. Average SMMR windspeed vs. average buoy windspeed (Feb. 1979–Oct. 1980).

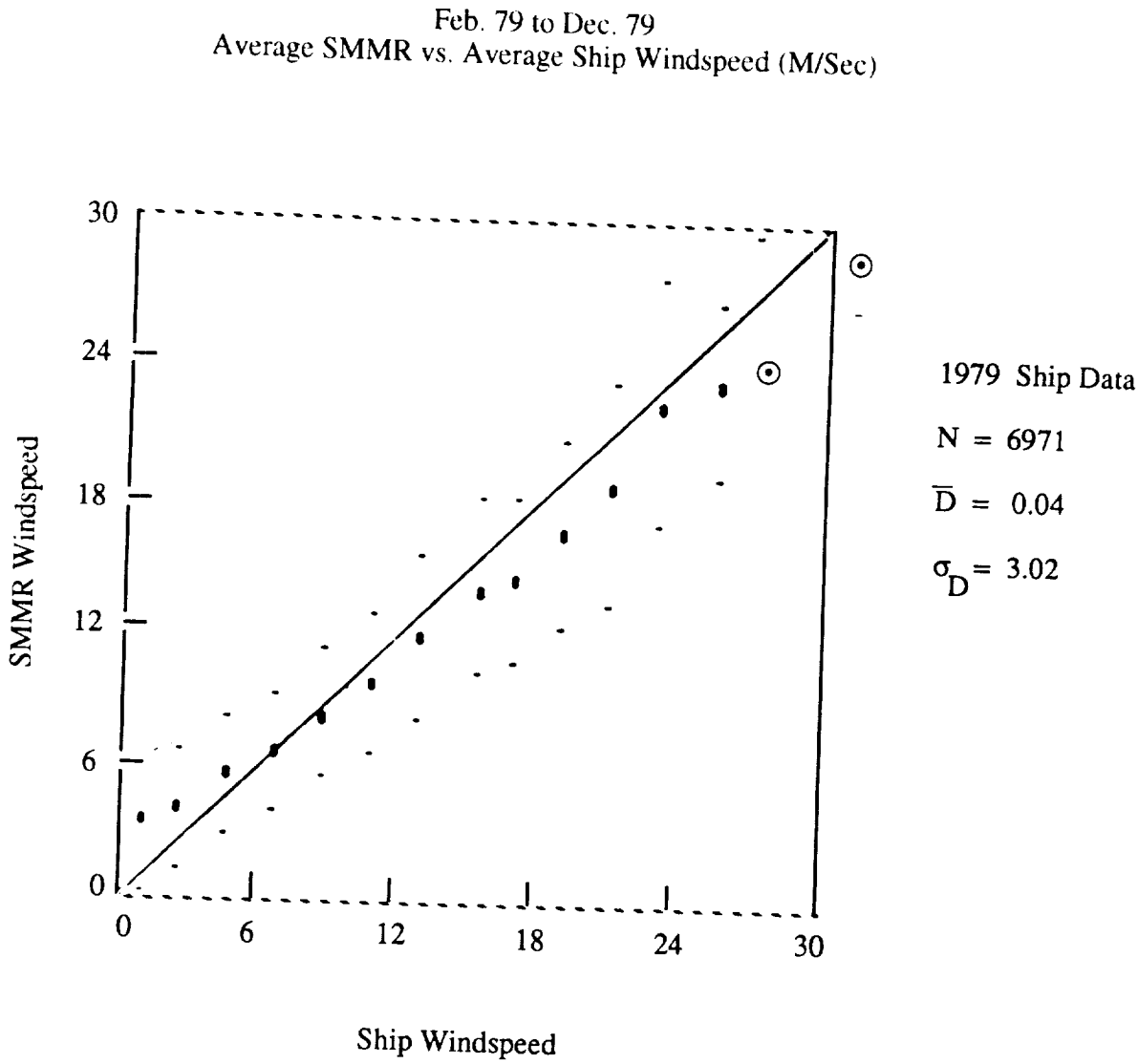

Figure 5.3. Average SMMR windspeed vs. average ship windspeed (Feb. 1979–Dec. 1979).

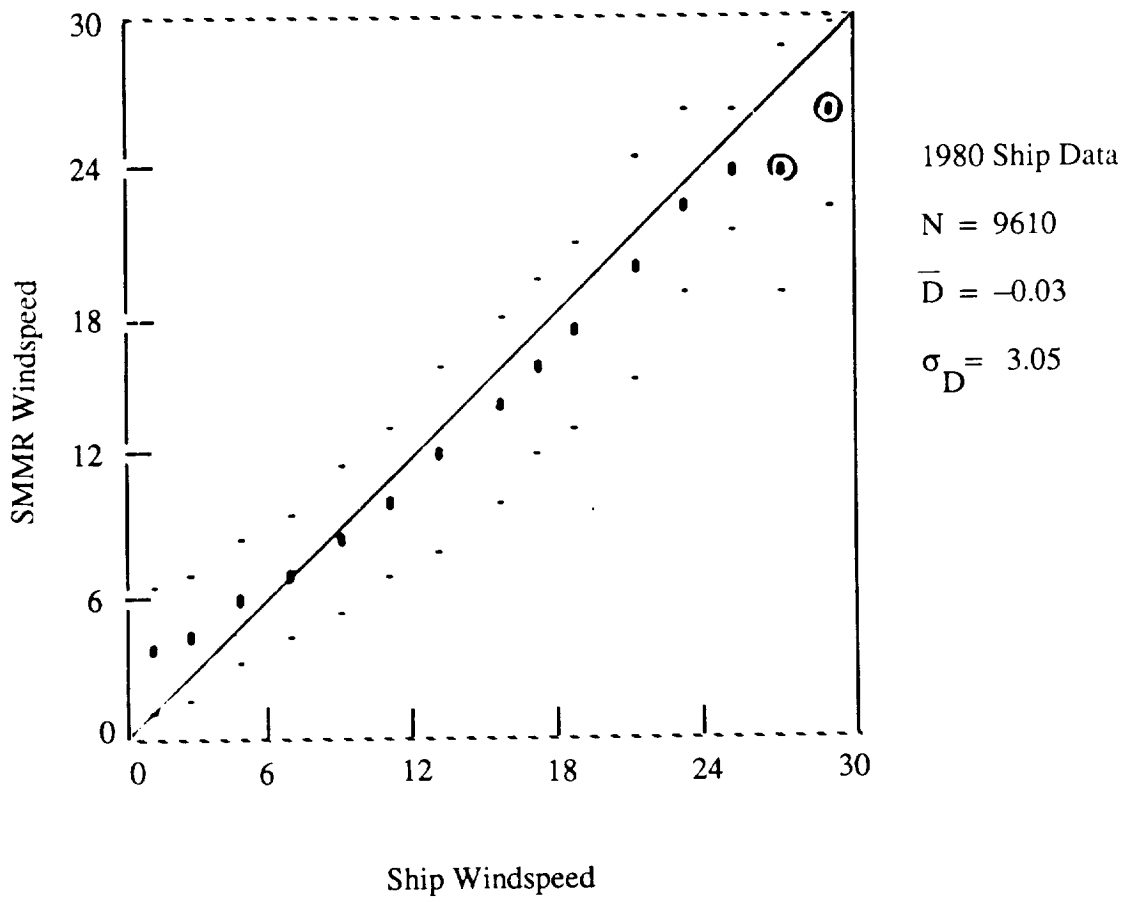

Figure 5.4. Average SMMR windspeed vs. average ship windspeed (Jan. 1980–Oct. 1980).

Table 5.2

Comparison of SMMR-Retrieved Windspeeds With Ship and Buoy Reports of 1979 and 1980 in Separate Latitude Bands

Latitude Region	$\bar{S}$	σ_S	$\bar{G}$	σ_G	$\bar{D}$	σ_D	N
60 N–45 N	9.02	4.67	9.01	4.58	0.01	3.16	3903
45 N–35 N	8.21	4.62	8.40	4.51	–0.19	3.12	4632
35 N–25 N	7.26	4.07	7.57	4.06	–0.30	2.96	2592
25 N–15 N	6.85	3.11	6.95	3.24	–0.10	2.67	1005
15 N–15 S	6.53	2.77	6.41	2.74	0.12	2.56	1987
15 S–35 S	7.69	3.48	7.14	3.37	0.55	2.98	1814
35 S–60 S	9.88	9.94	9.21	4.65	0.67	3.65	637

$\bar{S}$: Mean SMMR windspeed

$\bar{G}$: Mean ship-reported windspeed

$\bar{D}$: $\bar{S} - \bar{G}$, data with $|D| > 10$ are excluded

σ : Standard deviation

N : Number of samples

Feb. 79 to Oct. 80
Average SMMR and Average (SMMR-Ship) Windspeed (M/Sec) vs. Latitude

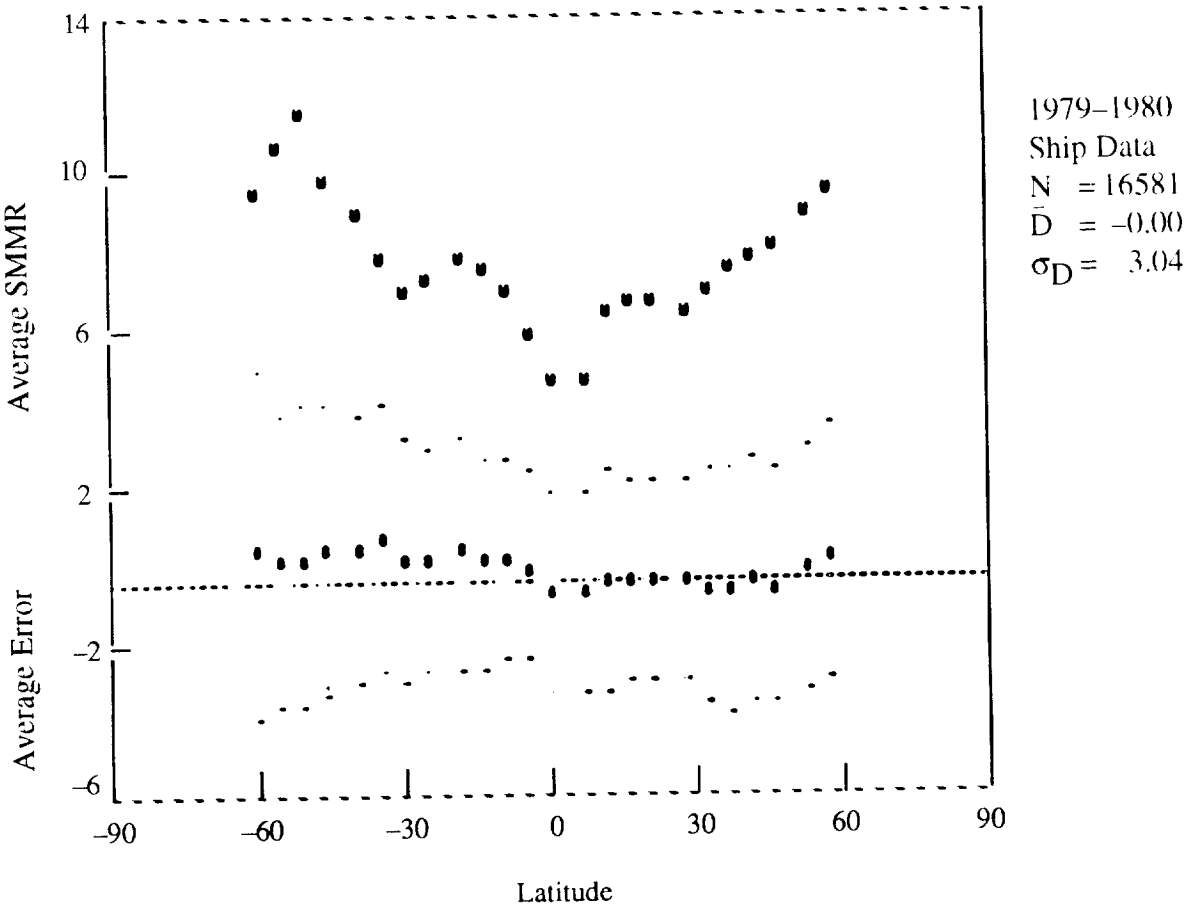

Figure 5.5. Average SMMR windspeed and average (SMMR-ship) windspeed vs. latitude (Feb. 1979–Oct. 1980).

Similar validations were performed for the SMMR windspeeds from Year 3 to Year 6. The number of available buoy reports dropped off significantly after 1981. Therefore, no statistically important samples were available for comparison. The results of comparisons for each month (daytime and nighttime data separately) from January 1979 to December 1984 are listed in Tables 5.3 through 5.11. The monthly mean differences between the SMMR and ship windspeeds are plotted in Figure 5.6, and the corresponding standard deviations of the difference are plotted in Figure 5.7. Except in January 1979, the monthly mean differences are consistent throughout the first 4 years. Starting from the 5th year, the difference increases, and there is a big increase during the 6th year. However, the standard deviation of the difference remains relatively uniform over the years.

The large increases in the retrieved windspeed in the 6th year may be understood in terms of the sensitivity of the windspeed retrieval algorithm to the input brightness temperatures. The results of the sensitivity analysis are shown in Table 5.12. The last column of the table lists the changes of retrieval values for a 1-degree increase of brightness temperature at the nominal temperature values listed in the third column. It shows that the algorithm is most sensitive to the change of the brightness temperature of the 10.7 H channel and is least sensitive to that of the 37 H channel. However, the observed abnormal behavior of the windspeed retrievals in the 6th year can by and large be explained by a combination of the increase of calibrated brightness temperatures for the 10.7 H channel and the decrease of those for the 10.7 V and 37 V channels.

The validation of Year-7 data is in progress but has not yet been completed. Corrective measures for the problem of calibration drift are also being studied.

Table 5.3

Comparison of SMMR and Ship Windspeeds (Daytime Data), 1979–1980

Month	W	σ_W	S	σ_S	D	σ_D	N	R
JAN. 79	7.59	5.14	8.41	4.36	–0.82	3.90	516	3.1
FEB. 79	9.77	4.37	8.70	4.47	1.07	3.07	417	1.2
MAR. 79	9.06	4.05	8.54	4.14	0.52	3.12	533	1.1
APR. 79	8.75	4.43	8.07	4.43	0.68	2.94	490	1.2
MAY 79	8.07	3.32	7.63	3.94	0.44	2.88	456	0.4
JUNE 79	7.37	3.15	7.15	3.50	0.22	2.76	449	0.7
JULY 79	6.20	3.16	6.46	3.16	–0.26	2.90	502	1.0
AUG. 79	6.71	3.41	7.07	3.52	–0.37	2.69	485	0.8
SEPT. 79	7.54	3.51	7.39	3.81	0.15	2.70	456	0.7
OCT. 79	9.25	4.67	9.34	5.29	–0.09	3.01	427	0.9
NOV. 79	9.33	4.13	8.75	4.24	0.58	3.16	403	0.7
DEC. 79	9.86	5.35	9.28	5.23	0.58	3.10	404	1.2
JAN. 80	9.18	4.29	8.96	4.49	0.23	3.01	605	1.5
FEB. 80	10.26	5.29	9.56	5.08	0.70	3.07	613	1.5
MAR. 80	8.82	4.17	8.44	4.21	0.39	3.03	755	0.9
APR. 80	8.35	3.75	7.82	3.87	0.52	2.92	638	0.6
MAY 80	7.98	3.87	7.86	3.94	0.11	3.11	699	1.3
JUNE 80	6.81	3.27	6.86	3.48	–0.05	2.96	589	1.0
JULY 80	7.36	3.66	7.05	3.46	0.31	2.96	624	0.3
AUG. 80	7.24	3.38	7.26	3.55	–0.02	2.96	611	1.1
SEPT. 80	7.41	3.56	7.69	3.81	–0.28	3.00	596	0.5
OCT. 80	9.38	4.50	9.15	4.78	0.24	3.26	605	1.0
NOV. 80	10.69	5.33	9.90	5.14	0.78	3.08	499	1.6
DEC. 80	10.12	4.63	9.47	4.70	0.65	3.31	579	1.0

W : Mean SMMR-derived windspeed
S : Mean ship-reported windspeed
D : W–S, data with $|D| > 10$ were excluded
σ : Standard deviation
N : Number of sample
R : Percentage of sample excluded

Table 5.4

Comparison of SMMR and Ship Windspeeds (Daytime Data), 1981–1982

Month	W	σ_W	S	σ_S	D	σ_D	N	R
JAN. 81	9.57	4.14	9.03	4.40	0.54	3.00	615	1.6
FEB. 81	9.94	4.69	9.81	4.77	0.13	3.43	554	1.8
MAR. 81	10.40	5.45	9.52	5.13	0.88	3.22	603	1.2
APR. 81	8.71	3.86	7.78	3.99	0.93	3.00	621	1.1
MAY 81	8.23	3.72	7.45	3.74	0.77	3.08	721	0.4
JUNE 81	7.69	3.19	7.22	3.21	0.46	2.89	552	1.1
JULY 81	7.26	3.21	6.76	3.19	0.50	2.90	508	0.8
AUG. 81	7.04	3.36	6.61	3.34	0.44	2.76	430	0.2
SEPT. 81	7.93	3.65	7.67	3.97	0.26	2.81	606	0.3
OCT. 81	8.49	3.66	8.14	4.13	0.35	2.94	562	0.4
NOV. 81	9.07	4.25	8.72	4.08	0.35	2.98	630	1.6
DEC. 81	9.89	4.49	9.24	4.69	0.65	3.05	630	0.5
JAN. 82	9.74	4.86	9.25	4.87	0.49	2.88	412	1.7
FEB. 82	9.29	4.46	8.72	4.50	0.57	3.26	497	2.2
MAR. 82	9.36	4.40	9.04	4.53	0.32	3.17	493	1.4
APR. 82	8.60	3.84	7.73	3.68	0.88	2.96	510	1.4
MAY 82	8.45	3.50	7.61	3.78	0.84	2.95	515	1.0
JUNE 82	8.30	4.01	7.49	3.98	0.81	2.94	473	1.5
JULY 82	7.12	3.29	7.04	3.50	0.08	2.62	456	0.7
AUG. 82	7.11	3.54	6.80	3.37	0.32	2.89	341	0.6
SEPT. 82	8.50	3.46	7.81	3.90	0.69	2.90	445	1.3
OCT. 82	9.72	4.03	8.47	4.40	1.25	3.02	488	2.5
NOV. 82	10.89	5.06	9.18	4.88	1.71	3.16	374	2.7
DEC. 82	11.00	4.87	9.61	4.89	1.39	3.11	396	0.8

W : Mean SMMR-derived windspeed
S : Mean ship-reported windspeed
D : W–S, data with $|D| > 10$ were excluded
σ : Standard deviation
N : Number of sample
R : Percentage of sample excluded

Table 5.5

Comparison of SMMR and Ship Windspeeds (Daytime Data), 1983–1984

Month	W	σ_W	S	σ_S	D	σ_D	N	R
JAN. 83	11.71	5.55	10.49	5.40	1.22	3.68	801	3.2
FEB. 83	11.11	4.99	9.59	4.83	1.52	3.14	525	2.7
MAR. 83	11.26	4.97	9.45	4.55	1.81	3.22	296	1.7
APR. 83	9.61	4.13	9.13	4.27	0.48	3.19	534	1.3
MAY 83	8.84	3.60	8.22	3.63	0.63	3.03	579	0.7
JUNE 83	9.19	3.67	7.90	3.77	1.28	3.04	416	1.0
JULY 83	9.20	3.34	7.55	3.66	1.65	2.92	489	0.6
AUG. 83	8.40	3.09	7.18	3.51	1.21	2.96	516	1.2
SEPT. 83	9.60	4.25	8.47	4.37	1.14	3.01	470	1.3
OCT. 83	10.45	3.81	8.47	3.82	1.98	3.04	494	1.2
NOV. 83	12.17	4.88	10.49	4.88	1.68	3.13	446	2.0
DEC. 83	10.74	4.58	9.10	4.67	1.64	2.83	476	1.7
JAN. 84	13.06	5.39	10.00	5.43	3.06	3.15	503	3.8
FEB. 84	12.14	4.55	8.77	4.64	3.37	2.73	544	3.1
MAR. 84	12.47	4.90	8.71	4.92	3.75	2.90	570	6.0
APR. 84	12.61	4.01	8.61	4.16	4.00	2.88	485	3.7
MAY 84	11.09	2.96	7.34	3.68	3.75	2.72	433	3.7
JUNE 84	10.89	3.10	7.17	3.65	3.72	2.72	479	1.7
JULY 84	10.51	2.85	6.88	3.34	3.63	2.56	481	1.7
AUG. 84	10.56	3.05	6.56	3.20	4.00	2.50	252	2.0
SEPT. 84	11.44	3.34	7.86	3.93	3.58	2.94	480	2.7
OCT. 84	12.39	3.65	8.80	4.27	3.59	3.08	562	2.7
NOV. 84	13.76	4.52	9.88	4.66	3.88	2.92	577	3.3
DEC. 84	13.55	4.55	9.79	4.83	3.76	2.90	501	3.4

W : Mean SMMR-derived windspeed
S : Mean ship-reported windspeed
D : W–S, data with $|D| > 10$ were excluded
σ : Standard deviation
N : Number of sample
R : Percentage of sample excluded

Table 5.6

Comparison of SMMR and Ship Windspeeds (Nighttime Data), 1979–1980

Month	W	σ_W	S	σ_S	D	σ_D	N	R
JAN. 79	6.08	5.44	9.26	4.43	–3.18	3.62	300	3.7
FEB. 79	7.83	4.58	8.38	4.31	–0.55	3.03	194	1.0
MAR. 79	8.23	5.42	8.56	5.03	–0.32	3.22	172	1.2
APR. 79	6.71	3.98	7.32	4.02	–0.61	2.95	171	0.0
MAY 79	6.67	3.58	7.17	3.37	–0.49	3.02	144	3.5
JUNE 79	5.72	3.47	6.68	3.08	–0.96	3.36	148	0.7
JULY 79	5.59	2.94	6.65	2.98	–1.05	2.83	239	0.4
AUG. 79	5.78	3.61	6.80	3.55	–1.02	3.38	221	1.4
SEPT. 79	7.18	4.76	7.62	4.20	–0.44	2.75	200	3.0
OCT. 79	7.44	4.91	8.03	4.27	–0.59	2.91	140	2.1
NOV. 79	8.28	4.58	8.87	3.86	–0.59	3.28	159	1.3
DEC. 79	8.55	5.31	8.83	4.73	–0.28	2.92	161	0.6
JAN. 80	9.44	5.81	9.66	5.19	–0.22	3.49	324	2.8
FEB. 80	8.49	5.22	8.74	4.71	–0.24	3.11	298	2.3
MAR. 80	7.71	5.03	8.39	4.53	–0.68	3.14	400	1.5
APR. 80	8.49	4.78	9.10	4.47	–0.61	3.03	398	1.5
MAY 80	6.87	3.23	7.29	3.56	–0.42	2.82	344	0.0
JUNE 80	6.32	3.29	6.54	2.95	–0.23	2.83	303	2.3
JULY 80	5.95	3.36	6.84	3.20	–0.89	2.94	326	2.1
AUG. 80	5.48	3.14	6.61	3.32	–1.13	2.68	292	2.1
SEPT. 80	7.11	3.54	7.66	3.51	–0.55	2.93	298	1.0
OCT. 80	8.46	4.45	8.56	4.36	–0.10	2.85	292	0.0
NOV. 80	8.64	4.70	9.03	4.48	–0.40	3.08	265	2.6
DEC. 80	7.79	4.81	8.37	4.47	–0.58	2.99	296	1.4

W : Mean SMMR-derived windspeed
S : Mean ship-reported windspeed
D : W–S, data with $|D| > 10$ were excluded
σ : Standard deviation
N : Number of sample
R : Percentage of sample excluded

Table 5.7

Comparison of SMMR and Ship Windspeeds (Nighttime Data), 1981–1982

Month	W	σ_W	S	σ_S	D	σ_D	N	R
JAN. 81	8.05	4.83	8.67	4.61	–0.62	3.11	319	3.4
FEB. 81	9.60	5.45	9.47	4.67	0.13	3.46	389	1.5
MAR. 81	8.80	5.51	8.82	5.07	–0.02	3.46	381	2.6
APR. 81	7.90	4.19	8.21	4.25	–0.31	2.90	375	1.6
MAY 81	6.94	4.09	7.08	3.71	–0.14	3.16	308	1.0
JUNE 81	6.49	3.05	6.94	3.30	–0.45	2.78	317	0.6
JULY 81	6.18	3.28	6.39	3.05	–0.20	2.67	298	1.7
AUG. 81	5.96	3.05	6.89	3.13	–0.93	2.72	266	0.4
SEPT. 81	6.67	3.73	7.45	3.77	–0.79	2.84	344	0.6
OCT. 81	7.10	3.78	7.84	3.84	–0.74	3.05	310	2.3
NOV. 81	8.52	4.80	8.52	4.17	–0.00	3.44	303	3.0
DEC. 81	7.81	4.64	8.77	4.06	–0.95	3.45	349	2.9
JAN. 82	9.14	5.15	9.36	4.54	–0.22	3.30	250	1.6
FEB. 82	8.32	4.76	8.60	3.98	–0.28	3.31	220	0.5
MAR. 82	9.03	5.17	9.28	4.52	–0.25	3.08	260	0.8
APR. 82	7.54	4.02	8.00	3.65	–0.46	2.67	263	1.1
MAY 82	7.28	4.03	7.48	3.74	–0.20	2.82	191	1.6
JUNE 82	7.30	3.90	7.68	3.48	–0.39	3.03	221	1.4
JULY 82	6.16	3.12	6.63	3.07	–0.46	2.43	200	0.0
AUG. 82	6.56	3.13	7.13	3.08	–0.57	2.85	137	0.7
SEPT. 82	7.53	3.28	7.69	3.37	–0.16	2.57	180	0.0
OCT. 82	7.92	5.49	8.40	4.71	–0.47	2.97	202	2.0
NOV. 82	9.06	5.45	9.19	4.70	–0.14	3.35	213	0.5
DEC. 82	9.19	6.39	8.19	4.91	0.29	3.87	194	6.2

W : Mean SMMR-derived windspeed
S : Mean ship-reported windspeed
D : W–S, data with $|D| > 10$ were excluded
σ : Standard deviation
N : Number of sample
R : Percentage of sample excluded

Table 5.8

Comparison of SMMR and Ship Windspeeds (Nighttime Data), 1983–1984

Month	W	σ_W	S	σ_S	D	σ_D	N	R
JAN. 83	10.61	6.13	9.79	4.98	0.82	3.56	522	3.1
FEB. 83	10.43	6.41	10.18	5.14	0.25	3.66	251	0.8
MAR. 83	9.73	4.64	9.48	4.49	0.25	3.25	137	1.5
APR. 83	8.93	3.99	8.36	3.73	0.57	3.00	302	2.3
MAY 83	9.20	3.65	8.25	3.41	0.95	2.78	243	1.2
JUNE 83	8.38	3.79	7.63	3.64	0.75	2.83	258	1.2
JULY 83	7.97	3.19	7.52	3.04	0.45	2.84	258	1.9
AUG. 83	7.54	3.24	7.18	3.17	0.36	2.78	234	1.3
SEPT. 83	8.05	3.54	7.97	3.77	0.07	2.92	197	1.0
OCT. 83	9.06	3.95	8.80	3.75	0.26	3.19	244	0.8
NOV. 83	10.29	5.25	9.14	4.31	1.15	3.18	212	1.9
DEC. 83	10.39	5.85	9.05	4.42	1.35	3.39	247	5.3
JAN. 84	11.79	5.07	8.69	4.31	3.10	3.12	247	6.1
FEB. 84	12.72	4.57	8.44	4.34	4.28	2.91	246	5.3
MAR. 84	13.04	4.68	8.72	4.50	4.32	2.84	266	6.4
APR. 84	12.39	3.78	8.04	4.14	4.34	2.92	224	3.1
MAY 84	12.64	3.66	7.53	3.53	5.10	2.86	188	5.3
JUNE 84	11.30	2.89	6.51	2.94	4.79	2.53	224	5.4
JULY 84	10.69	3.50	6.59	3.34	4.10	2.83	229	3.1
AUG. 84	10.76	3.06	6.34	2.87	4.41	2.58	136	2.2
SEPT. 84	11.81	3.60	7.59	3.82	4.22	2.69	217	3.2
OCT. 84	13.01	4.30	9.02	4.27	3.99	2.96	228	6.1
NOV. 84	13.66	5.10	9.40	4.84	4.26	3.26	250	6.0
DEC. 84	12.26	4.72	8.57	4.31	3.69	3.57	288	6.6

W : Mean SMMR-derived windspeed
S : Mean ship-reported windspeed
D : W–S, data with $|D| > 10$ were excluded
σ : Standard deviation
N : Number of sample
R : Percentage of sample excluded

Table 5.9

Comparison of SMMR and Ship Windspeeds (Day/Nighttime Data), 1979–1980

Month	W	σ_W	S	σ_S	D	σ_D	N	R
JAN. 79	7.04	5.30	8.72	4.40	–1.69	3.96	861	3.3
FEB. 79	9.15	4.52	8.60	4.42	0.55	3.15	611	1.1
MAR. 79	8.85	4.43	8.54	4.37	0.31	3.16	705	1.1
APR. 79	8.22	4.41	7.88	0.34	0.34	2.99	661	0.9
MAY 79	7.74	3.43	7.52	3.81	0.22	2.94	600	1.2
JUNE 79	6.96	3.31	7.03	3.41	–0.07	2.96	597	0.7
JULY 79	6.00	3.10	6.52	3.10	–0.52	2.90	741	0.8
AUG. 79	6.42	3.50	6.99	3.53	–0.57	2.93	706	1.0
SEPT. 79	7.43	3.93	7.46	3.93	–0.03	2.72	656	1.4
OCT. 79	8.80	4.79	9.02	5.08	–0.21	2.99	567	1.2
NOV. 79	9.03	4.29	8.78	4.14	0.25	3.23	562	0.9
DEC. 79	9.49	5.37	9.15	5.09	0.34	3.07	565	1.1
JAN. 80	9.28	4.87	9.20	4.75	0.07	3.19	929	1.9
FEB. 80	9.68	5.33	9.29	4.98	0.39	3.11	911	1.8
MAR. 80	8.44	4.52	8.42	4.33	0.02	3.11	1155	1.1
APR. 80	8.40	4.17	8.31	4.16	0.09	3.01	1036	1.0
MAY 80	7.61	3.71	7.67	3.82	–0.06	3.03	1043	0.9
JUNE 80	6.64	3.28	6.75	3.31	–0.11	2.92	892	1.5
JULY 80	6.88	3.62	6.98	3.37	–0.10	3.00	950	0.9
AUG. 80	6.67	3.41	7.05	3.49	–0.38	2.92	903	1.4
SEPT. 80	7.31	3.56	7.68	3.71	–0.37	2.98	894	0.7
OCT. 80	9.08	4.50	8.96	4.65	0.13	3.13	897	0.7
NOV. 80	9.98	5.21	9.60	4.94	0.37	3.13	764	2.0
DEC. 80	9.33	4.82	9.09	4.65	0.23	3.25	875	1.1

W : Mean SMMR-derived windspeed
S : Mean ship-reported windspeed
D : W–S, data with $|D| > 10$ were excluded
σ : Standard deviation
N : Number of sample
R : Percentage of sample excluded

Table 5.10

Comparison of SMMR and Ship Windspeeds (Day/Nighttime Data), 1981–1982

Month	W	σ_W	S	σ_S	D	σ_D	N	R
JAN. 81	9.05	4.44	8.91	4.48	0.15	3.09	934	2.2
FEB. 81	9.80	5.02	9.67	4.73	0.13	3.44	943	1.7
MAR. 81	9.78	5.52	9.25	5.12	0.53	3.34	984	1.7
APR. 81	8.40	4.00	7.94	4.09	0.46	3.02	996	1.3
MAY 81	7.84	3.88	7.34	3.74	0.50	3.13	1029	0.6
JUNE 81	7.25	3.19	7.12	3.25	0.13	2.88	869	0.9
JULY 81	6.86	3.27	6.62	3.14	0.24	2.84	806	1.1
AUG. 81	6.63	3.28	6.71	3.26	–0.08	2.82	696	0.3
SEPT. 81	7.47	3.73	7.59	3.90	–0.12	2.86	950	0.4
OCT. 81	8.00	3.76	8.03	4.03	–0.03	3.03	872	1.0
NOV. 81	8.89	4.44	8.66	4.11	0.24	3.14	933	2.0
DEC. 81	9.15	4.65	9.07	4.48	0.08	3.29	979	1.3
JAN. 82	9.51	4.98	9.29	4.74	0.22	3.06	662	1.7
FEB. 82	8.99	4.57	8.68	4.35	0.31	3.30	717	1.7
MAR. 82	9.25	4.68	9.13	4.53	0.12	3.15	753	1.2
APR. 82	8.24	3.94	7.82	3.67	0.42	2.93	773	1.3
MAY 82	8.13	3.68	7.58	3.77	0.56	2.95	706	1.1
JUNE 82	7.98	4.00	7.55	3.83	0.43	3.02	694	1.4
JULY 82	6.83	3.26	6.91	3.38	–0.08	2.58	656	0.5
AUG. 82	6.95	3.43	6.89	3.29	0.06	2.90	478	0.6
SEPT. 82	8.22	3.44	7.77	3.76	0.44	2.83	625	1.0
OCT. 82	9.19	4.58	8.45	4.49	0.74	3.10	690	2.3
NOV. 82	10.22	5.27	9.18	4.81	1.04	3.34	587	1.9
DEC. 82	10.41	5.48	9.38	4.91	1.03	3.41	590	2.5

W : Mean SMMR-derived windspeed
S : Mean ship-reported windspeed
D : W–S, data with $|D| > 10$ were excluded
σ : Standard deviation
N : Number of sample
R : Percentage of sample excluded

Table 5.11

Comparison of SMMR and Ship Windspeeds (Day/Nighttime Data), 1983–1984

Month	W	σ_W	S	σ_S	D	σ_D	N	R
JAN. 83	11.28	5.81	10.21	5.24	1.06	3.64	1323	3.2
FEB. 83	10.89	5.49	9.78	4.94	1.11	3.36	776	2.1
MAR. 83	10.78	4.91	9.46	4.53	1.32	3.31	433	1.6
APR. 83	9.36	4.10	8.85	4.10	0.51	3.12	836	1.7
MAY 83	8.95	3.62	8.23	3.57	0.72	2.96	822	0.9
JUNE 83	8.88	3.73	7.80	3.72	1.08	2.97	674	1.0
JULY 83	8.77	3.34	7.54	3.46	1.24	2.95	747	1.1
AUG. 83	8.13	3.16	7.18	3.40	0.95	2.93	750	1.2
SEPT. 83	9.14	4.12	8.31	4.21	0.83	3.02	667	1.2
OCT. 83	9.99	3.91	8.58	3.80	1.41	3.19	738	1.1
NOV. 83	11.56	5.08	10.05	4.74	1.51	3.15	658	2.0
DEC. 83	10.62	5.05	9.08	4.58	1.54	3.03	723	2.9
JAN. 84	12.64	5.32	9.57	5.12	3.07	3.14	750	4.5
FEB. 84	12.32	4.56	8.67	4.55	3.65	2.82	790	3.8
MAR. 84	12.65	4.84	8.71	4.79	3.93	2.89	836	6.1
APR. 84	12.54	3.94	8.43	4.16	4.11	2.89	709	3.5
MAY 84	11.56	3.26	7.40	3.63	4.16	2.83	621	4.2
JUNE 84	11.02	3.04	6.96	3.45	4.06	2.70	703	2.8
JULY 84	10.57	3.07	6.79	3.34	3.78	2.66	710	2.1
AUG. 84	10.63	3.05	6.49	3.09	4.14	2.53	388	2.1
SEPT. 84	11.56	3.42	7.78	3.90	3.78	2.88	697	2.9
OCT. 84	12.57	3.86	8.87	4.27	3.71	3.05	790	3.7
NOV. 84	13.73	4.70	9.73	4.72	3.99	3.03	827	4.1
DEC. 84	13.08	4.65	9.35	4.68	3.73	3.16	789	4.6

W : Mean SMMR-derived windspeed
S : Mean ship-reported windspeed
D : W–S, data with $|D| > 10$ were excluded
σ : Standard deviation
N : Number of sample
R : Percentage of sample excluded

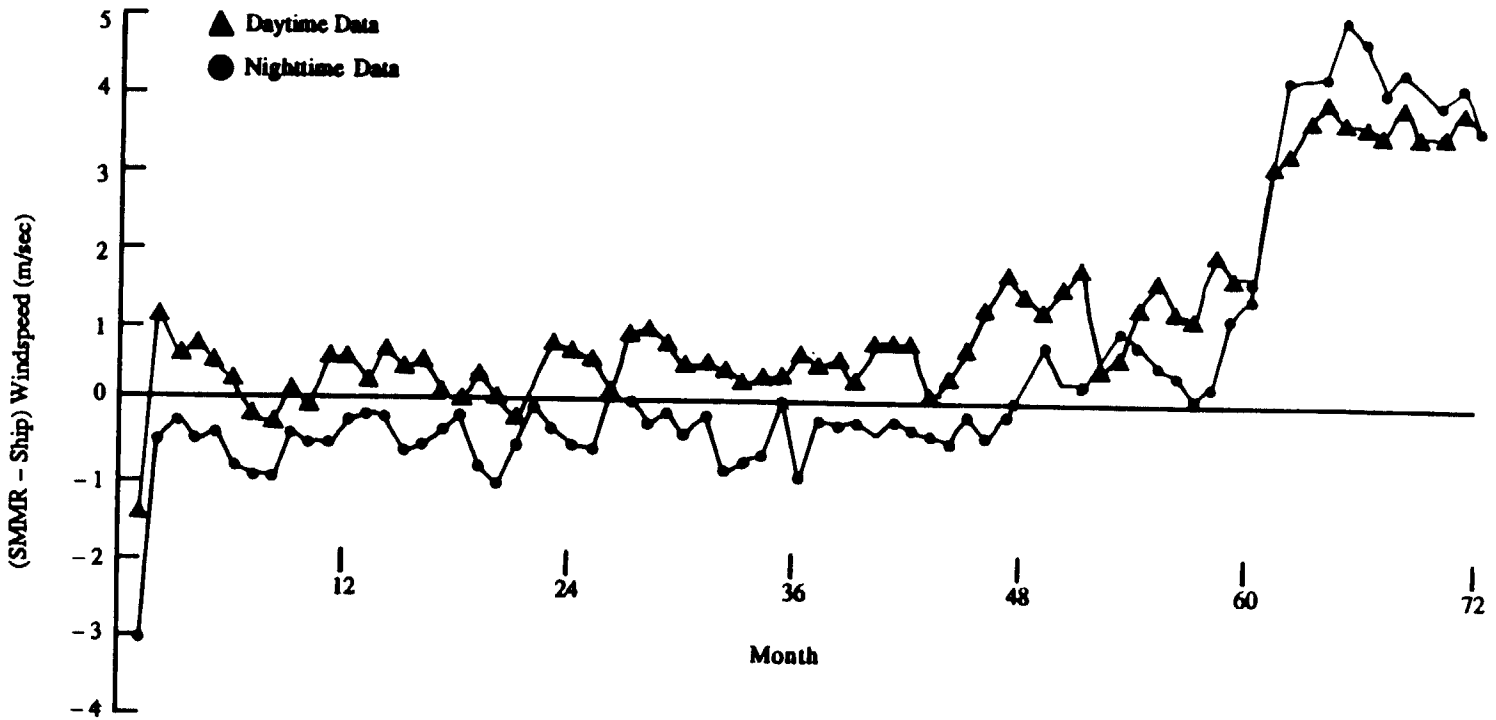

Figure 5.6. Monthly mean difference between SMMR windspeeds and ship measurements vs. time (Jan. 1979–Dec. 1984).

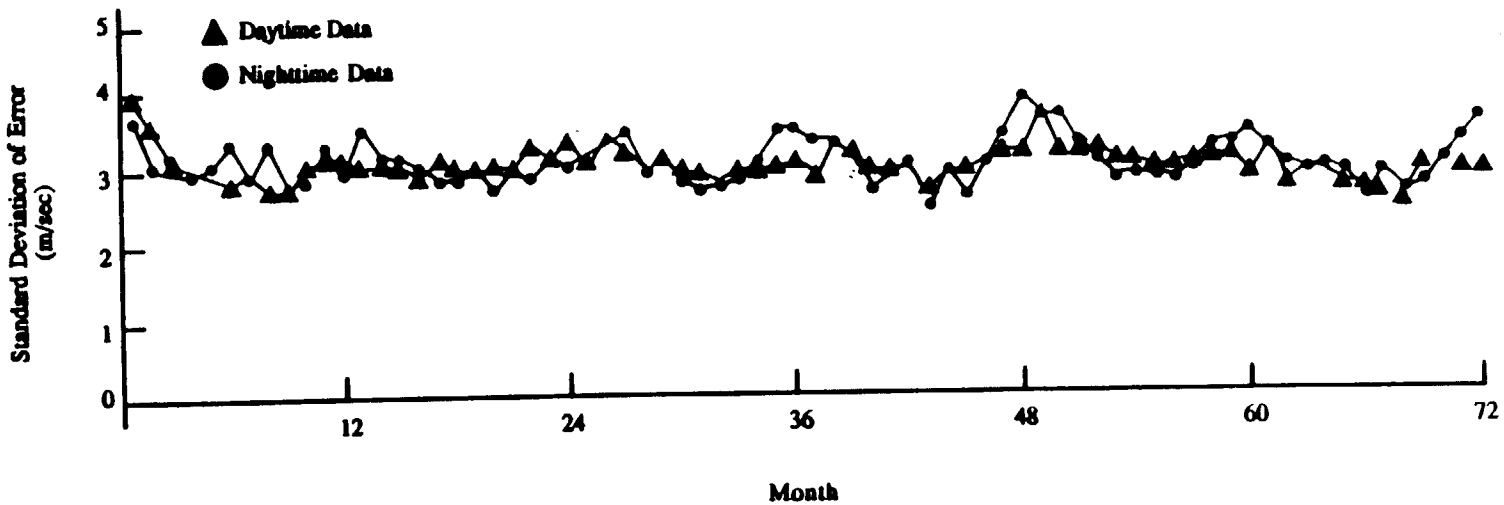

Figure 5.7. Monthly standard deviation of the difference between SMMR windspeeds and ship measurements vs. time (Jan. 1979–Dec. 1984).

Table 5.12

Sensitivity of Windspeed Algorithm

Channel	Formula	T_B(K)	$\frac{dw}{dT_B}$ (m/sec)
10.7 H	$\frac{-40.69}{T_{10V} - 285} + \frac{252.2\ T_{10V}}{(T_{10V} + T_{10H})^2} + 0.8813$	99	1.81
10.7 V	$40.69\ \frac{T_{10H} - 285}{(T_{10V} - 285)^2} - \frac{252.2\ T_{10H}}{(T_{10V} + T_{10H})^2}$	160	–0.86
37 H	$-\frac{10.38}{T_{37V} - 285}$	156	0.13
37 V	$10.38\ \frac{T_{37H} - 285}{(T_{37V} - 285)^2} - 0.3956$	203	–0.60

C-2

REFERENCES

Cavalieri, D. J., P. Gloersen, and W. J. Campbell. Determination of sea ice parameters with the Nimbus–7 SMMR. *J. Geophys. Res., 89,* 5355–5369, 1984.

Cavalieri, D. J., S. Martin, and P. Gloersen. Nimbus–7 SMMR observations of the Bering Sea ice cover during March 1979. *J. Geophys. Res., 88,* 1983.

Chang, A. T. C., and T. T. Wilheit. Remote sensing of water vapor, liquid water, and wind speed at the ocean surface by passive microwave techniques from the Nimbus–5 satellite. *Radio Science, 14,* 793–802, 1980.

Chang, H. D. Analysis of water vapor from the second year SMMR data. Report to the SMMR/NET Meeting, December 1983.

Chang, H. D., P. H. Hwang, T. T. Wilheit, A. T. C. Chang, D. H. Staelin, and P. W. Rosenkranz. Monthly distribution of precipitable water from the Nimbus–7 SMMR data. *J. Geophys. Res., 89(04),* 5328–5334, 1984.

Fu, C. C. Analysis of SMMR retrieved wind speed. Report to the SMMR/NET Meeting, December 1983.

Gloersen, P. Calibration of Nimbus–7 SMMR: II. Polarization mixing correction. *NASA TM 84976,* 1983.

Gloersen, P. and F. T. Barath. A scanning multichannel microwave radiometer for Nimbus–G and SEASAT–A. *IEEE J. Oceanic Eng., OE–2,* 172–178, 1977.

Gloersen, P. and D.J. Cavalieri. Reduction of weather effects in the calculation of sea ice concentration from microwave radiances. *J. Geophys. Res., 91,* 3913–3919, 1986.

Gloersen, P., D. J. Cavalieri, and W. J. Campbell. Derivation of sea ice concentration, age, and surface temperature from multispectral microwave radiances obtained with the Nimbus–7 Scanning Multichannel Microwave Radiometer. In *Oceanography From Space,* edited by J. R. F. Gower, pp. 823–829, Plenum Press, 1981.

Gloersen, P., D. J. Cavalieri, A. T. C. Chang, T. T. Wilheit, W. J. Campbell, O. M. Johannessen, K. B. Katsaros, K. F. Kunzi, D. B. Ross, D. Staelin, E. P. L. Windsor, F. T. Barath, P. Gudmandsen, E. Langham, and R. O. Ramseier. A summary of results from the first Nimbus–7 SMMR observations. *J. Geophys. Res., 89,* 5335–5344, 1984.

Gloersen, P., D. J. Cavalieri, and H. V. Soule. An alternative algorithm for correction of scanning multichannel radiometer polarization radiances using Nimbus–7 observed data. *NASA TM 80672,* 1980.

Grody, N. C., A. Gruber, and W. C. Chen. Atmospheric water content and the tropical Pacific derived from the Nimbus–6 scanning microwave spectrometer. *J. Appl. Meteorol., 19,* 986–996, 1980.

Han, D. Offset angle of polarization rotation for Nimbus–7 SMMR. SASC Technical Report, 1980.

Hogg, D. C., F. D. Guirand, J. B. Snider, M. T. Decker, and E. R. Westwater. A steerable dual channel microwave radiometer for measurement of water vapor and liquid in the troposphere. *J. Climate Appl. Meteor., 22,* 789–806, 1983.

Kim, S. T., D. Han, H. D. Chang. Analysis and correction of the brightness temperature measured in the 21 GHz horizontal channel of the Nimbus–7 Scanning Multichannel Microwave Radiometer. *SASC-T-5-5100-0004-00026-84,* 1984.

Milman, A. S. and T. T. Wilheit. SST's from the Nimbus–7 SMMR. Presented at the JPL SST Workshop, January 1983.

Milman, A. S. and T. T. Wilheit. Sea surface temperatures from the Scanning Multichannel Microwave Radiometer on Nimbus–7. *J. Geophys. Res., 90,* 11631–11641, 1985.

Nordberg, W., J. Conaway, D. B. Ross, and T. Wilheit. Measurements of microwave emission from a foam-covered, wind-driven sea. *J. Atmos. Sci., 28,* 429–435, 1971.

NORSEX Group. The Norwegian Remote Sensing Experiment (NORSEX) in a Marginal Ice Zone. *Science, 220,* 781–787, 1983.

Prabhakara, C., H. D. Chang, and A. T. C. Chang. Remote sensing of precipitable water over the oceans from Nimbus–7 microwave measurements. *J. Appl. Meteorol., 21,* 59–68, 1982.

Rosenkranz, P. W. Inversion of data from diffraction limited multiwavelength remote sensor. 2. Nonlinear dependence of observables on the geophysical parameters. *Radio Sci., 17,* 245–256, 1982.

Rosenkranz, P. W., D. H. Staelin, and N. C. Grody. Typhoon June (1975) viewed by scanning microwave spectrometer. *J. Geophys. Res., 83,* 1857–1868, 1978.

Staelin, D. H., K. F. Kunzi, R. L. Pettyjohn, R. K. L. Poon, R. W. Wilcox, and J. W. Waters. Remote sensing of atmospheric water vapor and liquid water with the Nimbus–5 microwave spectrometer. *J. Appl. Meteorol., 15(11),* 1204–1214, 1976.

Starr, V. P., J. P. Piexoto, and R. G. McKean. Pole-to-pole moisture conditions for the IGV. *Pure Appl. Geophys., 75,* 300–331, 1969.

Svendsen, E., K. Kloster, B. Farrelly, O. M. Johannessen, J. Johannessen, W. J. Campbell, P. Gloersen, D. Cavalieri, and C. Maetzler. NORSEX evaluation of the Nimbus–7 Scanning Multichannel Microwave Radiometer for Sea Ice Research. *J. Geophys. Res., 88,* 2781–2791, 1983.

Swift, C. T. Passive microwave remote sensing of the ocean—A review. *Boundary Layer Meteorol., 18,* 25–54, 1980.

Webster, W. J., Jr., T. T. Wilheit, D. B. Ross, and P. Gloersen. Spectral characteristics of the microwave emission from a wind-driven, foam-covered sea. *J. Geophys. Res., 81,* 3095–3099, 1976.

Wilheit, T. T. Microwave determination of oceanographic and meteorological parameters. *(COSPAR) Space Research, xx,* 15–20, 1980.

Wilheit, T. T. A model for the microwave emissivity of the ocean's surface as a function of wind speed. *IEEE Trans. Geosci. Electron., GE–17,* 244–249, 1979.

Wilheit, T. T. A review of application of microwave radiometry to oceanography. *Boundary Layer Meteorol., 13,* 277–293, 1978.

Wilheit, T. T. and A. T. C. Chang. An algorithm for retrieval of ocean surface and atmospheric parameters from the observations of the scanning multichannel microwave radiometer. *Radio Sci., 15,* 525–544, 1980.

Wilheit, T. T., J. Greaves, J. Gatlin, D. Han, B. M. Krupp, and A.S. Milman. Retrieval of ocean surface parameters from the Scanning Multichannel Microwave Radiometer on the Nimbus–7 satellite. *IEEE Trans. Geoscience and Remote Sensing, GE–22,* 133–143, 1984.

Zwally, H. J., J. C. Comiso, C. L. Parkinson, W. J. Campbell, F. D. Carsey, and P. Gloersen. Antarctic sea ice, 1973–1976: satellite passive-microwave observations. *NASA Spec. Publ. 459,* 206 pp., 1983.

LIST OF ACRONYMS, INITIALS, AND ABBREVIATIONS

°	Degree
Δ	Delta, change
%	Percent
C	Sea-ice total concentration
C_{FY}	First-year ice concentration
C_{MY}	Multiyear ice concentration
C_W	Open water amount
C_F	First-year ice fraction
C_M	Multiyear ice fraction
CELL	SMMR tapes containing calibrated brightness temperatures binned into Earth-located cells
CELL-ALL	Synonymous with cell
CELGEN	CELL generation program
EBCDIC	Extended Binary Coded Decimal Interchange Code
ESMR	Electrically Scanning Microwave Radiometer
FOV	Field-of-view
GHz	Gigahertz (10**9)
GMT	Greenwich Mean Time
GR	Gradient Ratio
Hz	Hertz (cycles per second)
ILT	Image Location Tape
ITCZ	Intertropical convergence zone
km	Kilometer
LO	Land/Ocean
LSB	Least significant bit
m	Meter
MAP-30	Mapped parameters of 37-GHz channel data tape
MAP-LO	Mapped form of PARM–LO
MAP-SS	Mapped form of PARM–SS
M/sec	Millisecond
MSB	Most significant bit
NASA	National Aeronautics and Space Administration
NMC	National Meteorological Center
NOPS	Nimbus Observation Processing System
NSW	Near-Surface Winds
PARM	SMMR tape containing geophysical parameters on the CELL grid
PARMAP	SMMR tape containing mapped parameters from PARM–LO and PARM–SS
PARMGN	Parameter generation

LIST OF ACRONYMS, INITIALS, AND ABBREVIATIONS (Continued)

PARM-LO	SMMR tape containing land/ocean parameters as computed from CELL-ALL tape
PARM-SS	SMMR tape containing sea-ice/ice-sheet parameters as computed from the CELL-ALL tape
PARM-30	SMMR tape containing 37-GHz brightness temperature on the CELL grid
PARM tape	Retrieved SMMR geophysical parameter tape
PR	Polarization Ratio
RFI	Radio Frequency Interface
rms	Root Mean Square
s/c	Spacecraft
SACC	Science and Applications Computing Center
sec	Second
SMMR	Scanning Multichannel Microwave Radiometer
SPEC	Specification
SST	Sea-Surface Temperature
TAT	Antenna Temperature Tape
TDF	Trailer Documentation File
UFO	User Formatted Output (Tape)
UTC	Universal Time Correction
WV	Water vapor

APPENDIX A PARM TAPE FORMAT

A.1 Common Features of PARM Tapes

All PARM tapes are 1600 bpi, 9-track tapes. They are generated on the IBM 3081 at the Science and Applications Computing Center (SACC) at the NASA/Goddard Space Flight Center. There are formats that are common to all three types of PARM tapes. In the following, the common features will be described first; formats that vary with type of PARM tape follow.

A.1.1 NOPS Standard Header File

The first file on PARM tapes is the Nimbus Observation Processing System (NOPS) Standard Header File, written in EBCDIC coded characters using odd parity. This file contains identifier, data coverage, and generation information. The NOPS Standard Header file contains two identical records of 630 bytes each. Each record is broken into five 126-character groups. The first group contains information of the contents of the tape. (Appendix B describes in detail the specifications of NOPS Standard Header Records.) The second group is left blank. The remaining groups may contain information at the discretion of the subsystem analyst.

A.1.2 Data File Structure

Starting with the second file, all files, except for the last two files, contain one orbit's data. The first logical record of each file contains the documentation information (see Section A.2.2) for that file. Each subsequent logical record, except the last physical record, contains data covering a time period equal to 30 scan periods (122.88 seconds). This covers an area roughly 780 by 787 km. The last physical record of each file is a dummy record filled with zeroes except for the first three bytes. The second to the last file of each tape is a dummy file consisting of one dummy record. The last file on a PARM tape is called a Trailer Documentation File (TDF).

A.1.3 Trailer Documentation File

The TDF consists of all NOPS Standard Header Records of the input tapes used in order of their access; that is, first in is first recorded. For details of TDF, see Appendix B.

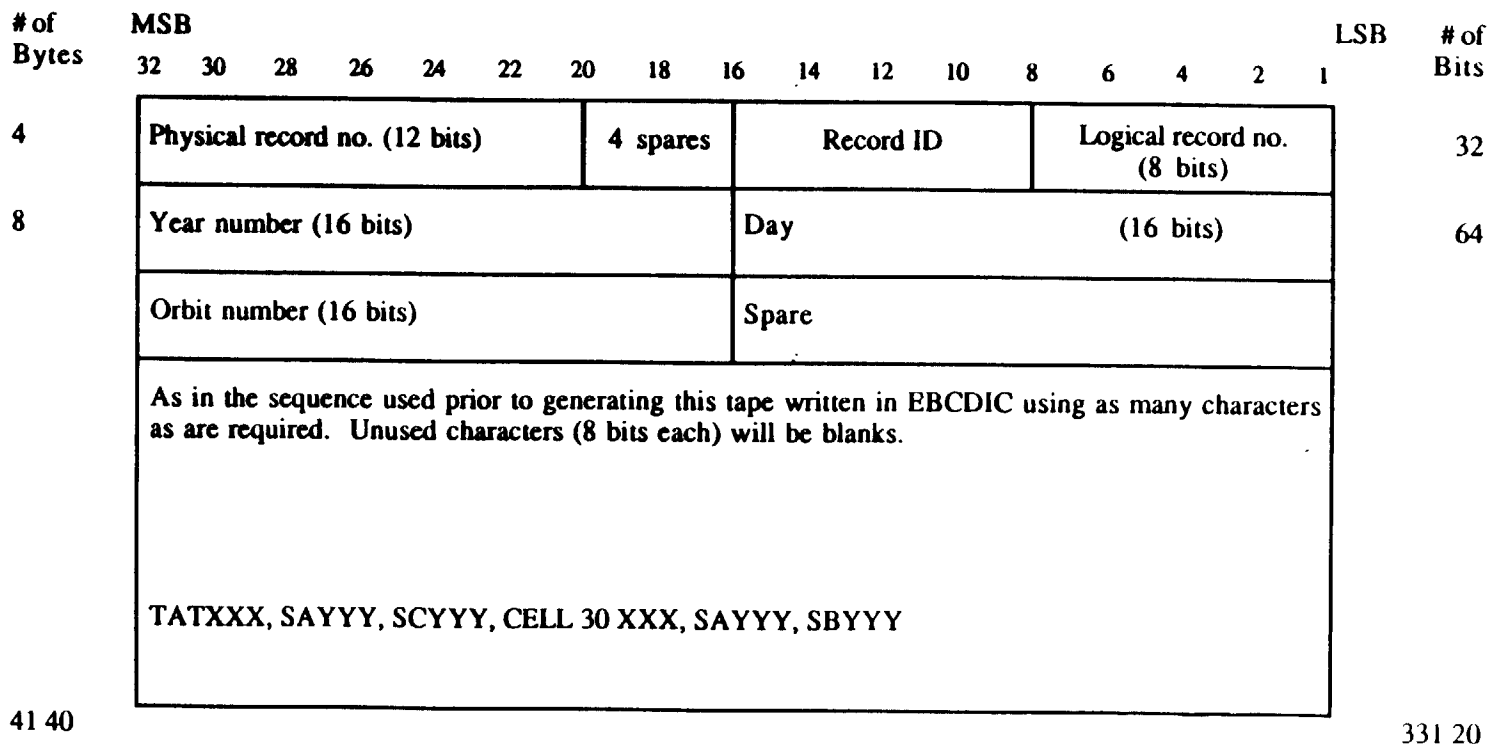

Figure A.1. SMMR PARM-LO Documentation Logical Record Format.

A.2 PARM-LO

A.2.1 Data File

The physical record is made up of three logical records. Each logical record contains 4140 bytes. There are two types of logical records: a Documentation Logical Record and a Data Logical Record. The Documentation Logical Record appears once as the first logical record of the first physical record in every data file. Figure A.1 shows the format of the Documentation Logical Record. The Data Logical Record contains data that cover a 780 x 787 km area using 5, 8, or 13 bands of 156 x 158 km, 97. 5 x 98. 5 km, or 60 x 61 km cells, respectively. The five bands of five cells per band group can handle up to four different land/ocean parameters. The eight bands of eight cells per band group were designed for a maximum of two land/ocean parameters, and the last group (13 bands of 13 cells) is set up for four sets of parameters. Each band, centered on the ground track of the spacecraft, is perpendicular to its velocity vector and is ascending in time. Figure A.2 shows the Data Logical Record format. This format was designed to be generated and read on 32-bit machines, but with selected information placed to make it easy to use on 24-bit machines. This tape contains parameters with resolutions of 156, 97. 5, and 60 km. Table A.1 contains a list of the parameters and parameter numbers.

A.2.2 Documentation Logical Record

The Documentation Logical Record is always located in the first logical record of the first record in a data file. The description of the first 12 bytes of information can be found in the Data Logical Record section (A.2.3). The rest of the logical record is used for describing the subroutine versions used in generating each SMMR tape up to and including this tape (i.e., TAT Tape and CELL-ALL). Figure A.1 illustrates the type of information written on this tape.

A.2.3 Data Logical Record

The data contained in Figure A.2 are defined as follows:

(1) Physical Record Number (12 bits) - This is the number of this record within a file. It starts at 1 and increments by 1 throughout the file. All logical records within a physical record carry the same identical number.

(2) Record ID (8 bits) - Identifies record type, the last physical record within a file, and records in the second to the last file on the tape. The most significant bit (MSB) is set to 1 if that physical record is the last one written in the file. The second MSB is set to 1 in all records within the second to the last file.

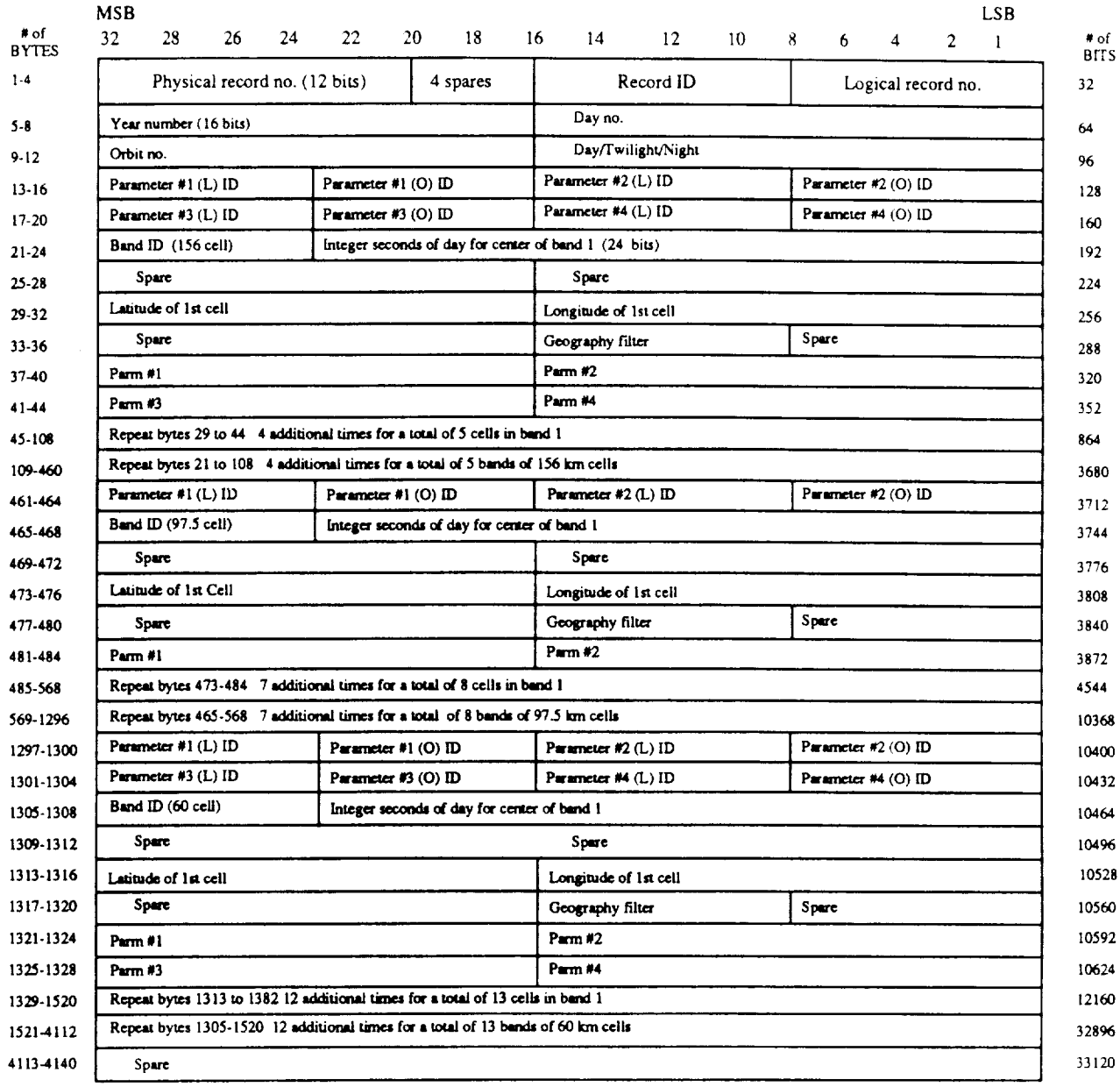

Figure A.2. SMMR PARM-LO Data Logical Record Format.

Table A.1

Parameters and Parameter ID Numbers on PARM-LO Tape

Parameter Number	Description of Parameter	Unit	Resolution
	Ocean Parameters		
1	Sea-Surface Windspeed*	-1 m/sec	97 km
4	Total Atmospheric Water Vapor	mgm/cm^2	60 km
5	Sea-Surface Temperature	0. 1 K	156 km
	Land Parameters		
6	6. 6-GHz Percent Polarization	0. 1 %	156 km
9	T6. 6 V	0. 1 K	156 km

*Year-1 windspeed data were not produced

The record ID's are located in the 6 least significant bits (LSB) and are shown below:

Type of Record	Record ID #
Documentation Logical Record	21
Data Logical Record	22
Dummy Logical Record	23

(3) Logical Record Number (8 bits) - This is the number of the logical record within a file. It starts at 1 and increments by 1 throughout the file.

(4) Year Number (16 bits) - Only the last two digits of the calendar year number are written on the tape (e.g., 78).

(5) Day Number (16 bits) - Day numbers range from 1 starting on January 1st to day 365 (or 366, if leap year).

(6) Orbit Number (16 bits) - An orbit is defined as starting at one descending node (one-half orbit after a NASA orbit) and ending at the following descending node. The orbit number does not change within a file.

(7) Parameter #1 through #2 ID (four or eight 8-bit words) - These ID numbers are used to identify which parameters are located in the data fields. Table A.1 describes the parameters and the associated parameter ID numbers. If the parameter ID number is zero, no valid data are available in the corresponding data field. The first word of each parameter pair is for the parameter number over land; the second word is for the parameter number over ocean. Since there are two or four data fields, a maximum of two or four sets of land/ocean parameter numbers can be output depending on which bandsize (resolution) is required. They may be identical for over land and ocean or may be different. The geography filter will be used to determine whether the data are over land or ocean.

(8) Day/Twilight/Night - Code describing illumination of spacecraft (s/c) and illumination of Earth (cells) in the FOV:

0 = Day (both s/c and cells illuminated)
1 = Twilight (s/c illuminated, cells in shadow)
2 = Night (both s/c and cells in shadow)

(9) Band Number ID (8 bits) - This number identifies the type of band and the cell within each band. It is a combination of a band number and the type of band.

Type of Band	Range of Band Numbers
5 Bands of 5 Cells/Band	51 to 55
8 Bands of 8 Cells/Band	81 to 88
13 Bands of 13 Cells/Band	101 to 113

(10) Integer Seconds of the Day for Center of Band (24 bits) - The GMT corresponds to the center of the band and is given in integer seconds of the day.

(11) Latitude of Cell (16 bits) - Each cell latitude is given in hundredths of degrees, where -9000 is the South Pole and 9000 is the North Pole. The latitude is given for the center of the cell.

(12) Longitude of Cell (16 bits) - The longitude is given for the center of the cell, in hundredths of degrees from the 0° Greenwich Meridian westward to -18000 and eastward to +18000.

(13) Data for Parameters 1 to 4 (two or four 16-bit words) - The data output depends on Item #7, parameter ID. The parameter specified in Parameter ID #1 is output in the Parameter 1 data field, etc. When there are no data for one of the parameters, its parameter ID number is set to zero. If no parameters can be

computed at any resolution from the input data, no logical records are written. Table A.2 shows the parameter position of each parameter in the parameter data field.

Table A.2

Parameters and Their Positions in PARM-LO Tape

Parameter Description	Resolution of Cell	Geographic Filter	Parameter Position
6. 6-GHz Percent Polarization	156 km	Land	1
Sea-Surface Temperature	156 km	Ocean	1
T6. 6 V	156 km	Land	2
Windspeed*	97 km	Ocean	1
Water Vapor	60 km	Ocean	3

*Year-1 windspeed data were not produced

(14) Season Geography Filter (8 bits) - The filter determines where and under what conditions a measurement was made. These flags are defined as follows:

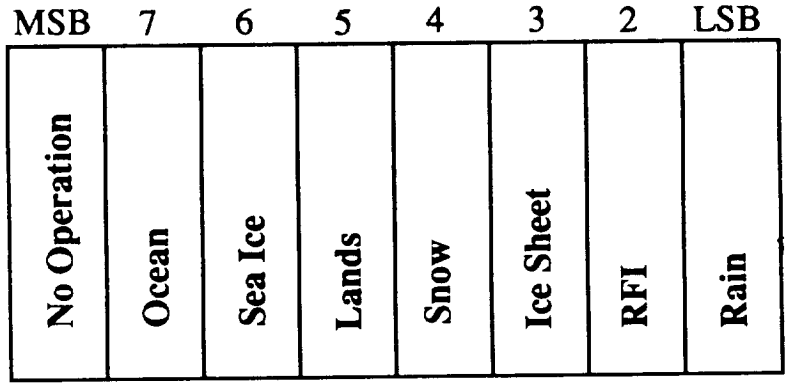

1 = True or Yes
0 = No or Not True

RFI: Radio Frequency Interference

(15) Spare - All spares are filled with zeros unless specified otherwise.

A.3 PARM-SS

A.3.1 Data File

The physical record is made up of three logical records. Each logical record contains 4140 bytes. There are two types of logical records: a Documentation Logical Record and a Data Logical Record. The Documentation Logical Record appears once as the first logical record of the first physical record in every data file. Figure A.3 shows the format of the Documentation Logical Record.

The Data Logical Record contains data that cover a 780 x 787 km area using 5, 8, or 13 bands of 156 x 158 km, 97. 5 x 98. 5 km or 60 x 61 km cells, respectively. The five bands of five cells per band group can handle up to four different land/ocean parameters. The eight bands of eight cells per band group were designed for a maximum of two land/ocean parameters. The last group (13 bands of 13 cells) is set up for four sets of parameters.

Each band is centered on the ground track of the spacecraft, is perpendicular to its velocity vector, and is ascending in time. Figure A.4 shows the Data Logical Record format. This format was designed to be generated and read on 32-bit machines but with selected information placed to make it easy to use on 24-bit machines.

This tape contains parameters at resolutions of 156, 97. 5, and 60 km. Table A.3 contains a list of the parameters and parameter numbers.

A.3.2 Documentation Logical Record

The Documentation Logical Record is always located in the first logical record of the first physical record in a data file. The description of the first 12 bytes of information can be found in Section A.3.3. The rest of the logical record is used for describing the subroutine versions used in generating each SMMR tape up to and including this tape (i.e., TAT Tape and CELL-ALL). See Figure A.3 for an example of the type of information written to this tape.

A.3.3 Data Logical Record

The data contained in Figure A.4 are defined as follows:

(1) Physical Record Number (12 bits) - This is the number of this record within a file. It starts at 1 and increments by 1 throughout the file. All logical records within a physical record will carry the same identical number.

(2) Record ID (8 bits) - Identifies record type, the last physical record within a file, and records in the second to the last file on the tape. The MSB will be set to 1 if that physical record is within the second to the last file.

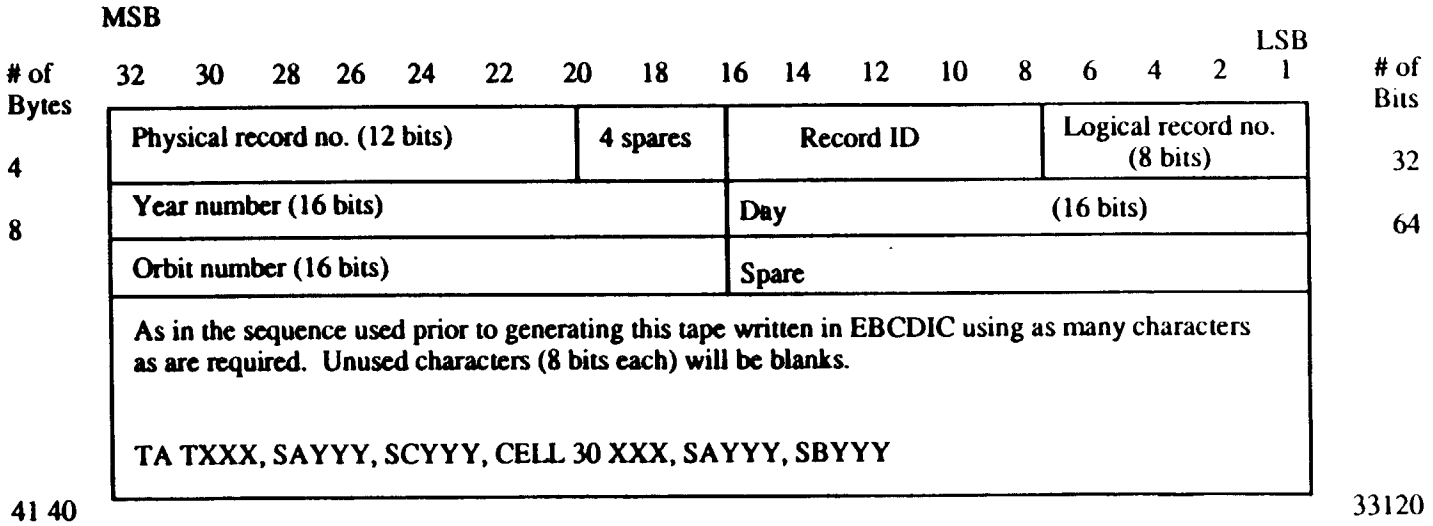

Figure A.3. SMMR PARM–SS Documentation Logical Record Format.

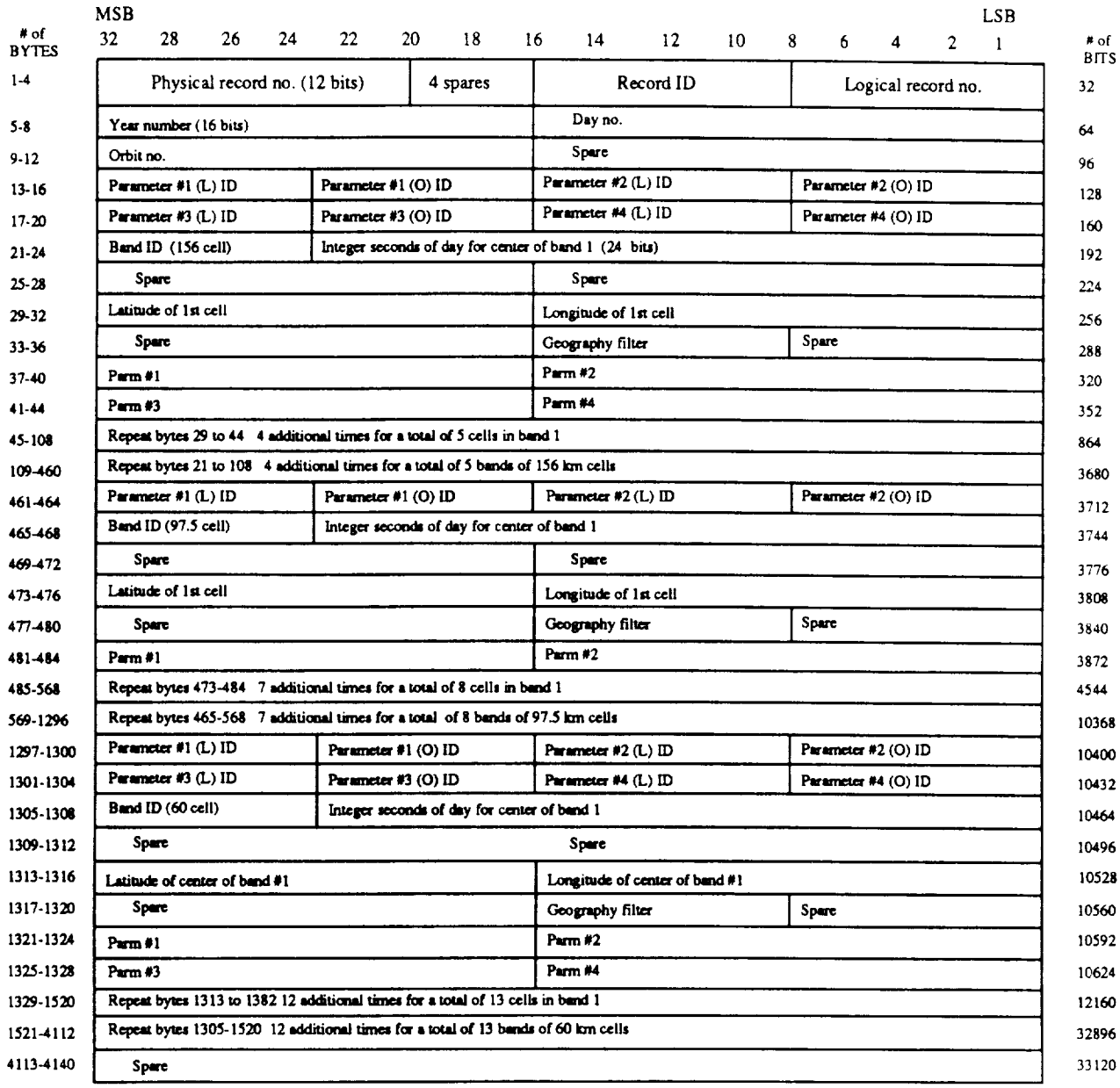

Figure A.4. SMMR PARM–SS Data Logical Record Format.

Table A.3

Parameters and Parameter ID Numbers on PARM–SS Tape

Parameter Number	Description of Parameter	Unit	Resolution
	Ocean Parameters		
5	Sea-Surface Temperature	0. 1 °C	156 km
1	Sea-Surface Windspeed	0. 1 °C m/sec	97. 5 km
	Sea-Ice Parameters		
11	Sea-Ice Concentration	10^{-1}%	60 km
5	Sea-Ice Surface Temperature	10^{-1} K	156 km
12	Multiyear Ice Fraction*	10^{-1}%	60 km
13	18-GHz Percent Polarization	10%	60 km
	Land/Snow Parameters		
16	T37 H – T18 H	0. 1 K	60 km
14	2(T37 V – T18 V)/ (T37 V + T18 V)	0. 1 K	156 km
15	T18 V	0. 1 K	156 km
17	Snow (Yes/No)†		60 km
	Ice-Sheet Parameters		
14	T6. 6 V	0. 1 K	156 km
18	T18 V	0. 1 K	60 km
19	T10. 7 V	0. 1 K	97. 5 km
15	T6. 6 H	0. 1 K	156 km

* This parameter is computed over the Northern Hemisphere only

† Parameter not produced for Year-1 data

The record ID's are located in the 6 LSB and are shown below:

Type of Record	Record ID #
Documentation Logical Record	24
Data Logical Record	25
Dummy Logical Record	26

(3) Logical Record Number (8 bits) - This is the number of the logical record within a file. It starts at 1 and increments by 1 throughout the file.

(4) Year Number (16 bits) - Only the last two digits of the calendar year number are written on the tape (e.g., 78).

(5) Day Number (16 bits) - Day numbers range from 1 starting on January 1st to day 365 (or 366, if leap year).

(6) Orbit Number (16 bits) - An orbit is defined as starting at one descending node (one-half orbit after a NASA orbit) and ending at the following descending node. The orbit number does not change within a file.

(7) Parameter #1 through #4 ID (four or eight 8-bit words) - These ID numbers are used to identify which parameters are located in the data fields. Table A.3 describes the parameters and the associated parameter ID numbers. The first word of each parameter pair is for the ID of the parameter over land and the second word is for the ID of the parameter over ocean. Since there are two or four data fields, a maximum of two or four sets of land/ocean parameter ID numbers can be output depending on which band size (resolution) is required. They may be identical for over land and ocean or may be different. The geography filter will be used to determine whether the data are over land or ocean.

(8) Day/Twilight/Night (8 bits) - Code describing illumination of spacecraft (s/c) and illumination of Earth (cells) in the FOV:

0 = Day (both s/c and cells illuminated)
1 = Twilight (s/c illuminated, cells in shadow)
2 = Night (both s/c and cells in shadow)

(9) Band Number ID (8 bits) - This number is a combination of a band number and the type of band.

Type of Band	Range of Band Numbers
5 Bands of 5 Cells/Band	51 to 55
8 Bands of 8 Cells/Band	81 to 88
13 Bands of 13 Cells/Band	101 to 113

(10) Integer Seconds of the Day for Center of Band (24 bits) - The GMT corresponds to the center of the band and is given in integer seconds of the day.

(11) Latitude of Cell (16 bits) - Each cell latitude is given in hundredth of degrees, where –9000 is the South Pole and 9000 is the North Pole. The latitude is given for the center of the cell.

(12) Longitude of Cell (16 bits) - The longitude is given for the center of the cell, in hundredth of degrees from the 0° Greenwich Meridian westward to –18000 and eastward to +18000.

(13) Data for Parameters 1 to 4 (two or four 16-bit words) - The data output depends on Item #6, parameter ID. The parameter specified in Parameter ID #1 is output in the Parameter 1 data field and whatever parameter is specified in Parameter ID #2 is output in Parameter #2 data fields, etc. When there are no data for one of the parameters, its parameter ID number is set to zero. If not a single parameter at any resolution can be computed from the input data, no logical records are written. Table A.4 shows the parameter position of each parameter in the parameter data field.

Table A.4

Parameters and Their Positions in PARM-SS Tape

Parameter Description	Resolution of Cell	Geographic Filter	Parameter Position
Gradient Ratio	156 km	Land/Snow	1
$T_{6,6}$	156 km	Ice Sheet	1
Sea-Surface Temperature	156 km	Ocean	1
Ice-Surface Temperature	156 km	Sea Ice	1
T_{18V}	156 km	Land/Snow	2
$T_{6.6H}$	156 km	Ice Sheet	2
Sea-Surface Windspeed	97. 5 km	Ocean	1
$T_{10.7V}$	97. 5 km	Ice Sheet	1
$T_{37H-T18H}$	60 km	Land/Snow	1
Ice Concentration	60 km	Sea Ice	1
18-GHz Percent Polarization	60 km	Sea Ice	2
Snow (Yes/No)	60 km	Land/Snow	3
T_{18V}	60 km	Ice Sheet	3
Multiyear Ice Fraction	60 km	Sea Ice	3

(14) Season Geography Filter (8 bits) - The filter determines where and under what conditions a measurement was made. These flags are defined as follows:

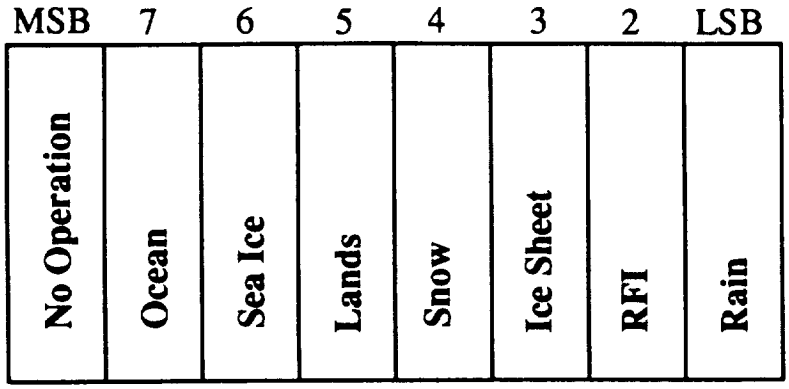

1 = True or Yes
0 = No or Not True

RFI: Radio Frequency Interference

(15) Spare - All spares are filled with zeros unless specified otherwise.

A.4 PARM–30

A.4.1 Data File

The physical record is made up of two logical records. Each logical record contains 8352 bytes. There are two types of logical records: a Documentation Logical Record and a Data Logical Record. The Documentation Logical Record appears once as the first logical record of the first physical record in every data file. Figure A.5 shows the format of the Documentation Logical Record.

The Data Logical Record contains data which cover a 780 x 787 km area using 26 bands of 26 30 x 30 km cells. Each band is centered on the subsatellite track, is perpendicular to its velocity vector, and is ascending in time. Figure A.6 shows the format of the Data Logical Record. This format was designed to be read on 32- or 24-bit machines. This tape contains sea-ice concentration in 30-km resolution.

A.4.2 Documentation Logical Record

The Documentation Logical Record is always located in the first logical record of the first physical record in a data file. The description of the first 8 bytes of information can be found in the Data Logical Record section. The rest of the logical record is used for describing the subroutine versions used in generating each SMMR tape up to and including this tape (i.e., TAT Tape, CELL-ALL, and PARM–30 Tapes). See Figure A.5 for an example of the type of information written to this tape.

A.4.3 Data Logical Record

The data contained in Figure A.6 are defined as follows:

(1) Physical Record Number (12 bits) - This is the number of this record within a file. It starts at 1 and increments by 1 throughout the file. Both logical records within a physical record will carry the same identical number.

(2) Record ID (8 bits) - Identifies record type, the last physical record within a file, and records in the second to the last file on the tape. The MSB will be set to 1 if that physical record is within the second to the last file. The second MSB is set to 1 in all records within the second to the last file.

Type of Record	Record ID #
Documentation Logical Record	27
Data Logical Record	28
Dummy Logical Record	29

(3) Logical Record Number (8 bits) - This is the number of the logical record within a file. It starts at 1 and increments by 1 throughout the file.

(4) Year Number (16 bits) - Only the last two digits of the calendar year number are written on the tape (e.g., 78).

(5) Day Number (16 bits) - Day numbers range from 1 starting on January 1st to day 365 (or 366, if leap year).

(6) Orbit Number (16 bits) - An orbit is defined as starting at one descending node (one-half orbit after a NASA orbit) and ending at the following descending node. The orbit number does not change within a file.

(7) Parameter #1 and #2 ID (four 8-bit words) - These ID numbers are used to identify which parameters are located in the data fields. All parameters on this tape must be output as 30-km resolution data. If the parameter ID number is zero, no valid data are available in the corresponding data field. The first word of each parameter pair is for the ID of the parameter over land, and the second word is for the ID of the parameter over ocean. Since there is only one parameter on the PARM–30 tape (ice concentration in 30-km resolution), this parameter ID is written in the Parameter 1 slot. The geography filter will be used to determine whether the data is over land or ocean.

(8) Day/Twilight/Night - Code describing illumination of spacecraft (s/c) and illumination of Earth (cells) in the FOV.

0 = Day (both s/c and cells illuminated)
1 = Twilight (s/c illuminated, cells in shadow)
2 = Night (both s/c and cells in shadow)

(9) Band Number ID (8 bits) - This number is a combination of a band number and the type of band.

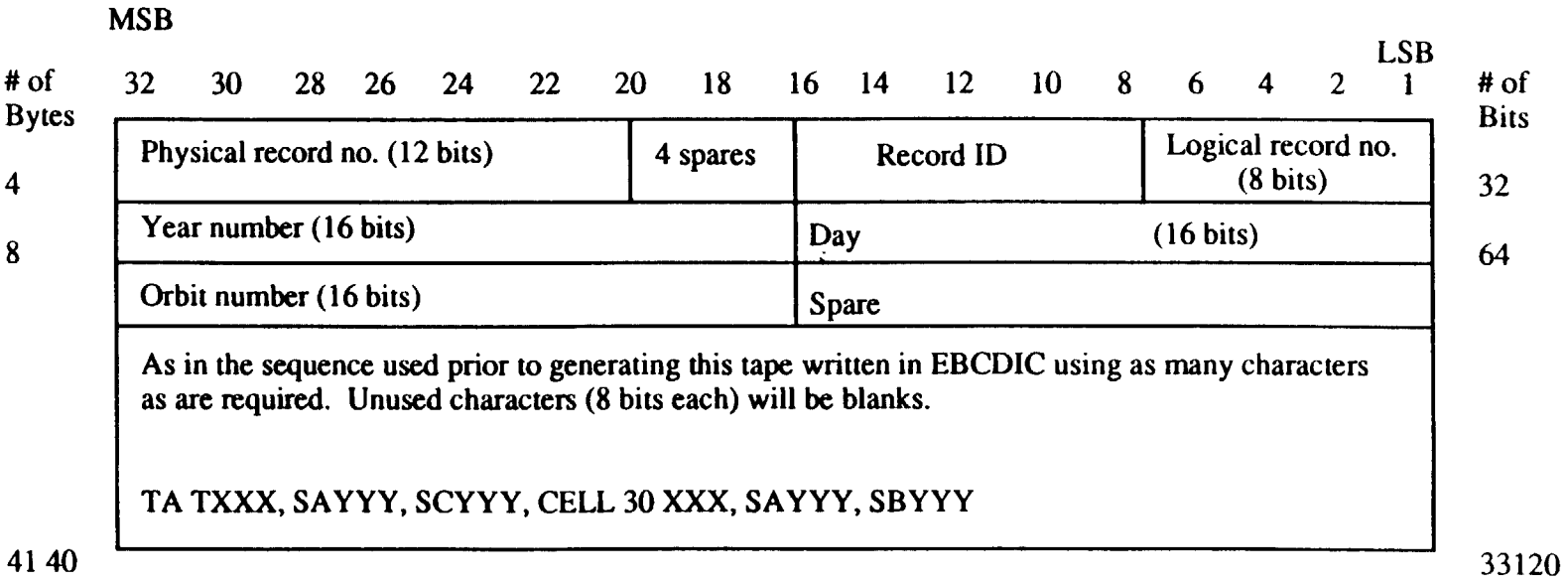

Figure A.5. SMMR PARM-30 Documentation Logical Record Format.

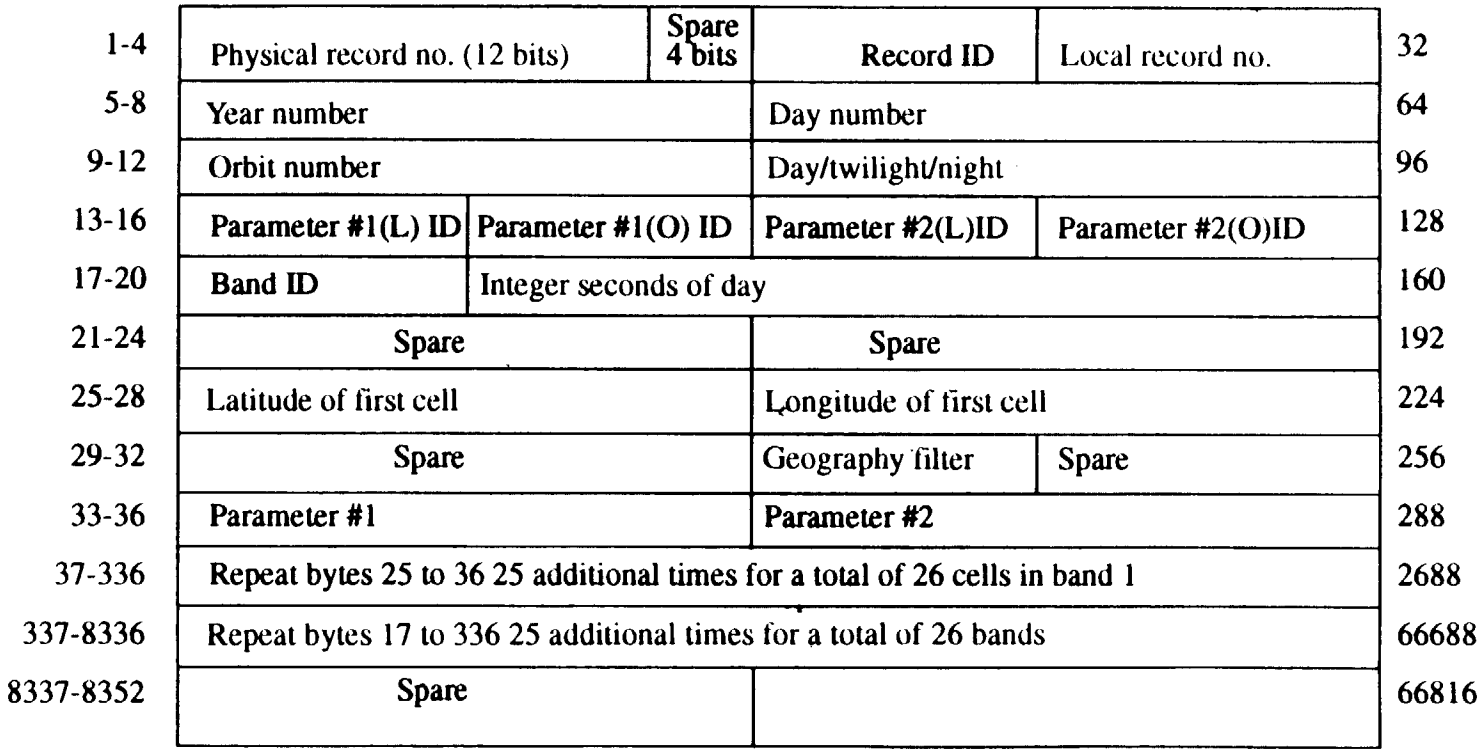

Figure A.6. SMMR PARM-30 Data Logical Record Format.

Type of Band	Range of Band Numbers
26 Bands of 26 Cells/Band	1 to 26

(10) Integer Seconds of the Day for Center of Band (24 bits) - The GMT corresponding to the center of the band is given in integer seconds of the day.

(11) Latitude of Cell (16 bits) - Each cell latitude is given in hundredth of degrees where -9000 is the South Pole and 9000 is the North Pole. The latitude is given for the center of the cell.

(12) Longitude of Cell (8 bits) - The longitude is given for the center of the cell, in hundredth of degrees from the 1° Greenwich Meridian westward to -18000 and eastward to +18000.

(13) Parameters 1 and 2 (two 16-bit words) - The data output are sea-ice concentrations in 30-km resolution over ocean in parameter 1 position.

(14) Season Geography Filter (8 bits) - The filter determines where and under what conditions a measurement was made. These flags are defined as follows:

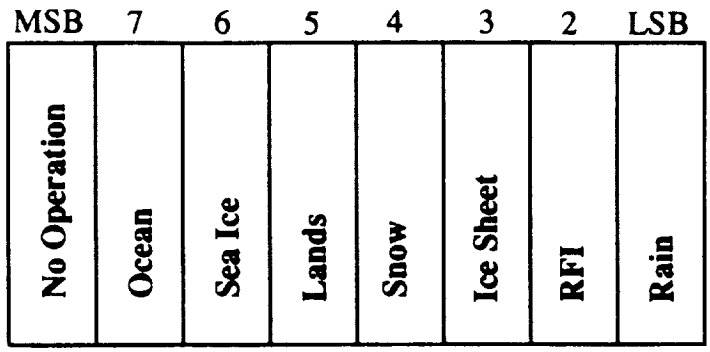

1 = True or Yes
0 = No or Not True

RFI: Radio Frequency Interference.

(15) Spare - All spares are filled with zeros unless specified otherwise.

APPENDIX B SPECIFICATION OF STANDARD HEADER FILE AND TRAILER DOCUMENTATION FILE

B.1 Standard Header File

The Standard Header File is the first file of the tape. It consists of two identical physical records of 630 EBCDIC characters and is followed by an end-of-file mark.

($_b$ = blank)

The first 126 characters of the record consist of:

*NIMBUS-7$_b$NOPS$_b$SPEC$_b$NO$_b$TXXXXXX (characters 1-30)

(XXXXXX = tape specification number)

$_b$SQ$_b$NO$_b$XXYYYYY-Z (characters 31-46)

(XX = PDF code BG = PARM-30,
BH = PARM-LO, BI = PARM-SS,
YYYYY = sequence number,
Z = copy number)

$_b$SMMR$_b$SACC$_b$TO$_b$IPD$_b$ (characters 47-64)

$_b$STRT$_b$19XX$_b$DDD$_b$HHMMSS$_b$ (characters 65-87)
(start year, day of year, hours,
minutes, seconds)

TO$_b$19XX$_b$DDD$_b$HHMMSS$_b$ (characters 88-106)
(End date and time of data)

GEN$_b$19XX$_b$DDD$_b$HHMMSS$_b$ (characters 107-126)
(Date and time when the tape was generated)

The rest of the record contains blanks or more information when required.

Example:

*NIMBUS-7$_b$NOPS$_b$SPEC$_b$No$_b$T234121$_b$SQ$_b$NO$_b$BH90321-2

$_b$SMMR$_b$SACC$_b$TO$_b$IPD$_{bb}$START$_b$1979$_b$032$_b$000432$_b$

TO$_b$1900$_b$00O$_b$000000$_b$GEN^{b}1980$_b$232$_b$221045$_b$ followed by 504 blanks

indicate SMMR PARM-LO tape:

Sequence no. 90321, copy 2
data starting on: day 32 of 1979 at 00:04:32
data ending on: unavailable
tape generated on: day 232 of 1980 at 22:10:45

B.2 Trailer Documentation File (TDF)

The TDF consists of all NOPS standard header records (nonduplicated) that relate to products that have gone into the making of the current product. Documentation records will be sequenced in accordance with their access; that is, first in is the first recorded. Every record in the TDF is 630 bytes in length.

The first record of this file will serve to identify the file as a TDF. This is accomplished by placing asterisks in characters 1 to 10 followed by NOPS TRAILER DOCUMENTATION FILE FOR TAPE PRODUCT T (SPEC NO (6 digits)) GENERATED ON DDD HHH MM. The second physical record will be a repeat of the NOPS standard header record for this tape with the provision that data referring to the end-time are correct for the data set. Following the first two physical records will be an accumulation of TDF's of all input tapes. For those products that require more than one tape, the TDF will appear on the last tape only.

APPENDIX C PARM TAPE DATA SET

C.1 Available Year-1 Data

YEAR	DAY	START ORBIT	END ORBIT	YEAR	DAY	START ORBIT	END ORBIT
78	302	66	79	79	10	1074	1087
78	303	80	92	79	12	1103	1116
78	304	93	106	79	14	1131	1143
78	305	108	120	79	16	1157	1171
78	306	121	134	79	18	1185	1198
78	307	135	148	79	20	1214	1226
78	308	149	162	79	22	1241	1254
78	309	163	175	79	24	1269	1282
78	310	176	189	79	26	1296	1309
78	311	190	203	79	28	1323	1337
78	312	204	217	79	30	1351	1365
78	313	218	231	79	31	1379	1379
78	314	232	245	79	32	1380	1392
78	315	246	258	79	34	1406	1419
78	316	259	272	79	36	1435	1448
78	317	273	286	79	38	1462	1475
78	318	287	300	79	40	1490	1503
78	319	301	314	79	42	1518	1531
78	320	327	328	79	43	1545	1545
78	321	329	341	79	44	1546	1558
78	322	342	342	79	46	1573	1586
78	323	356	369	79	48	1601	1614
78	325	383	397	79	50	1628	1641
78	327	412	424	79	52	1656	1669
78	329	438	452	79	54	1684	1696
78	331	467	480	79	56	1711	1724
78	333	494	507	79	58	1739	1752
78	334	508	508	79	59	1753	1758
78	335	521	534	79	60	1767	1779
78	337	549	563	79	62	1794	1807
78	338	576	577	79	64	1821	1835
78	339	578	590	79	66	1849	1862
78	341	604	618	79	68	1876	1890
78	343	632	646	79	70	1905	1918
78	345	661	673	79	72	1933	1945
78	347	688	701	79	73	1946	1946
78	349	716	729	79	74	1960	1973
78	351	743	756	79	76	1987	2001
78	353	771	784	79	77	2015	2015
78	355	798	812	79	78	2016	2028
78	356	825	825	79	80	2043	2056
78	357	826	839	79	82	2071	2084
78	359	853	867	79	84	2099	2111
78	361	881	894	79	86	2125	2139

YEAR	DAY	START ORBIT	END ORBIT	YEAR	DAY	START ORBIT	END ORBIT
78	363	909	922	79	88	2157	2166
78	365	936	949	79	90	2181	2194
79	2	965	978	79	92	2209	2222
79	4	992	1005	79	94	2236	2249
79	6	1020	1033	79	96	2264	2277
79	8	1047	1060	79	98	2291	2305
79	100	2321	2332	79	176	3369	3383
79	102	2348	2360	79	178	3398	3410
79	104	2376	2388	79	180	3424	3437
79	105	2402	2402	79	182	3453	3466
79	106	2403	2415	79	183	3479	3480
79	108	2430	2443	79	184	3481	3493
79	110	2457	2471	79	186	3507	3521
79	111	2484	2485	79	188	3536	3549
79	112	2486	2498	79	190	3565	3576
79	114	2513	2526	79	192	3591	3604
79	116	2541	2553	79	194	3618	3632
79	117	2567	2567	79	196	3647	3659
79	118	2568	2581	79	198	3673	3687
79	120	2595	2609	79	200	3704	3714
79	122	2623	2637	79	202	3729	3742
79	123	2650	2650	79	204	3759	3769
79	124	2651	2664	79	206	3784	3797
79	125	2665	2672	79	208	3812	3824
79	126	2679	2692	79	210	3840	3853
79	128	2707	2719	79	212	3868	3880
79	130	2734	2747	79	214	3895	3908
79	132	2761	2775	79	216	3923	3935
79	133	2788	2789	79	218	3950	3963
79	134	2790	2802	79	220	3977	3991
79	136	2817	2830	79	222	4006	4018
79	138	2844	2857	79	224	4033	4046
79	139	2871	2872	79	226	4061	4074
79	140	2873	2885	79	227	4088	4088
79	142	2900	2913	79	228	4089	4101
79	144	2928	2941	79	230	4115	4128
79	145	2954	2954	79	232	4143	4156
79	146	2955	2968	79	234	4172	4184
79	148	2982	2996	79	236	4198	4212
79	150	3010	3023	79	237	4225	4226
79	152	3037	3051	79	238	4227	4239
79	154	3066	3079	79	239	4253	4253
79	155	3092	3093	79	240	4254	4267
79	156	3094	3106	79	242	4281	4295
79	158	3121	3134	79	244	4310	4322
79	160	3148	3162	79	246	4337	4350
79	161	3175	3176	79	248	4364	4378
79	162	3177	3189	79	250	4392	4405
79	164	3203	3217	79	252	4419	4433
79	166	3232	3244	79	254	4447	4461
79	167	3258	3258	79	256	4475	4487
79	168	3259	3272	79	258	4502	4516
79	170	3286	3299	79	260	4530	4543

YEAR	DAY	START ORBIT	END ORBIT
79	172	3314	3327
79	173	3341	3341
79	174	3342	3355
79	266	4614	4625
79	268	4641	4654
79	270	4669	4682
79	271	4696	4696
79	272	4697	4709
79	274	4723	4737
79	276	4751	4764
79	277	4778	4778
79	278	4779	4792
79	280	4806	4820
79	282	4834	4847
79	283	4861	4861
79	284	4862	4875
79	286	4890	4903
79	288	4917	4929
79	290	4944	4958
79	292	4972	4985
79	293	5000	5000
79	294	5001	5013
79	296	5028	5041
79	298	5056	5069
79	300	5084	5096
79	302	5111	5124
79	304	5139	5151

YEAR	DAY	START ORBIT	END ORBIT
79	262	4559	4571
79	264	4586	4599
79	265	4613	4613

C.2 Available Year-2 Data

YEAR	DAY	START ORBIT	END ORBIT
79	306	5166	5179
79	308	5194	5207
79	309	5221	5221
79	310	5222	5234
79	312	5248	5262
79	314	5276	5290
79	315	5304	5304
79	316	5305	5317
79	318	5331	5344
79	320	5360	5373
79	322	5387	5400
79	324	5414	5427
79	326	5442	5455
79	328	5470	5483
79	330	5498	5511
79	332	5525	5538
79	334	5553	5565
79	336	5580	5594
79	338	5609	5621
79	340	5636	5649
79	342	5663	5676
79	344	5691	5704
79	346	5718	5732
79	348	5746	5760
79	350	5775	5787
79	352	5802	5815
79	354	5830	5842
79	356	5856	5869
79	358	5884	5898
79	360	5913	5925
79	362	5940	5953
79	364	5967	5981
80	1	5996	6008
80	3	6023	6036
80	4	6050	6050
80	5	6051	6063
80	7	6078	6090
80	9	6106	6119
80	11	6134	6146
80	13	6160	6173
80	15	6188	6202
80	16	6216	6216
80	17	6217	6228
80	19	6243	6257
80	21	6271	6284
80	22	6299	6299
80	23	6300	6312
80	25	6326	6340
80	27	6355	6367
80	29	6382	6395

YEAR	DAY	START ORBIT	END ORBIT
80	31	6409	6423
80	33	6437	6451
80	35	6464	6478
80	37	6493	6506
80	39	6521	6533
80	41	6548	6561
80	43	6576	6589
80	44	6603	6603
80	45	6604	6616
80	46	6617	6617
80	47	6630	6644
80	49	6659	6671
80	51	6686	6699
80	53	6714	6727
80	55	6741	6754
80	57	6769	6782
80	59	6796	6809
80	60	6824	6824
80	61	6825	6837
80	63	6851	6865
80	65	6880	6892
80	66	6907	6907
80	67	6908	6920
80	69	6935	6948
80	71	6963	6975
80	73	6990	7003
80	75	7018	7031
80	77	7045	7058
80	79	7073	7086
80	81	7100	7114
80	82	7128	7128
80	83	7129	7141
80	85	7155	7169
80	87	7183	7197
80	88	7211	7211
80	89	7212	7224
80	91	7239	7252
80	93	7267	7279
80	95	7294	7307
80	97	7322	7335
80	98	7349	7349
80	99	7350	7362
80	101	7377	7390
80	103	7404	7418
80	105	7433	7445
80	107	7459	7473
80	109	7488	7500
80	110	7515	7515
80	111	7516	7528
80	113	7543	7556

YEAR	DAY	START ORBIT	END ORBIT
80	115	7571	7584
80	117	7598	7611
80	119	7625	7638
80	121	7654	7666
80	123	7681	7694
80	125	7708	7722
80	127	7737	7750
80	129	7764	7777
80	131	7792	7804
80	132	7819	7819
80	133	7820	7832
80	135	7846	7860
80	137	7875	7887
80	138	7902	7902
80	139	7903	7915
80	141	7929	7943
80	142	7957	7957
80	143	7958	7970
80	145	7985	7998
80	147	8012	8026
80	149	8041	8053
80	151	8068	8081
80	153	8096	8109
80	155	8123	8136
80	157	8150	8164
80	159	8179	8191
80	161	8206	8219
80	163	8233	8246
80	165	8262	8274
80	167	8289	8302
80	169	8317	8330
80	171	8344	8357
80	173	8372	8385
80	175	8400	8413
80	176	8414	8427
80	177	8428	8440
80	179	8454	8468
80	181	8483	8496
80	182	8510	8510
80	183	8511	8523
80	185	8537	8551
80	187	8566	8578
80	189	8593	8606
80	191	8620	8634
80	193	8648	8661
80	195	8676	8689
80	197	8704	8717
80	199	8732	8744
80	201	8759	8772
80	203	8787	8799

YEAR	DAY	START ORBIT	END ORBIT
80	204	8813	8814
80	205	8815	8827
80	207	8842	8855
80	209	8870	8882
80	210	8896	8897
80	211	8898	8910
80	213	8925	8937
80	215	8952	8965
80	217	8980	8993
80	219	9008	9021
80	220	9035	9035
80	221	9036	9048
80	223	9063	9076
80	225	9091	9103
80	226	9118	9118
80	227	9119	9131
80	229	9145	9159
80	231	9173	9186
80	232	9201	9201
80	233	9202	9214
80	235	9228	9241
80	236	9256	9256
80	237	9257	9269
80	238	9283	9283
80	239	9284	9297
80	240	9298	9298
80	241	9311	9322
80	242	9339	9339
80	243	9340	9352
80	245	9367	9380
80	247	9394	9408
80	248	9422	9422
80	249	9423	9435
80	250	9436	9436
80	251	9450	9463
80	253	9477	9489
80	254	9505	9505
80	255	9506	9518
80	257	9533	9546
80	259	9560	9573
80	260	9587	9587
80	261	9588	9601
80	263	9615	9629
80	265	9643	9656
80	267	9671	9684
80	269	9699	9712
80	270	9726	9726
80	271	9727	9739
80	273	9754	9767
80	275	9781	9795

YEAR	DAY	START ORBIT	END ORBIT
80	277	9810	9822
80	278	9823	9823
80	279	9836	9850
80	281	9864	9877
80	282	9891	9891
80	283	9892	9905
80	285	9919	9933
80	286	9947	9947
80	287	9948	9960
80	289	9975	9988
80	291	10003	10016
80	293	10030	10043
80	295	10058	10071
80	297	10085	10098
80	298	10113	10113
80	299	10114	10126
80	301	10141	10154
80	303	10169	10181
80	304	10196	10196
80	305	10197	10209

C.3 Available Year-3 Data

YEAR	DAY	START ORBIT	END ORBIT
80	307	10223	10237
80	308	10251	10251
80	309	10252	10264
80	311	10279	10292
80	313	10306	10319
80	315	10334	10347
80	317	10362	10375
80	319	19389	10402
80	321	10417	10430
80	323	10445	10458
80	325	10472	10486
80	326	10500	10500
80	327	10501	10512
80	329	10528	10541
80	331	10555	10568
80	333	10583	10596
80	335	10611	10624
80	337	10638	10652
80	339	10666	10679
80	341	10693	10707
80	342	10721	10721
80	343	10722	10734
80	344	10735	10735
80	345	10749	10762
80	347	10777	10789
80	348	10804	10804
80	349	10805	10817
80	351	10831	10845
80	353	10860	10872
80	354	10886	10886
80	355	10887	10900
80	357	10914	10928
80	358	10942	10942
80	359	10943	10955
80	361	10970	10983
80	363	10998	11011
80	365	11025	11039
81	1	11053	11066
81	3	11080	11094
81	5	11108	11121
81	6	11122	11122
81	7	11135	11148
81	9	11163	11177
81	11	11191	11204
81	12	11205	11205
81	13	11218	11232
81	15	11247	11260
81	17	11274	11287
81	18	11288	11288
81	21	11329	11342
81	22	11356	11356
81	23	11357	11370
81	25	11384	11398
81	27	11412	11425
81	29	11439	11453
81	31	11467	11481
81	33	11496	11508
81	34	11509	11510
81	35	11522	11536
81	37	11550	11564
81	38	11577	11578
81	39	11579	11591
81	41	11605	11619
81	42	11632	11633
81	43	11634	11646
81	44	11660	11660
81	45	11661	11674
81	47	11688	11702
81	49	11716	11730
81	51	11744	11757
81	53	11771	11785
81	54	11798	11799
81	55	11800	11812
81	56	11813	11813
81	57	11826	11840
81	59	11854	11867
81	60	11881	11882
81	61	11883	11895
81	63	11909	11923
81	65	11937	11951
81	67	11965	11978
81	69	11993	12006
81	71	12020	12033
81	73	12047	12061
81	75	12075	12089
81	76	12102	12103
81	77	12104	12116
81	79	12131	12144
81	81	12158	12172
81	82	12185	12186
81	83	12187	12199
81	84	12200	12200
81	85	12213	12227
81	87	12241	12255
81	89	12269	12282
81	91	12296	12310
81	93	12324	12337
81	95	12352	12365

YEAR	DAY	START ORBIT	END ORBIT
81	19	11301	11315
81	99	12407	12420
81	101	12435	12448
81	103	12462	12476
81	105	12490	12503
81	107	12518	12531
81	109	12545	12559
81	111	12573	12586
81	113	12600	12614
81	115	12628	12641
81	117	12656	12669
81	119	12683	12697
81	121	12711	12724
81	123	12739	12752
81	125	12767	12780
81	126	12794	12794
81	127	12795	12808
81	129	12822	12835
81	131	12849	12863
81	132	12877	12877
81	133	12878	12890
81	135	12904	12918
81	137	12932	12946
81	138	12960	12960
81	139	12961	12973
81	141	12987	13001
81	143	13015	13029
81	145	13043	13056
81	147	13070	13084
81	149	13098	13112
81	151	13126	13139
81	153	13153	13167
81	155	13181	13194
81	157	13208	13222
81	159	13236	13250
81	160	13264	13264
81	161	13265	13277
81	162	13278	13278
81	163	13291	13305
81	165	13319	13333
81	167	13347	13360
81	169	13374	13388
81	171	13402	13416
81	172	13429	13429
81	173	13430	13443
81	175	13457	13471
81	177	13485	13499
81	179	13512	13526
81	181	13540	13554
81	183	13568	13581
81	185	13595	13609

YEAR	DAY	START ORBIT	END ORBIT
81	97	12379	12393
81	187	13623	13636
81	188	12637	13651
81	189	13652	13664
81	191	13678	13692
81	193	13706	13720
81	194	13733	13734
81	195	13735	13747
81	197	13761	13775
81	199	13789	13803
81	200	13816	13816
81	201	13817	13830
81	203	13845	13858
81	205	13872	13886
81	206	13899	13899
81	207	13900	13913
81	209	13927	13941
81	211	13955	13968
81	212	13969	13969
81	213	13982	13996
81	215	14010	14023
81	216	14038	14038
81	217	14039	14051
81	219	14065	14079
81	221	14093	14107
81	223	14122	14134
81	224	14135	14135
81	225	14148	14162
81	227	14176	14190
81	229	14204	14217
81	231	14231	14245
81	233	14260	14272
81	235	14287	14300
81	237	14314	14328
81	239	14342	14355
81	241	14369	14383
81	243	14397	14411
81	245	14425	14438
81	247	14452	14468
81	249	14480	14494
81	250	14507	14507
81	251	14508	14521
81	253	14536	14549
81	255	14563	14576
81	257	14591	14604
81	259	14618	14632
81	261	14646	14660
81	263	14673	14687
81	265	14701	14715
81	267	14729	14742
81	269	14756	14770

YEAR	DAY	START ORBIT	END ORBIT
81	271	14784	14798
81	272	14811	14812
81	273	14813	14825
81	275	14839	14853
81	277	14867	14881
81	278	14894	14894
81	279	14895	14908
81	281	14922	14936
81	283	14950	14963
81	285	14978	14991
81	287	15005	15019
81	289	15033	15046
81	290	15060	15060
81	291	15061	15074
81	293	15088	15102
81	295	15116	15129
81	297	15143	15157
81	299	15171	15185
81	301	15199	15212
81	303	15226	15240

C.4 Available Year-4 Data

YEAR	DAY	START ORBIT	END ORBIT
81	305	15255	15268
81	306	15281	15281
81	307	15282	15295
81	309	15309	15323
81	311	15337	15350
81	312	15364	15364
81	313	15365	15378
81	315	15392	15405
81	317	15420	15433
81	319	15448	15461
81	321	15475	15489
81	323	15503	15516
81	325	15530	15544
81	327	15558	15571
81	328	15585	15586
81	329	15587	15599
81	331	15613	15627
81	333	15642	15655
81	335	15670	15682
81	337	15696	15710
81	339	15724	15737
81	340	15751	15751
81	341	15752	15765
81	343	15779	15793
81	345	15807	15821
81	347	15834	15848
81	349	15862	15876
81	351	15890	15903
81	352	15904	15904
81	353	15917	15931
81	355	15945	15959
81	357	15973	15986
81	359	16001	16014
81	361	16028	16042
81	362	16055	16055
81	363	16056	16069
81	365	16083	16096
82	2	16111	16124
82	4	16139	16152
82	6	16166	16180
82	7	16193	16194
82	8	16195	16207
82	10	16221	16235
82	12	16249	16263
82	13	16277	16277
82	14	16278	16290
82	16	16304	16318
82	18	16332	16346
82	19	16359	16360
82	22	16387	16401
82	24	16415	16429
82	26	16443	16456
82	28	16470	16483
82	30	16498	16511
82	32	16526	16539
82	34	16553	16567
82	35	16580	16581
82	36	16582	16594
82	38	16608	16622
82	40	16636	16650
82	42	16664	16677
82	43	16678	16678
82	44	16691	16705
82	46	16720	16733
82	48	16747	16760
82	50	16774	16788
82	52	16802	16816
82	53	16829	16829
82	54	16830	16843
82	56	16857	16871
82	58	16886	16898
82	60	16913	16926
82	62	16941	16954
82	64	16968	16981
82	66	16996	17009
82	68	17024	17037
82	69	17050	17051
82	70	17052	17064
82	72	17078	17092
82	74	17106	17119
82	76	17134	17147
82	78	17161	17175
82	80	17189	17202
82	82	17218	17230
82	84	17245	17258
82	86	17272	17285
82	88	17300	17313
82	90	17327	17341
82	92	17355	17369
82	94	17383	17396
82	96	17410	17424
82	98	17438	17451
82	100	17465	17479
82	102	17493	17507
82	103	17520	17521
82	104	17522	17534
82	106	17548	17562
82	108	17576	17590

YEAR	DAY	START ORBIT	END ORBIT
82	20	16361	16373
82	110	17605	17617
82	112	17631	17645
82	114	17659	17673
82	115	17686	17686
82	116	17687	17700
82	118	17715	17728
82	119	17729	17729
82	120	17742	17755
82	121	17769	17769
82	122	17770	17783
82	124	17797	17811
82	126	17825	17838
82	128	17852	17866
82	130	17880	17894
82	131	17908	17908
82	132	17909	17921
82	134	17935	17949
82	136	17963	17977
82	137	17990	17991
82	138	17992	18004
82	140	18018	18032
82	142	18046	18060
82	143	18073	18073
82	144	18074	18087
82	146	18101	18115
82	148	18129	18142
82	149	18156	18156
82	150	18157	18170
82	152	18184	18197
82	154	18212	18225
82	156	18239	18253
82	158	18267	18281
82	159	18294	18295
82	160	18296	18308
82	162	18322	18336
82	164	18350	18364
82	165	18377	18378
82	166	18379	18391
82	168	18406	19419
82	170	18433	18447
82	172	18461	18474
82	174	18488	18502
82	176	18516	18530
82	178	18544	18557
82	180	18571	18585
82	182	18599	18612
82	184	18626	18640
82	186	18654	18668
82	188	18682	18695
82	189	18696	18696
82	109	17603	17604
82	190	18709	18723
82	192	18737	18751
82	193	18764	18765
82	194	18766	18778
82	198	18821	18834
82	199	18848	18848
82	200	18849	18861
82	202	18875	18889
82	204	18903	18916
82	206	18931	18944
82	208	18958	18972
82	210	18986	18999
82	214	19042	19055
82	218	19097	19109
82	222	19152	19165
82	224	19179	19193
82	226	19207	19221
82	230	19263	19276
82	232	19290	19303
82	233	19317	19317
82	234	19318	19331
82	236	19346	19359
82	238	19373	19387
82	240	19401	19414
82	242	19428	19442
82	244	19456	19469
82	246	19484	19497
82	248	19511	19525
82	249	19538	19539
82	250	19540	19552
82	252	19566	19580
82	254	19594	19608
82	256	19622	19635
82	258	19649	19663
82	260	19677	19691
82	261	19704	19704
82	262	19705	19718
82	264	19732	19746
82	266	19760	19774
82	267	19787	19787
82	268	19788	19801
82	270	19815	19829
82	272	19843	19857
82	273	19870	19870
82	274	19871	19884
82	276	19898	19912
82	278	19926	19939
82	280	19953	19967
82	282	19981	19995
82	284	20013	20022

YEAR	DAY	START ORBIT	END ORBIT
82	286	20036	20050
82	288	20064	20078
82	289	20091	20092
82	290	20093	20105
82	292	20119	20133
82	294	20147	20161
82	295	20174	20174
82	296	20175	20188
82	298	20202	20216
82	300	20230	20244
82	301	20257	20257
82	302	20258	20271
82	304	20285	20299

C.5 Available Year-5 Data

YEAR	DAY	START ORBIT	END ORBIT
82	306	20313	20326
82	308	20340	20354
82	310	20368	20382
82	312	20396	20409
82	314	20423	20437
82	316	20451	20465
82	317	20478	20479
82	318	20480	20492
82	320	20506	20520
82	322	20534	20548
82	324	20562	20575
82	326	20589	20603
82	328	20617	20631
82	329	20644	20644
82	330	20645	20658
82	332	20672	20686
82	334	20700	20714
82	335	20727	20727
82	336	20728	20741
82	338	20755	20769
82	340	20783	20796
82	341	20797	20797
82	342	20810	20824
82	344	20838	20852
82	345	20865	20866
82	346	20867	20879
82	348	20893	20907
82	350	20921	20935
82	351	20948	20949
82	352	20950	20962
82	354	20976	20990
82	356	21004	21018
82	357	21031	21031
82	358	21032	21044
82	360	21059	21073
82	362	21087	21101
82	363	21114	21114
82	364	21115	21128
83	1	21143	21156
83	3	21170	21184
83	5	21197	21211
83	6	21212	21212
83	7	21225	21239
83	9	21253	21266
83	11	21280	21294
83	13	21308	21322
83	15	21336	21349
83	17	21363	21377
83	19	21391	21405

YEAR	DAY	START ORBIT	END ORBIT
83	21	21420	21432
83	23	21446	21460
83	25	21474	21488
83	26	21489	21501
83	27	21502	21515
83	29	21529	21543
83	31	21557	21570
83	33	21585	21598
83	35	21612	21626
83	37	21640	21653
82	39	21667	21681
82	41	21695	21709
82	42	21722	21723
82	43	21724	21736
82	44	21747	21750
82	45	21751	21764
82	47	21778	21792
83	48	21805	21806
83	49	21807	21819
83	50	21830	21833
83	51	21834	21847
83	52	21857	21861
83	53	21862	21875
83	54	21888	21889
83	55	21890	21902
83	57	21916	21930
83	50	21944	21957
83	60	21971	21971
83	61	21972	21985
83	63	21999	22013
83	65	22027	22040
83	67	22054	22068
83	69	22082	22096
83	71	22110	22123
83	73	22137	22151
83	75	22165	22179
83	77	22193	22206
83	79	22220	22234
83	81	22248	22262
83	82	22275	22276
83	83	22277	22289
83	85	22303	22317
83	87	22331	22345
83	88	22358	22358
83	89	22359	22372
83	91	22387	22400
83	93	22414	22427
83	94	22441	22441
83	95	22442	22455

YEAR	DAY	START ORBIT	END ORBIT
83	20	21418	21419
83	97	22469	22483
83	98	22496	22497
83	99	22498	22510
83	101	22524	22538
83	102	22539	22539
83	103	22552	22566
83	105	22580	22593
83	107	22607	22621
83	108	22622	22622
83	109	22635	22649
83	110	22662	22663
83	111	22664	22676
83	113	22690	22704
83	115	22719	22731
83	116	22745	22746
83	117	22747	22759
83	119	22773	22787
83	121	22802	22814
83	122	22828	22828
83	123	22829	22842
83	125	22856	22870
83	127	22886	22897
83	128	22911	22911
83	129	22912	22925
83	131	22940	22953
83	133	33967	22981
83	134	22982	22982
83	135	22995	23008
83	137	23022	23036
83	138	23049	23050
83	139	23051	23063
83	140	23064	23065
83	141	23077	23091
83	143	23105	23119
83	144	23132	23133
83	145	23134	23146
83	147	23160	23174
83	148	23175	23175
83	149	23188	23202
83	151	23216	23229
83	153	23244	23257
83	154	23258	23258
83	155	23272	23284
83	157	23300	23312
83	158	23313	23313
83	159	23327	23340
83	160	23341	23341
83	161	23354	23367
83	163	23381	23395
83	165	23409	23423

YEAR	DAY	START ORBIT	END ORBIT
83	96	22456	22456
83	167	23438	22450
83	169	23465	23478
83	171	23492	23506
83	172	23507	23507
83	173	23522	23533
83	174	23534	23535
83	175	23548	23561
83	176	23562	23562
83	177	23576	23589
83	178	23590	23590
83	179	23605	23616
83	180	23617	23618
83	181	23631	23644
83	183	23658	23672
83	185	23686	23837
83	187	23714	23727
83	189	23742	23727
83	191	23769	23782
83	193	23797	23810
83	195	23824	23837
83	197	23852	23865
83	199	23880	23893
83	201	23907	23920
83	203	23935	23948
83	205	23963	23976
83	206	23990	23990
83	207	23991	24003
83	209	24018	24031
83	211	24045	24059
83	212	24072	24073
83	213	24074	24086
83	215	24101	24114
83	217	24128	24142
83	219	24156	24169
83	221	24183	24197
83	223	24211	24224
93	224	24238	24238
93	225	24239	24252
83	227	24266	24280
83	229	24294	24307
83	230	24321	24321
83	231	24322	24335
83	233	24349	24363
83	235	24377	24390
83	237	24405	24418
83	239	24432	24446
83	241	24460	24473
83	243	24487	24501
83	245	24515	24529
83	246	24542	24543

YEAR	DAY	START ORBIT	END ORBIT
83	247	24544	24556
83	249	24571	24584
93	251	24598	24611
83	252	24625	24625
83	253	24626	24639
83	255	24653	24667
83	257	24681	24694
83	258	24708	24708
83	259	24709	24722
83	261	24736	24750
83	263	24764	24778
83	265	24791	24805
83	267	24819	24833
83	269	24847	24860
83	271	24874	24888
83	273	24902	24916
83	274	24929	24930
83	275	24931	24943
83	277	24957	24971
83	279	24985	24999
83	281	25013	25026
83	283	25040	25054
83	285	25068	25082
83	287	25096	25109
83	288	25110	25110
83	289	25124	25137
83	291	25151	25165
83	292	25178	25178
83	293	25179	25192
83	295	25207	25220
83	297	25234	25247
83	298	25261	25261
83	299	25262	25275
83	201	25289	25303
83	303	25318	25330

C.6 Available Year-6 Data

YEAR	DAY	START ORBIT	END ORBIT
83	305	25344	25358
83	307	25373	25386
83	309	25400	25413
83	311	25427	25441
83	313	25455	25469
83	314	25482	25483
83	315	25484	25496
83	317	25510	25524
83	319	25539	25552
83	321	25567	25579
83	323	25594	25607
83	325	25622	25635
83	327	25649	25662
83	329	25676	25690
83	331	25705	25717
83	332	25731	25731
83	333	25732	25745
83	335	25759	25773
83	337	25787	25800
83	339	25814	25828
83	341	25842	25856
83	342	25869	25870
83	343	25871	25883
83	345	25898	25911
83	347	25925	25939
83	348	25952	25953
83	349	25954	25966
83	351	25980	25994
83	353	26008	26022
83	354	26035	26035
83	355	26036	26049
83	357	26063	26077
83	359	26091	26105
83	360	26118	26118
83	361	26119	26132
83	363	26146	26160
83	365	26174	26187
84	2	26201	26214
84	4	26229	26243
84	5	26256	26257
84	6	26258	26270
84	8	26285	26298
84	10	26312	26325
84	11	26339	26340
84	12	26341	26353
84	14	26367	26381
84	16	26396	26408
84	17	26422	26423
84	18	26424	26436
84	22	26478	26492
84	23	26505	26505
84	24	26506	26519
84	26	26533	26547
84	28	26561	26575
84	30	26589	26602
84	32	26616	26630
84	34	26644	26657
84	36	26672	26685
84	38	26699	26712
84	40	26728	26740
84	41	26741	26741
84	42	26756	26768
84	44	26782	26796
84	45	26810	26810
84	46	26811	26823
84	48	26837	26851
84	49	26852	26852
84	50	26866	26879
84	51	26892	26893
84	52	26894	26906
84	54	26921	26934
84	56	26949	26962
84	57	26975	26975
84	58	26976	26989
84	60	27003	27017
84	62	27032	27045
84	64	27059	27072
84	66	27086	27099
84	68	27114	27128
84	70	27141	27154
84	72	27169	27183
84	73	27196	27197
84	74	27198	27210
84	76	27224	27238
84	78	27252	27266
84	79	27279	27280
84	80	27281	27293
84	82	27307	27321
84	84	27335	27348
84	85	27363	27363
84	86	27364	27376
84	87	27377	27377
84	88	27390	27404
84	90	27420	27432
84	92	27447	27459
84	93	27460	27460
84	94	27473	27487
84	95	27501	27501

YEAR	DAY	START ORBIT	END ORBIT
84	20	26450	26464
84	98	27529	27542
84	99	27543	27543
84	100	27557	27569
84	101	27584	27584
84	102	27585	27597
84	103	27610	27611
84	104	27612	27625
84	106	27640	27653
84	107	27666	27667
84	108	27668	27680
84	110	27695	27708
84	112	27724	27736
84	113	27750	27750
84	114	27751	27763
84	115	27764	27764
84	116	27778	27791
84	118	27806	27819
84	120	27834	27846
84	122	27861	27874
84	123	27888	27888
84	124	27889	27902
84	126	27916	29792
84	128	27944	27957
84	130	27972	27984
84	132	27999	28012
84	134	28027	28040
84	136	28055	28067
84	138	28082	28095
84	140	28110	28123
84	142	28138	28150
84	143	28151	28151
84	144	28165	28178
84	146	28193	28206
84	147	28220	28220
84	148	28221	28223
84	149	28234	29234
84	150	28248	29261
84	152	28276	28289
84	153	28303	28303
84	154	28304	28316
84	156	28332	29344
84	157	28345	29345
84	158	28359	28372
84	160	28386	28399
84	161	28400	28400
84	162	28414	29427
84	164	28442	28455
84	166	28469	28482
84	168	28497	28510
84	169	28524	28524

YEAR	DAY	START ORBIT	END ORBIT
84	96	27502	27514
84	170	28525	28537
84	172	28552	28565
84	174	28580	28592
84	176	28608	28620
84	177	28621	28621
84	178	28635	29648
84	180	28663	28676
84	181	28690	28690
84	182	28691	28703
84	183	28704	28704
84	184	28718	28731
84	186	28746	28758
84	187	28773	28773
84	188	28774	29786
84	190	28801	28814
84	192	28829	28842
84	194	28856	28869
84	196	28884	28897
84	198	28912	28924
84	200	28939	28952
84	202	28967	28980
84	204	28995	29007
84	206	29022	29034
84	208	29050	29063
84	209	29064	29064
84	210	29078	29090
84	212	29105	29118
84	214	29133	29146
84	216	29160	29173
84	217	29174	29175
84	218	29188	29201
84	220	29216	29229
84	221	29243	29243
84	222	29244	29256
84	224	29271	29284
84	238	29465	29477
84	240	29492	29505
84	242	29520	29533
84	244	29548	29560
84	246	29576	29588
84	247	29589	29590
84	248	29605	29616
84	249	29617	29630
84	250	29631	29643
84	252	29659	20671
84	254	29685	29699
84	256	29714	29726
84	258	29740	29754
84	260	29770	29781
84	262	29797	29809

YEAR	DAY	START ORBIT	END ORBIT
84	264	29823	29837
84	266	29852	29865
84	268	29879	29892
84	270	29907	29920
84	271	29934	29934
84	272	29935	29947
84	274	29962	29975
84	276	29990	30003
84	278	30018	30030
84	280	30045	30057
84	281	30058	30058
84	282	30073	30086
84	284	30101	30113
84	286	30129	30141
84	288	30156	20169
84	289	30182	30183
84	290	30184	30196
84	292	30210	30224
84	294	30240	30252
84	295	30266	30266
84	296	30267	30279
84	298	30293	30307
84	300	30322	30335
84	301	30336	30348
84	302	30349	30362
84	304	30376	30390

C.7 Available Year-7 Data

YEAR	DAY	START ORBIT	END ORBIT
84	306	30405	30417
84	307	30431	30431
84	308	30432	30445
84	310	30459	30473
84	312	30487	30500
84	314	30515	30528
84	316	30543	30556
84	317	30557	30557
84	318	30571	30583
84	319	30584	30585
84	320	30598	30611
84	321	30612	30612
84	322	30625	30639
84	323	30653	30653
84	324	30654	30666
84	326	30680	30694
84	328	30709	30722
84	329	30735	30736
84	330	30737	30749
84	332	30763	30777
84	334	30791	30805
84	335	30818	30818
84	336	30819	30819
84	338	30846	30860
84	339	30861	30861
84	340	30875	30888
84	341	30889	30889
84	342	30902	30915
84	343	30916	30916
84	344	30930	30943
84	345	30944	30944
84	346	30958	30871
84	347	30972	30972
84	348	30985	30998
84	349	30999	30999
84	350	31012	31026
84	351	31027	31027
84	352	31041	31054
84	354	31069	31081
84	355	31082	31082
84	356	31096	31109
84	357	31110	31110
84	358	31124	31136
84	359	31137	31137
84	360	31151	31164
84	361	31165	31165
84	362	31179	31192
84	363	31193	31206
84	364	31207	31219
84	366	31234	31247
85	1	31348	31248
85	2	31262	31275
85	3	31276	31289
85	4	31290	31302
85	5	31303	31303
85	6	31317	31330
85	7	31331	31331
85	8	31345	31358
85	10	31372	31385
85	11	31386	31386
85	12	31400	31413
85	13	31414	31414
85	14	31428	31440
85	15	31454	31454
85	16	31455	31468
85	17	31469	31469
85	18	31483	31496
85	19	31497	31497
85	20	31510	31524
85	22	31538	31551
85	24	31566	31579
85	26	31593	31606
85	28	31621	31634
85	29	31635	31635
85	30	31648	21661
85	31	31675	21676
85	32	31677	21689
85	34	31704	31717
85	36	31731	31745
85	37	31758	31759
85	38	31760	31772
85	40	31786	31800
85	42	31814	31827
85	44	31842	31855
85	45	31856	31856
85	46	31869	31883
85	47	31884	31884
85	48	31897	31910
85	50	31925	31938
85	51	31939	31939
85	52	31952	31966
85	54	31980	31993
85	56	32007	32021
85	58	32035	32049
85	59	32050	32050
85	60	32063	32076
85	62	32091	32104
85	64	32118	32132

YEAR	DAY	START ORBIT	END ORBIT
84	265	31220	31220
85	66	32146	32159
85	68	32174	32187
85	69	23188	32188
85	70	32201	32215
85	71	32216	32229
85	72	32230	32242
85	73	32243	32243
85	74	32256	32270
85	75	32271	32271
85	76	32285	32297
85	78	32312	32325
85	79	32326	32327
85	80	32340	32353
85	81	32367	32367
85	82	32368	32380
85	84	32395	32408
85	86	32423	23436
85	88	32450	32463
85	90	32478	32491
85	92	32506	32519
85	93	32532	32533
85	94	32534	32546
85	96	32560	32574
85	98	32589	32602
85	99	32616	32616
85	100	32617	32629
85	102	32644	32657
85	104	32672	32685
85	105	32699	32699
85	106	32700	32712
85	108	32727	32737
85	110	32755	32768
85	111	32781	32781
85	112	32782	32795
85	114	32810	32823
85	116	32838	32850
85	118	32865	32878
85	119	32879	32879
85	120	32893	33905
85	122	32921	32931
85	124	32948	32961
85	125	32962	32962
85	126	32976	32989
85	127	33003	33003
85	128	33004	33016
85	129	33017	33017
85	130	33031	33044
85	132	33059	33072
85	134	33086	33099
85	136	33114	33127

YEAR	DAY	START ORBIT	END ORBIT
85	65	32133	32133
85	138	33142	33155
85	140	33169	33182
85	142	33197	33210
85	144	33225	33238
85	146	33253	33265
85	148	33280	33293
85	150	33308	33321
85	152	33336	33348
85	154	33363	33376
85	156	33391	33403
85	158	33418	33431
85	160	33446	33459
85	161	33473	33473
85	162	33474	33486
85	164	33501	33514
85	165	33515	33515
85	166	33529	33542
85	168	33557	33569
85	170	33584	33597
85	172	33612	33624
85	173	33639	33639
85	174	33640	33652
85	176	33668	33678
85	178	33695	33708
85	180	33722	33735
85	182	33750	33763
85	183	33764	33764
85	184	33778	33791
85	186	33806	33818
85	187	33819	33819
85	188	33833	33846
85	189	33847	33860
85	190	33861	33873
85	192	33888	33901
85	193	33902	33902
85	194	33916	33929
85	195	33930	33931
85	196	33944	33956
85	198	33971	33984
85	200	33999	34012
85	202	34028	24039
85	204	34054	34067
85	206	34082	34095
85	207	34096	34109
85	208	34110	34122
85	210	34137	34150
85	212	34165	34178
85	214	34193	34205
85	216	34220	34233
85	218	34248	34260

YEAR	DAY	START ORBIT	END ORBIT
85	220	34276	34288
85	221	34289	24289
85	222	34303	34316
85	224	34331	34344
85	226	34358	34371
85	228	34386	34399
85	339	34400	34400
85	230	34414	34426
85	232	34441	34454
85	234	34469	34482
85	236	34497	34509
85	238	34524	34537
85	240	23552	34565
85	241	34579	24579
85	242	34580	34592
85	244	34607	24620
85	246	34635	34647
85	248	34663	34675
85	250	34690	34703
85	252	34718	24731
85	254	34746	34758
85	256	34773	34786
85	257	34787	34787
85	258	34801	34814
85	260	34829	34841
85	262	34856	34869
85	264	34884	34896
85	266	34911	34924
85	268	34939	34952
85	270	34967	34979
85	272	34994	35007
85	274	35022	35035
85	276	35050	35062
85	278	35077	35090
85	280	35105	35118
85	281	35132	35132
85	282	35133	35145
85	284	35160	35173
85	286	35188	35200
85	288	35216	35228
85	290	35243	35256
85	291	35270	35270
85	292	35271	35283
85	294	35298	35311
85	296	35326	35339
85	298	35354	35367
85	300	35381	35392
85	302	35409	35422
85	304	35436	35449

★U.S. GOVERNMENT PRINTING OFFICE: 1992 - 627 - 064/66001

REPORT DOCUMENTATION PAGE

Form Approved
OMB No. 0704-0188

1. AGENCY USE ONLY (Leave blank)	2. REPORT DATE	3. REPORT TYPE AND DATES COVERED
	August 1992	Reference Publication

4. TITLE AND SUBTITLE

Nimbus-7 Scanning Multichannel Microwave Radiometer (SMMR) PARM Tape User's Guide

5. FUNDING NUMBERS

JON-936-0390901-25
C - NAS5-29386

6. AUTHOR(S)

D. Han, P. Gloersen, S.T. Kim, C.C. Fu, R.P. Cebula, D. MacMillan

7. PERFORMING ORGANIZATION NAME(S) AND ADDRESS(ES)

Goddard Space Flight Center
Greenbelt, MD 20771

8. PERFORMING ORGANIZATION REPORT NUMBER

92B00104
Code 936

9. SPONSORING/MONITORING AGENCY NAME(S) AND ADDRESS(ES)

National Aeronautics and Space Administration
Washington, D.C. 20546-0001

10. SPONSORING/MONITORING AGENCY REPORT NUMBER

NASA RP-1284

11. SUPPLEMENTARY NOTES

D. Han and P. Gloersen, Goddard Space Flight Center, Greenbelt, MD; S.T. Kim and C.C. Fu, Computer Sciences Corp., Rockville, MD; R.P. Cebula, Hughes STX Corp., Lanham, MD; D. MacMillan, Interferometrics, Inc., Vienna, VA

12a. DISTRIBUTION/AVAILABILITY STATEMENT

Unclassified - Unlimited
Subject Category 48

12b. DISTRIBUTION CODE

13. ABSTRACT (Maximum 200 words)

The Scanning Multichannel Microwave Radiometer (SMMR) instrument onboard the Nimbus-7 spacecraft collected data from October 1978 until June 1986. The data have been processed to physical parameter level products. Geophysical parameters retrieved include sea-surface temperatures, sea-surface windspeed, total column water vapor, and sea-ice parameters. These products are stored on PARM-LO, PARM-SS, and PARM-30 tapes. In this document, the geophysical parameter retrieval algorithms and the quality of these products are described for the period between November 1978 and October 1985. Additionally, data formats and data availability are included.

14. SUBJECT TERMS

SMMR, SST, windspeed, water vapor, sea ice, passive microwave, remote sensing

15. NUMBER OF PAGES
152

16. PRICE CODE
A08

17. SECURITY CLASSIFICATION OF REPORT	18. SECURITY CLASSIFICATION OF THIS PAGE	19. SECURITY CLASSIFICATION OF ABSTRACT	20. LIMITATION OF ABSTRACT
Unclassified	Unclassified	Unclassified	UL